Development of Efficient Intensity based Registration Techniques for Multi-modal Brain Images

Smita Pradhan

Department of Electrical Engineering,
National Institute of Technology, Rourkela,
Rourkela-769 008, Odisha, India.
Aug, 2016.

Development of Efficient Intensity based Registration Techniques for Multi-modal Brain Images

Dissertation submitted in partial fulfillment
of the requirements of the degree of

Doctor of Philosophy

in

Electrical Engineering

by

Smita Pradhan

(Roll No: 511EE107)

Under the Supervision of

Dr. Dipti Patra

Department of Electrical Engineering,
National Institute of Technology, Rourkela,
Rourkela-769 008, Odisha, India

2011-2016

Dedicated

to

My Parents

and my $\sqrt{}$ *Aunty Mummy*

Certificate

This is to certify that the thesis entitled **"Development of Efficient Intensity based Registration Techniques for Multi-modal Brain Images"** *by* **Smita Pradhan**, *submitted to the National Institute of Technology, Rourkela for the award of Doctor of Philosophy in Electrical Engineering, is a record of bonafide research work carried out by her in the Department of Electrical Engineering, under my supervision. I believe that this thesis fulfills part of the requirements for the award of degree of Doctor of Philosophy.The results embodied in the thesis have not been submitted for the award of any other degree elsewhere.*

Place: Rourkela
Date: 23^{rd} August, 2016

Dr. Dipti Patra
Associate Professor
Department of Electrical Engineering
National Institute of Technology, Rourkela
Rourkela-769 008, Odisha, India.

Acknowledgment

I thank God for protecting me from what I thought, I wanted and blessing me with what I didn't know I needed.

I would like to acknowledge my gratitude to a number of people who have helped me in different ways for the successful completion of my thesis. I would like to express my sincerest gratitude to my guide Dr. Dipti Patra, Associate Professor, Department of Electrical Engineering, National Institute of Technology, Rourkela but for whose deft guidance this thesis would not have seen the light of the day. Her erudite scholarship, prudent observations, perceptive critical comments and painstaking efforts to improve the quality of my work, have been steering me in the proper direction of research, from beginning to end. Moreover, her profound patience and kind understanding have helped me to overcome the same particularly in difficult times, when the odd seemed invincible and insurmountable.

I am also grateful to Prof. R K Sahu, Director, N.I.T. Rourkela, for his inspiring words. I wish to place on record my thanks to our Ex-Director Prof. S. K. Sarangi for his motivated words and constant support towards research. I also show my sincere gratitude to Prof. J. K. Satapathy, HOD, Electrical Engineering, for his valuable comments, which helped me to complete my research work. I humbly acknowledge the creative criticism and constructive suggestions of Prof. Anup K. Panda (Chairman), Prof. Samit Ari, and Prof. Pankaj K. Sa, committee members, while scrutinizing my research work. My completion of this thesis could not have been accomplished without the support of Prof. Akrur Behera, Dept. of Mathematics.

I ventilate my deep sense of gratitude to Prof. Susmita Das and Prof. K.R.Subhashini for their learned advice and constant encouragement. I appreciate immensely the invaluable time lent to me by Dr. Sucheta Panda and sonologist Dr. Hemalata Satapathy for their long discussion about my research. I am also grateful to all the staff members and research scholars of the Department of Electrical Engineering for their co-operations and support throughout this period. I am thankful to Yogananda sir, Sushant sir, Prajna mam, Suvranshu, Sunil, Astik, Himanshu, Sushant, Lazarous, Umesh, Deepak, Achala, Sushree, and Rajashree for their co-operations throughout this period.

Finally, I owe my loving thanks to my parents, uncle, aunty, brothers, sisters, sister-in-laws, brother-in-laws, niece, and nephew. Without their encouragement, understanding and love it would have been impossible for me to finish this work.

Smita Pradhan

Abstract

Recent advances in medical imaging have resulted in the development of many imaging techniques that capture various aspects of the patients anatomy and metabolism. These are accomplished with image registration: the task of transforming images on a common anatomical coordinate space. Image registration is one of the important task for multi-modal brain images, which has paramount importance in clinical diagnosis, leads to treatment of brain diseases. In many other applications, image registration characterizes anatomical variability, to detect changes in disease state over time, and by mapping functional information into anatomical space. This thesis is focused to explore intensity-based registration techniques to accomplish precise information with accurate transformation for multi-modal brain images. In this view, we addressed mainly three important issues of image registration both in the rigid and non-rigid framework, i.e. i) information theoretic based similarity measure for alignment measurement, ii) free form deformation (FFD) based transformation, and iii) evolutionary technique based optimization of the cost function.

Mutual information (MI) is a widely used information theoretic similarity measure criterion for multi-modal brain image registration. MI only defines the quantitative aspects of information based on the probability of events. For justification of the information of events, qualitative aspect i.e. utility or saliency is a necessitate factor for consideration. In this work, a novel similarity measure is proposed, which incorporates the utility information into mutual information, known as Enhanced Mutual Information (EMI). It is found that the maximum information gain using EMI is higher as compared to that of other state of arts. The utility or saliency employed in EMI is a scale invariant parameter, and hence it may fail to register in case of projective and perspective transformations. To overcome this bottleneck, salient region (SR) based Enhance Mutual Information (SR-EMI) is proposed, a new similarity measure for robust and accurate registration. The proposed SR-EMI based registration technique is robust to register the multi-modal brain images at a faster rate with better alignment.

As the structural content of brain images are important during treatment planning, the rigid transformation based registration fails to capture local deformation of surfaces. Hence, non-rigid based registration is essential for brain image analysis, which can be performed on FFD-based transformation. In this transformation, the image grid is applied to find the deformed region of a brain. Though B-spline interpolation is popularly used for non-rigid transformation, it fails to register intra tissues of brain by property of its sensitivity to the distribution of intensity and the local deformations. To overcome this problem, penalized spline (P-spline) interpolation is introduced, but it increases the computation time. An adaptive P-spline (AP-spline) based interpolation

scheme is proposed, to reduce the computational burden, which interpolates only for the local deformation of the image grid rather than the whole image. The proposed AP-spline interpolation based registration is found to be more efficient than that of the P-spline and B-spline based registration approach.

As the functions of the similarity measure with respect to the transformation parameters are non-linear and non-convex, local optimization based method may not be appropriate to obtain the optimal solution of the parameters. For optimum transformation, an evolutionary based hybrid optimization technique is proposed using the notion of Bacterial Foraging Algorithm (BFA) and quantum-behaved particle swarm optimization (QPSO) method, named as bacterial foraging - quantum-behaved particle swarm optimization (BF-QPSO) algorithm. For global search, BF is adopted with a local search using QPSO in the step of chemotaxis. The proposed algorithm is found to be efficient regarding faster converge rate and less mean registration error as compared to PSO, QPSO, BFA and BF-PSO based registration algorithm.

All the proposed registration schemes are validated with simulated as well as real multi-modal brain images.

Keywords: Image registration, multi-modal images, mutual information, spline interpolation, evolutionary optimization techniques.

List of Acronyms

Acronym	Description
CT	Computed Tomography
PD	Proton Density
MRI	Magnetic Resonance Imaging
NMR	Nuclear Magnetic Resonance
PET	Positron Emission Tomography
SPECT	Single Photon Emission Computed Tomography
FMRI	Functional Magnetic Resonance Imaging
MI	Mutual Information
SMI	Spatial Mutual Information
NMI	Normalized Mutual Information
RMI	Regional Mutual Information
QMI	Qualitative-Quantitative Mutual Information
EMI	Enhanced Mutual Information
SM	Similarity Measure
PDF	Probability Density Function
SR	Salient Region
FFD	Free form Deformation
B-spline	Basis Spline
P-spline	Penalized Spline
NURBS	Non-uniform Rational B-spline
AP-spline	Adaptive Penalized Spline
PSO	Particle Swarm Optimization
QPSO	Quantum behaved Particle Swarm Optimization
BFA	Bactrial Foraging Algorithm
BF-PSO	Bactrial Foraging-Particle Swarm Optimization
BF-QPSO	Bactrial Foraging-Quantum behaved Particle Swarm Optimization
MRE	Mean Registration Error
TRE	Target Registration Error
PSNR	Peak Signal-to-Noise Ratio
NCC	Normalized Cross Correlation
MSE	Mean Squared Error
RMS	Root Mean Square
UQI	Universal Quality Index
SSIM	Structural Similarity Index Measure
CBI	Checker Board Image

Contents

Certificate i

Acknowledgement ii

Abstract iii

List of Acronyms v

List of Figures ix

List of Tables xiii

1 Introduction 1

1.1 Image Registration . . . 2

1.2 Classification of Image Registration Methods . . . 3

1.2.1 Registration bases . . . 3

1.2.2 Classification based on Image Dimensions . . . 3

1.2.3 Transformation based Image Registration . . . 4

1.2.4 Modalities . . . 4

1.3 Medical Image Registration . . . 5

1.3.1 Image Acquisition Artifacts . . . 6

1.3.2 Multi-modality Challenges . . . 7

1.3.3 Ill-Posedness . . . 7

1.3.4 Ambiguous Correspondences . . . 7

1.3.5 Computational Challenges . . . 8

1.4 Reviewed Literature . . . 8

1.5 Motivation . . . 10

1.6 Objectives of Thesis . . . 10

1.7 Thesis Contributions . . . 11

1.8 Organization of Thesis . . . 13

2 Image Registration using Mutual Information based Similarity Measure 16

2.1 Introduction . . . 17

2.2 Materials and Methods . . . 18

2.2.1 Intensity-based Image Registration . . . 18

2.2.2 Similarity Measures . . . 19
2.2.3 Information Theoretic based Similarity Measure . . . 20
2.3 Proposed Registration Framework . . . 27
2.3.1 Information Measure . . . 27
2.3.2 Proposed Similarity Measure: Enhanced Mutual Information . . . 28
2.3.3 Image Registration using Enhanced Mutual Information . . . 30
2.4 Simulation and Results . . . 31
2.4.1 Performance Evaluation Measures . . . 32
2.4.2 Registration Function . . . 33
2.4.3 Robustness of Registration Scheme . . . 44
2.5 Summary . . . 48

3 Image Registration using Affine Invariant Saliency based Similarity Measure 49
3.1 Introduction . . . 50
3.2 Materials and Methods . . . 51
3.2.1 Visual Saliency . . . 52
3.2.2 Scale Saliency . . . 53
3.3 Proposed Registration Framework . . . 55
3.3.1 Salient Region (SR) . . . 56
3.3.2 Proposed Affine Invariant Similarity Measure . . . 57
3.3.3 Image Registration using SR-EMI . . . 58
3.4 Simulation and Results . . . 59
3.4.1 MR T1, T2 and PD weighted image data set . . . 61
3.4.2 Pre and post operative brain MR image data set . . . 62
3.5 Summary . . . 68

4 Non-rigid Image Registration using Spline based Interpolation 69
4.1 Introduction . . . 70
4.2 Materials and Methods . . . 72
4.2.1 Transformation Model . . . 72
4.2.2 Free Form Deformation based Transformation . . . 72
4.2.3 Spline based Image Transformation . . . 73
4.2.4 Non-rigid Image Registration using B-spline Interpolation . . . 76
4.3 Proposed Registration Framework . . . 76
4.3.1 Smoothing Spline . . . 77
4.3.2 Proposed P-spline Interpolation based Image Registration . . . 78
4.3.3 Knot Selection . . . 78
4.3.4 Proposed Adaptive P-spline Interpolation based Image Registration 79
4.4 Simulation and Results . . . 80

4.4.1 MR image data set 81
4.4.2 Pre and post operative brain MR image data set 90
4.5 Summary 92

5 Hybrid Evolutionary Technique for Transformation Optimization 93
5.1 Introduction 94
5.2 Materials and Methods 95
5.2.1 Powell's Optimization Technique 95
5.2.2 Particle Swarm Optimization Algorithm 95
5.2.3 Quantum behaved Particle Swarm Optimization Algorithm 96
5.2.4 Bacterial Foraging Algorithm 98
5.3 Proposed Optimization Algorithm: Hybrid BF-QPSO 101
5.4 Simulation and Results 103
5.4.1 Axial MR T1 and deformed T1 image data set 104
5.4.2 Coronal MR T1 and deformed T1 image data set 109
5.4.3 Pre and post operative brain MR image data set 110
5.5 Summary 117

6 Conclusion and Future Scopes 118
6.1 Summary of the Work 118
6.2 Future Scope of Research 121

List of Figures

1.1 Image registration framework 3
1.2 Multi-modal brain Images 5
1.3 Thesis organization 14

2.1 Block diagram of intensity based image registration framework 19
2.2 Illustration of relationship between an image region with its neighborhoods and joint distribution 25
2.3 Block diagram of proposed image registration framework 30
2.4 (a) Reference image, (b) Floating image translated along x axis, (c) Paired image before registration, (d-h) Registered image and (i-m) Paired image after registration using NMI (Viola), SMI (Pluim), RMI (Russakoff), QMI (Luan) and EMI (proposed) scheme respectively for Case I 37
2.5 (a) Reference image, (b) Floating image translated along y axis, (c) Paired image before registration, (d-h) Registered image and (i-m) Paired image after registration using NMI (Viola), SMI (Pluim), RMI (Russakoff), QMI (Luan) and EMI (proposed) scheme respectively for Case II 38
2.6 (a) Reference image, (b) Floating image rotated about x axis, (c) Paired image before registration, (d-h) Registered image and (i-m) Paired image after registration using NMI (Viola), SMI (Pluim), RMI (Russakoff), QMI (Luan) and EMI (proposed) scheme respectively for Case III 39
2.7 (a) Reference image, (b) Floating image translated and rotated about x axis, (c) Paired image before registration, (d-h) Registered image and (i-m) Paired image after registration using NMI (Viola), SMI (Pluim), RMI (Russakoff), QMI (Luan) and EMI (proposed) scheme respectively for Case IV 40
2.8 (a) Reference image, (b) Scaled floating image, (c) Paired image before registration, (d-h) Registered image and (i-m) Paired image after registration using NMI (Viola), SMI (Pluim), RMI (Russakoff), QMI (Luan) and EMI (proposed) scheme respectively for Case V 41

2.9 Similarity measures with respect to geometrical transformation for Case III: using RMI (a) Rotation along x axis r_x, (b) Translation along x-axis t_x, (c) Translation along y-axis t_y; using SMI (d) Rotation about x axis r_x, (e) Translation along x-axis t_x (f) Translation along y-axis t_y; using QMI (g) Rotation about x axis r_x, (h) Translation along x-axis t_x, (i) Translation along y-axis t_y; using Proposed EMI (j) Rotation about x axis r_x, (k) Translation along x-axis t_x, (l) Translation along y-axis t_y . . 42
2.10 Similarity measures with respect to geometrical transformation for Case IV: using RMI (a) Rotation along x axis r_x, (b) Translation along x-axis t_x, (c) Translation along y-axis t_y; using SMI (d) Rotation about x axis r_x, (e) Translation along x-axis t_x, (f) Translation along y-axis t_y; using QMI (g) Rotation about x axis r_x (h) Translation along x-axis t_x (i) Translation along y-axis t_y; using Proposed EMI (j) Rotation about x axis r_x (k) translation along x-axis t_x (l) translation along y-axis t_y . . . 43
2.11 Percentage of successful registration for initial transformation with TRE values for Case III 45
2.12 Comparison of Similarity measures for Case III 45
2.13 Percentage of successful registration for initial transformation with TRE values for Case IV 46
2.14 Comparison of Similarity measures for Case IV 46

3.1 Example of visual saliency 51
3.2 Block diagram of proposed image registration scheme 55
3.3 Example of finding salient regions with ellipse 57
3.4 (a,c) PD image, Pre operative brain MR image respectively, and (b,d) Extracted salient regions with affine invariant saliency 58
3.5 (a,d,g,j,m) Input images, (b,e,h,k,h) Saliency using scale invariant saliency, and (c,f,i,l,o) Saliency using affine invariant saliency 60
3.6 (a) Reference image, (b) Floating image; CBI image after registration using SR-EMI, EMI and QMI based registration scheme respectively for transformation: (c-e) Rotated about x-axis, (f-h) Translated along x axis, and (i-k) Translated along y-axis for Case I 64
3.7 (a) Reference image, (b) Floating image; CBI image after registration using SR-EMI, EMI and QMI based registration scheme respectively for transformation: (c-e) Rotated about x-axis, (f-h) Translated along x axis and (i-k) Translated along y-axis for Case II 65

3.8 (a) Reference image, (b) Floating image, (c) CBI before registration, (d-f) Registered image, (g-i) CBI after registration, (j-l) Difference image after registration using SR-EMI, EMI and QMI based registration scheme respectively for Case IV 66
3.9 Comparison of SM value using proposed SR-EMI, proposed EMI and QMI based registration for all Cases 67
3.10 Comparison of MRE using proposed SR-EMI, proposed EMI and QMI based registration for all Cases 67

4.1 (a) Reference image grid, (b) Floating image grid, (c) Interpolation of transformed floating image to reference image 74
4.2 Block diagram of non-rigid image registration 77
4.3 (a) Reference image, (b) Floating image, (c) Difference image before registration, (d-g) Registered image using B-spline, P-spline, NURBs and AP-spline transformation, (h-k) Corresponding final transformed grid, (l-o) Difference image after registration for Case I 84
4.4 Convergence of different transformation method for Case I 85
4.5 RMS error curve for different transformation method for Case I 85
4.6 (a) Reference image, (b) Floating image, (c) Difference image before registration, (d-g) Registered image using B-spline, P-spline, NURBs and AP-spline transformation, (h-k) Corresponding final transformed grid, (l-o) Difference image after registration for Case II 86
4.7 Convergence of different transformation method for Case II 87
4.8 RMS error curve for different transformation method for Case II 87
4.9 (a) Reference image, (b) Floating image, (c) Difference image before registration, (d-g) Registered image using B-spline, P-spline, NURBs and AP-spline transformation, (h-k) Corresponding final transformed grid, (l-o) Difference image after registration for Case III 89
4.10 (a) Reference image, (b) Floating image, (c-f) Registered image using B-spline, P-spline, NURBs and AP-spline transformation, (g-j) Corresponding difference images, (k-n) Final transformed grid after registration for Case IV 91

5.1 Example of PSO 96
5.2 Flow chart of QPSO 97
5.3 Flow chart of proposed BF-QPSO 101

5.4 (a) Reference image, (b) Floating image, (c-e) Registered images using BFA, QPSO, BF-QPSO with AP-spline interpolation and SR-EMI similarity measure, (f-h) Corresponding difference images, (i-k) Final transformed grid respectively for Case I 106
5.5 RMS error for different optimization methods for Case I 107
5.6 SM value for different optimization methods for Case I 107
5.7 (a) Reference image, (b) Floating image, (c-e) Registered image using BFA, QPSO, BF-QPSO with AP-spline interpolation and SR-EMI similarity measure, (f-h) Corresponding difference images, (i-k) Final transformed grid respectively for Case II 108
5.8 (a) Reference image, (b) Floating image, (c) Paired image before registration, (d-f) Registered image using BFA, QPSO, BF-QPSO with AP-spline interpolation and SR-EMI similarity measure, (g-i) Final transformed grid, (j-l) Paired image after registration respectively for Case III 114
5.9 (a) Reference image, (b) Floating image, (c) Paired image before registration, (d-f) Registered image using BFA, QPSO, BF-QPSO with AP-spline interpolation and SR-EMI similarity measure, (g-i) Final transformed grid (j-l) Paired image after registration respectively for Case IV 115
5.10 RMS error for different optimization methods for Case IV 116
5.11 SM value for different optimization methods for Case IV 116

List of Tables

2.1 Performance Measures for all Cases 36
2.2 Comparison of rigid transformation parameters, and computational time for Case (I-IV) 44

3.1 Performance Measures for all Cases 62

4.1 Performance Measures for Case I 83
4.2 Performance Measures for Case II 88
4.3 Performance Measures for Case III 88
4.4 Performance Measures for Case IV 90

5.1 Performance Measures for Case I 109
5.2 Performance Measures for Case II 110
5.3 Performance Measures for Case III 111
5.4 Performance Measures for Case IV 112

Chapter 1

Introduction

In this chapter, we start with a general description of image registration from the perspective of its applications, followed by its classification with different criteria. The reason behind multi-modal brain image registration and the techniques developed towards rigid and non-rigid registrations are also described along with the literature review. The objectives of the thesis as well as a brief on thesis organization are included in this chapter.

1.1 Image Registration

Registration is an important task in image processing, where images are to be matched, captured from different sensors or different viewpoints at different times [1]. The goal of image registration is to find the optimal transformation that best aligns the structures of interest in the input images. It is a crucial step for image analysis in which valuable information is gained from the combination of various data sources like in image fusion, change detection, and multichannel image restoration [2]. Registration has potential applications in remote sensing (multispectral classification, environmental monitoring, change detection, image mosaicing, weather forecasting, creating super-resolution images, integrating information into geographic information systems (GIS)), in cartography (map updating), in computer vision (target localization, automatic quality control), in astrophotography, and most importantly in medicine (combining computer tomography (CT) and nuclear magnetic resonance (NMR) data to obtain more complete information about the patient, monitoring tumor growth, treatment verification, comparison of the patients data with anatomical atlases) etc.

Since information gained from two images acquired through different sensors are usually complementary in nature, alignment of useful data is often desired. Therefore, it is necessary to transform one image to align geometrically with the other one so that the difference between their spatial information can be easily observed. Image registration is used to align a pair of images in the same coordinate system in order to get comprehensive information from different acquired images. Out of two images in a pair, one image is considered as the reference image and the other one as the floating image, which is transformed to align geometrically with respect to the reference one. The image registration framework is shown in Fig. 1.1. It can be broadly divided into three tasks:

Similarity measure: The similarity measure helps in measuring the degree of alignment between reference and floating images. Generally, there are two kinds of similarity metric, namely, feature-based metric and intensity-based metric.

Transformation: A transformation is a mapping of locations of points in one image to new locations in another. The transformation applied to register the images depends on the degrees of freedom. It may be categorized as either rigid transformation (translation and rotation), or non-rigid transformation (affine, perspective, curve, etc.).

Optimization: The goal of the optimization step is to search for the maximum or minimum value of the similarity measure adopted. For the registration, the optimum of the cost function is assumed to correspond to the transformation that correctly register the input images.

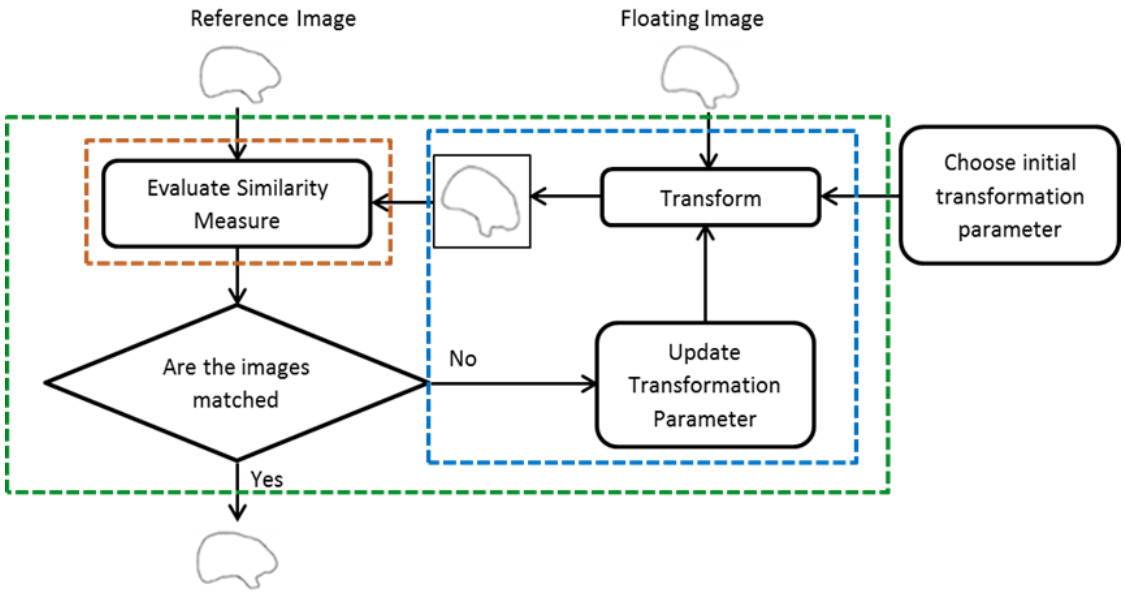

Figure 1.1: Image registration framework

1.2 Classification of Image Registration Methods

Image registration methods can be classified into various categories based on different aspects. A brief description is included in this section.

1.2.1 Registration bases

Image registration can be performed by extracting different information from input images. Based on the kind of information, it can be classified into landmark-based and intensity-based methods.

In **landmark-based** image registration, the choice of landmarks highly depends on the shape of the objects in images. Hence, corresponding feature location is a challenging task. Also, preprocessing of images, such as image segmentation, is often needed before the registration, which may affect the robustness of registration performance.

In **intensity-based** image registration, only intensity values of the images are used to perform the task. Although it requires more computation than landmark-based image registration, intensity-based image registration is considered more suitable for real time as it does not require the preprocessing step. Hence, in this thesis, we exclusively focus on intensity-based image registration.

1.2.2 Classification based on Image Dimensions

The dimensions of the reference and the floating images taken are assumed to be same, i.e. 2D-2D and 3D-3D image registration. The dimensions can also be different, for example, in 2D-3D image registration, the reference image is in two dimensions

and the floating image is in three dimensions. Registering those two images requires transforming the three-dimensional floating image, including mapping a 3D data volume onto a 2D image, to align with the 2D reference image.

1.2.3 Transformation based Image Registration

Image registration can be classified into rigid and non-rigid image registration according to the transformation type.

In **rigid image registration**, floating images are considered as rigid bodies, and only rotation and translation are included in the transformation parameter sets. For example, three degrees of freedom is considered when floating images are in two dimensions (rotation through one axis and translation in two dimensions), and six degrees of freedom is considered when floating images are in three dimensions (rotation through three axes and translation in three dimensions).

In **non-rigid image registration**, in addition to rigid transformations, deformable (e.g., affine, projective, curved, etc.) transformations are also considered, which requires comparatively more degrees of freedom than rigid-based image registration. Transform-based image registration mostly depends on the characteristics of objects in the image. If the attributes of objects indicate that corresponding objects are deformed (e.g., brain, livers), it is more suitable to perform non-rigid image registration. Though non-rigid image registration is essential, the computational complexity is high due to its high degrees of freedom. Rigid registration is usually performed first to align the images approximately and to reduce the computational complexity. Subsequently, non-rigid registration is employed to get more accurate alignment between the given two deformable objects. In this thesis, we focus on how to perform rigid and non-rigid image registrations efficiently and accurately.

1.2.4 Modalities

Image registration can also be classified into mono-modality and multi-modality depending on sources of input images. If the same sensor produces both the images with the same physical parameters, the kind of registration is called **mono-modality image registration**. In mono-modality image registration, the reference and the floating images have the same or similar intensity values when they are registered.

Multi-modality image registration refers to the case where the images are captured by different sensors or the same sensor with different physical parameters. Fig. 1.2 shows an example of various modalities of brain images such as MRI, angiography, CT, ultrasound, SPECT, and PET, etc. In multi-modal image registration, different sensors or different physical parameters result in different intensity values between the reference and the floating images.

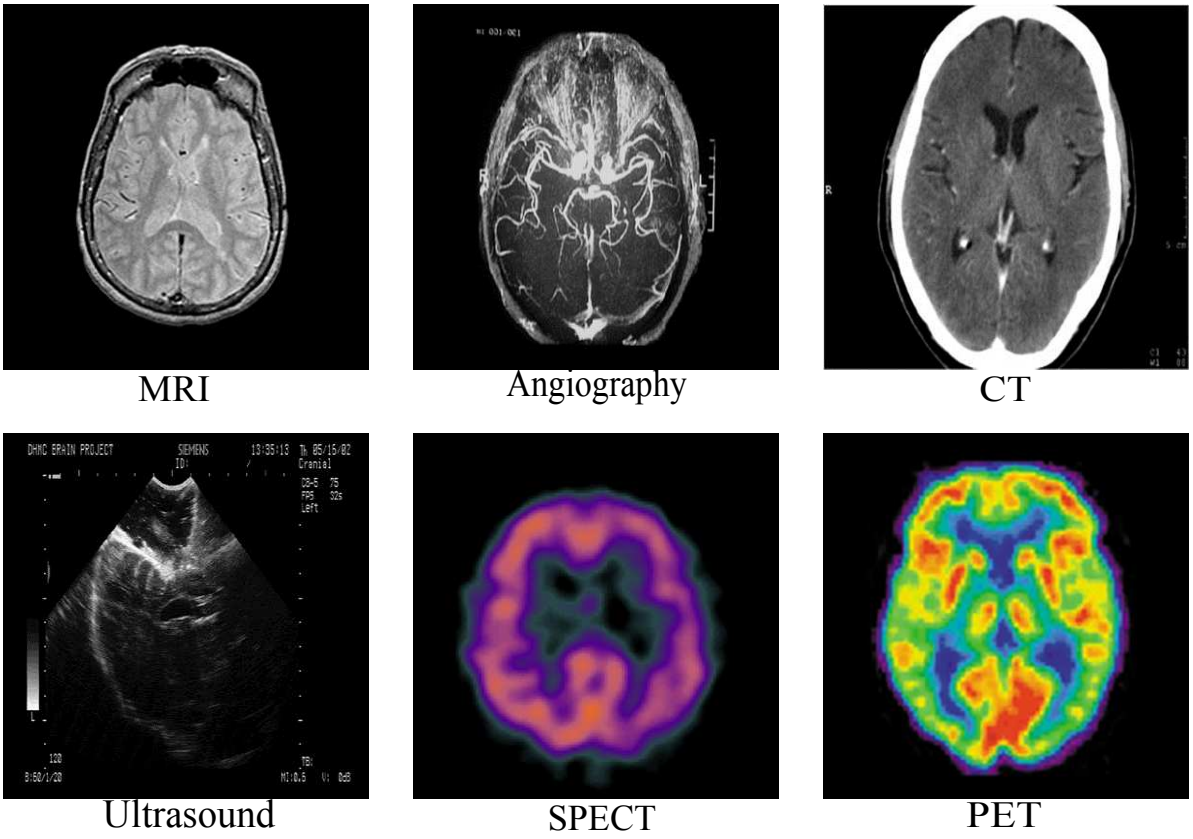

Figure 1.2: Multi-modal brain Images

1.3 Medical Image Registration

Image registration is essential for making the medical images more ready and more suitable to improve the quality of health-care service, and hence it is applicable widely in the areas including medical database management, medical image retrieval, telemedicine, and e-health. It also contributes significantly in computer-assisted surgery as well as intra-subject, inter-subject and inter-modality analysis, registration with atlases, quantification and qualification of feature, shapes and sizes, elastography, distortion compensation, motion detection and compensation, etc. [3].

Medical image registration has been extensively investigated, and a large number of software-based algorithms have been proposed alongside the developed hardware-based solutions (for instance, the combined PET/CT scanners). Among the comprehensive software-based registration, the feature-based techniques are more computationally efficient but require a preprocessing step to extract the features to be used in registration, which makes this category of registration user-intensive and user-dependent. The intensity-based scheme provides an automatic solution to avoid user interface in the registration process. However, this type of registration is computationally complex. Particularly, image registration is a data-driven and case-orientated research area. It is a challenging task to select the most suitable and usable technique for a

particular requirement of a data set captured from various imaging scanners. For instance, although maximization of MI has been recognized as one of the most robust registration methods, however it cannot always give an accurate solution for each class of registration. An automated and accurate registration is more desirable. The combined imaging devices such as PET/CT provide an expensive hardware-based solution. However, even this expensive registration method is also not suitable to provide the accurate registration, and thus software-based solution is required to fix the mean registration caused by patient motions between the imaging sessions. The rapid advances in imaging techniques raised more challenges in registration area to generate more accurate and efficient algorithms in a clinically acceptable time frame.

Diagnosis and prediction of brain disorders are easy due to development of imaging tools using computer techniques. Previously computed tomography was used for clinical applications. Nowadays other imaging techniques such as magnetic resonance imaging (MRI), positron emission tomography (PET), single photon emission computed tomography (SPECT), functional magnetic resonance imaging (fMRI) are more popular, used for radiotherapy and surgical procedure. These advanced techniques help physicians to detect the disease or unhealthy condition and diagnose exact and supplementary information about the location of a tumor in brain. Different modalities in brain imaging are utilized to characterize various aspects of the patient being imaged. Although this opens the possibility to fuse these different types of information, also poses significant challenges from an image registration point of view based on the following factors.

1.3.1 Image Acquisition Artifacts

Brain image acquisition techniques can produce artifacts, such as noise, motion artifacts and intensity inhomogeneities. As a consequence, image registration techniques must be designed to be as robust as possible to these type of image acquisition artifacts.

A Noise and Intensity Inhomogeneities

Noise is an inherent artifact in brain imaging. Even though the acquisition parameters of a scanner may be tuned to minimize these artifacts, they are seldom completely removed. Intensity inhomogeneities correspond to a variation in intensity as a result of spatial position. These changes in intensity can usually be modeled as a multiplicative bias field. This type of artifact is often produced by Magnetic Resonance (MR) scanners. The main causes for these artifacts to occur is due to inhomogeneities of the magnetic field of the scanner and the patient's position. These can hamper the robustness and accuracy of intensity-based registrations considerably since the intensity in the images is not spatially consistent.

B Motion Artifacts

The motion of patients inside the scanner may produce misalignment between acquisition slices, which is usually problematic for registration algorithms. Furthermore, natural motion such as cardiac or respiratory motion may also be troublesome.

1.3.2 Multi-modality Challenges

As brain images from different modalities are usually acquired with different scanners and thus at different points in time, the anatomical features of the images might have different spatial arrangements. Furthermore, different modalities show different anatomical or functional properties of the brain being imaged, which makes registration methods more challenging since the fusion is not clinically relevant if the images are not adequately aligned.

1.3.3 Ill-Posedness

As previously mentioned, image registration involves an optimization on a search space of a dimensionality that can be in the order of hundreds, if the transformation to be estimated is non-rigid. Non-rigid registration becomes an ill-posed problem in the Hadamard sense. Hadamard states three conditions for a problem to be well-posed: The existence of a solution, the uniqueness of a solution, and the continuous dependency of the solution on the initial conditions.

Non-rigid registration problems usually violate the last two conditions. As a consequence, regularization terms or models are needed to reduce the space of solutions as much as possible and obtain stable results. Even though a substantial amount of research on non-rigid registration of brain images has been devoted to different regularization models [4–8], it still remains an open problem that has to be taken into account when designing registration algorithms.

1.3.4 Ambiguous Correspondences

Ambiguous correspondences between two medical images arise when one of them depicts biological features not present in the other. For example, when registering a brain image of a healthy subject with a brain image of a subject with brain pathology, such as lesions or tumors. These ambiguous correspondences can be a challenging task for image registration, that can lead to perform unexpectedly in those areas. This is particularly the case for intensity-based registration approaches.

1.3.5 Computational Challenges

In medical image analysis, registration is required for the estimation of non-linear transformation of the images. For this, non-rigid registration is used, which is a time-consuming process, as 3D medical imaging acquisition techniques have higher number of voxels. This signifies the underlying non-rigid transformations may need to be defined by some parameters. There is a trade-off between accuracy and speed, where a compromise has to be made. This compromise tends to be application driven. For example, image-guided surgery usually requires real-time registrations, whereas computational anatomy or longitudinal studies can be performed during days or sometimes even weeks without compromising the clinical applicability of the outcomes.

1.4 Reviewed Literature

The different registration methodologies have been discussed with their advantages and drawbacks. 2D image registration has been developed by geometrical transformation of overlapped images of the different complexity of unimodal images [9]. A brief review of image registration methodologies in different application is presented in [10]. In the medical image analysis, image registration techniques are categorized into intensity or feature based. The main steps of intensity based registration are similarity measures, geometric transformations, optimization and accuracy assessment techniques [10, 11]. For multi-modal images, entropy, and mutual information have been used as matching criteria for clinical image alignment [12, 13].

Intensity-based image registration were used to optimize the transformation parameter by optimizing the similarity measure by automatic algorithms. For multi-modal image registration, mutual information has been used as similarity metric. But the registration accuracy depends on the metric value limits due to interpolation. Shekhar *et al.* investigated on deformed ultrasound volumes of thoracic and abdominal organs with different transformations based on mutual information measure [14]. Though maximization of mutual information (MI)-based objective function over a regular grid of splines results the better, the computational complexity depends on the compliance of the transformation of smaller structures in the image. Number of degrees of freedom in the transformation has to be reduced to speed up the technique [15]. To reduce the computational cost of the registration procedure, Andronache *et al.* mapped the intensity of small patches instead of MI measures [16]. Local neighborhood concept for distinctive structure of small patches has been introduced to calculate the similarity measure [17]. This method is extended to self-similarity weighted graph-based implementation of α-mutual information (α-MI) for non-rigid image registration by taking local structures. The (α-MI) measure was robust against signal non-stationarity

and intensity distortions and used SeSaMI as the similarity measure in a standardized cost function with B-spline deformation field to achieve non-rigid registration [18].

In medical imaging, interpolation is required for processing such as resampling and compression [19]. In the analysis of serial structural MRI data, mapping of local tissue pattern over time was a challenging task. Rueckert *et al.* has modeled the global and local motion of breast MRI using affine transformation followed by B-spline [20]. In 2006, they extended the free-form deformation model and they proposed diffeomorphic non-rigid registration algorithm [21]. Deformable image registration is an essential tool in medical image processing. The overview of deformable registration methods are presented in [22]. Splines are familiar to deal with interpolation and discretization problem. The applications of spline in image processing is reviewed in [23]. Applications of B-spline in image processing are discussed in [24, 25]. Zhuang *et al.* used a set of control points in FFD and proposed a weighted non-rigid registration scheme [26]. Khader *et al.* also presented a non-rigid image registration technique using cubic B-spline interpolation to model the deformation of floating image and matched with the reference image by minimizing the similarity measure optimized by quasi-Newton optimization technique [27]. As the basis functions of B-spline are smooth, the singularities in the deformation field can be avoided by the regularization of the function. To enforce the local invertibility, sometimes the B-spline bases are penalized with conventional Jacobian penalty in the grid points. Chun *et al.* incorporated simple penalty approach into non-rigid image registration techniques [28]. For estimation of the forward and inverse transformation of an image, another intensity-based similarity metric has been proposed, which reduces the negative effects of outliers [29].

Though B-spline are fascinating for nonparametric modeling, it is complicated to find the optimal number of position of knots, which permits restricted controls over smoothness. To overcome this problem penalty has been added to B-splines with a large number of knots [30]. Deformable image registration is an important tool that combines the multi-modal image datasets for analysis of motion detection and compensation. The popular DIR algorithms models the displacement vector field with local shape control is B-spline. Jacobson *et al.* presented two-dimensional deformable image registration scheme for CT images and extended it to automatic non-uniform scheme with a comparison to uniform schemes [31]. To visualize the brain surfaces of male and female, Rajapakse *et al.* used Non-Uniform Rational B-Splines (NURBS) [32]. NURBs provides an alternative to FFD-based on B-spline with more flexibility and accuracy. It is extended to 3D images and simulated with real images to avoid the local minima with improved performance [33]. Lahmiri *et al.* classified the healthy brain from Alzheimer's disease or mild cognitive impairment using SVM [34].

For the optimization of similarity measure, local methods or global methods can

be used. Local methods such as steepest descent gradient, Powell's direction set usually trap in the local optimum and result mean-registration error. So, estimation of good initial transformation parameters are necessary. Simulated annealing (SA), genetic algorithm (GA) and particle swarm optimization (PSO) are some popular global optimization techniques used in image registration [35, 36]. Though GA is a powerful method for global optimization, it requires high computation time and lacks the fine tuning capability. Costin *et al.* described about the Bio-Inspired Optimization Strategy for medical image registration [37].

1.5 Motivation

In intensity based registration methods, images from different modalities display complementary information about the object in images with different intensity maps. Therefore, similarity measures used for multi-modal image registration must be insensitive to differing intensity maps. The information theoretic approach inspires us for the development of enhanced (new) similarity measure for addressing intensity based rigid image registration of the brain. Unfortunately, all types of image misalignment can not be solved by rigid image registration. Hence, non-rigid transformations are usually considered to account for image deformations. For that, registration using non-rigid transforms remains a challenging task. These methods vary in their robustness, complexity, and sophistication. Also, the registration process is complicated as there may be mean registration error. Fast and accurate, automated, intensity-based medical image registration is of great utility to clinicians and researchers. However, the high computational demand of registration can lead to prohibitively lengthy execution times in imaging workflows. For instance, registration must be performed within minutes for applications in intra-operative imaging and image-guided surgery, so as not to delay procedures. Also, brain atlas creation and clinical studies often require the accurate and reliable registration of hundreds or thousands of image pairs. To date, the enormous computational requirements of registration methods have largely precluded their use at interactive or near real-time speeds on desktop computers. In order to become an accepted tool in day-to-day practice, registration algorithms must be designed to execute and generate accurate results within the acceptable time.

1.6 Objectives of Thesis

In this thesis, image registration of multi-modal brain images has been considered in the intensity domain. The registration is addressed both in the rigid and non-rigid framework. The thesis is focused on the development of efficient registration methods which could register multi-modal brain images accurately with less computation time.

For evaluation, multi-modal images are taken, such as Computed Tomography (CT), Magnetic Resonance Imaging (MRI)-T1 weighted, T2 weighted, and PD, etc. Also, the frontal, sagittal and axial images along with pre and post-operative medical images are considered for image registration in both rigid and non-rigid framework. The objectives of this thesis are as follows:

- Proposition of information theoretic based similarity measure to attain the qualitative and quantitative information for efficient registration of brain images.
- Development of advanced registration schemes using both scale and affine invariant saliency measure incorporated in similarity measure.
- Development of fast and accurate FFD-based transformation method for addressing non-rigid registration of multi-modal brain images.
- Development of efficient optimization technique for transformation associated with cost function to obtain the maximum similarity measure.
- Performance analysis of proposed methods and validation with multi-modal brain image data.

1.7 Thesis Contributions

This dissertation aims at developing advanced registration methodologies for medical images, and specifically for brain images. The registration problem is addressed both in the rigid and non-rigid framework using the intensity-based approach. The chapter-wise contributions of the thesis are summarized as follows:

- **Chapter 2:** In this chapter, the thesis aims at developing an information theoretic based novel similarity measure for brain image registration in intensity-based rigid transformation framework. In this work, mutual information-based similarity measure is employed for alignment measurement. The qualitative information is incorporated through the utility factor or saliency, using which, a new weighted information measure is proposed named as Enhanced Mutual Information (EMI). The information gain using EMI is compared with that of existing qualitative-quantitative mutual information (QMI) [38]. It is mathematically proved that, the maximum information is gained in case of EMI as compared to QMI.
- The proposed EMI takes care of both qualitative and quantitative measure of relative information. A new registration algorithm is proposed based on EMI, and the performance of the same is analyzed for multi-modal rigid registration of brain images. It is found that, the performance of the proposed scheme is better than

that of other state of arts. The algorithm is validated with simulated as well as real brain MR images considering rigid transformation, i.e. translation, rotation, and scaling.

- **Chapter 3:** In the previous chapter, the utility or saliency used in similarity measure is a scale invariant weighting factor. Due to this, EMI based registration method may fail to register properly in case of affine transformation. An attempt has been made to overcome this difficulty, by incorporating an affine invariant saliency into the similarity measure, which is invariant to the projective and perspective transformation. In addition to it, the saliency is computed on all pixels of the image which adds computational burden. Therefore, using affine invariant salient region (SR), a new information measure is proposed named as Salient Region Enhanced Mutual Information (SR-EMI). The gained information through SR-EMI in the proposed registration scheme could register the images efficiently as compared to EMI based registration scheme. The performance analysis shows that the SR-EMI based registration algorithm outperforms the similar existing algorithms regarding mean registration error and other performance criteria.

- **Chapter 4:** Though the incorporation of salient region as saliency enhances the similarity measure, it suffers when the images are geometrically deformed. For example, the radiological analysis of soft tissue of the brain with some abnormal cells is a challenging task in rigid registration process. Effort has been made to overcome these challenges with the development of an efficient non-rigid transformation scheme for image registration. In this chapter, the registration problem is formulated in non-rigid framework and spline based interpolation has been performed for non-rigid transformation. B-spline based interpolation scheme fails to reform the local deformations that are present in the soft tissues of brain images. Hence, Penalized spline (P-spline) is incorporated by penalizing the image grid with a regularization term. This regularization term helps in smoothing the deformed image grid. It is found that P-spline interpolation based registration method outperforms the B-spline interpolation based registration method.

- The computation time in case of P-spline interpolation is more due to the penalty term at each grid point of the whole image. In order to reduce the computational burden, an adaptive P-spline (AP-spline) based interpolation method is proposed, where the penalty term is adaptively weighted, and only takes care of the locally deformed grid of the floating image instead of the whole image grid. The proposed AP-spline interpolation based registration algorithm is successfully validated with geometrically distorted brain images as well as pre and post-operative brain images. The comparison analysis of convergence rate and RMS error shows the

efficacy of the proposed P-spline and AP-spline interpolation based registration methods. The convergence rate is found to be faster, and the RMS error is found to be least in case of the proposed AP-spline method as compared to other state-of-art methods.

- **Chapter 5:** Optimization of cost function is a crucial step in image registration. The cost function is the similarity measure, which consists of a number of degrees of freedom of the transformation, is to be optimized for proper registration. The choice of initial transformation is a challenging task to get an optimum parameter. Hence, the solution is adoption of nature-inspired optimization techniques. In this chapter, the registration problem is formulated for both rigid and non-rigid transformation. Due to large number of degrees of freedom in non-rigid registration, Powell's optimization technique fails to converge properly. A hybrid evolutionary based optimization technique is proposed using the notion of both bacterial foraging (BF) and quantum-behaved particle swarm optimization method (QPSO). For a global search, BF is adopted with a local search using QPSO in the step of chemotaxis for faster convergence and to reduce the computation time. The proposed BF-QPSO optimization algorithm could be successfully validated with non-rigid brain images. The performance measure of the proposed scheme outperforms the other existing state-of-arts. The performance of proposed hybrid BF-QPSO optimization technique is found to be better than other existing evolutionary based optimization techniques, such as PSO, BFA, QPSO, BF-PSO, etc.

1.8 Organization of Thesis

The thesis is organized into the following chapters. An overview of the chapter organization is shown in Fig. 1.3.

Chapter 1: Introduction

This chapter deals with formal description of the image registration process, its classification based on various criteria, a brief literature on medical image registration with an emphasis to the brain images. The thesis objectives, research contributions as well as chapter organization are also included here.

Chapter 2: Image Registration using Mutual Information based Similarity Measure

This chapter deals with information theoretic based similarity measure used for rigid registration followed by detailed description of the existing state-of-arts. A

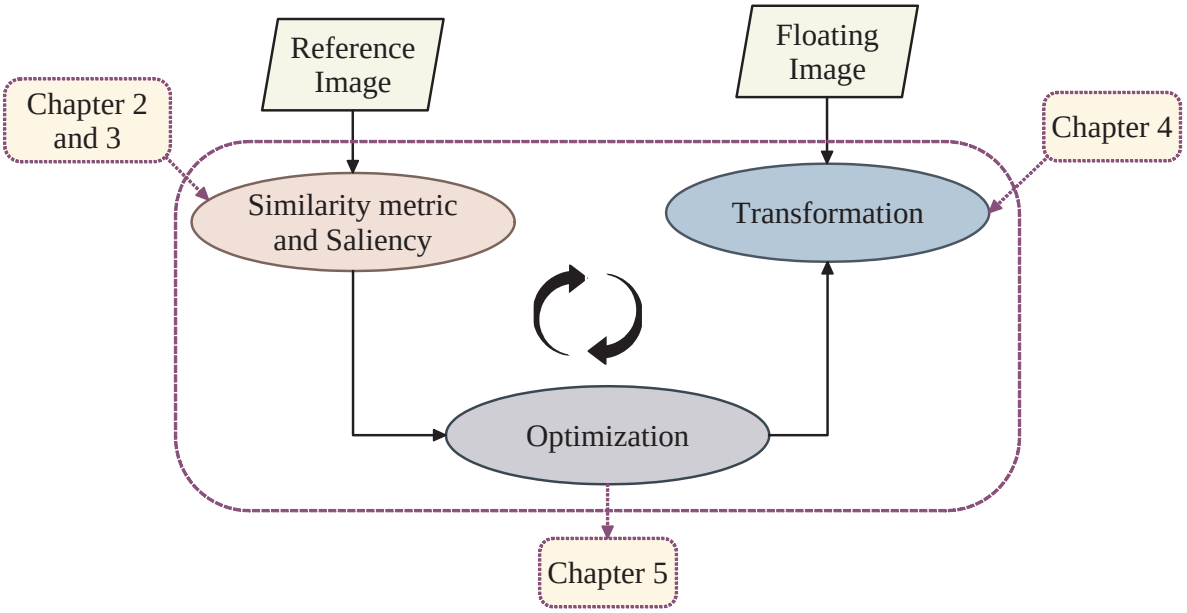

Figure 1.3: Thesis organization

new similarity measure is proposed named as Enhanced Mutual Information (EMI), exhibiting the relative information of both images. Both qualitative and quantitative information is incorporated into mutual information using the utility factor or saliency. The performance of the proposed similarity measure is compared with other existing similarity measures. An algorithm is designed for the registration scheme using EMI as similarity measure. Simulation and results are presented for simulated as well as real brain images with rigid transformations.

The maximum information obtained through proposed similarity measure EMI for registration is described in the **APPENDIX A**.

Chapter 3: Image Registration using Affine Invariant Saliency-based Similarity Measure

In this chapter, affine transformation based similarity measure is proposed. Affine invariant salient region is incorporated into the saliency for formulating EMI based registration scheme. The proposed SR-EMI algorithm is validated with CT and MR image data sets. The performance analysis is also included for exhibiting the efficiency of proposed registration method.

Chapter 4: Nonrigid Image Registration using Spline based Interpolation

In this chapter, we present the non-rigid registration of deformed floating image with respect to the reference image. P-spline based interpolation method is proposed to reform the image grid of the deformed floating image properly, by using a penalty

term to the B-spline bases during registration. An adaptive P-spline (AP-spline) based interpolation methods is also proposed to reduce the computation burden by penalizing the local deformed grid adaptively. The proposed algorithm is validated with inter and intra operative brain MR image data set. The performance analysis of the proposed non-rigid registration method is also presented.

Chapter 5: Hybrid Evolutionary Technique for Transformation Optimization

In this chapter, the local and global optimization technique for similarity measure within a given class of geometric, affine, and non-rigid transformations are studied. To find the optimum transformation parameters, for more accurate mapping hybridized evolutionary technique BF-QPSO is proposed. The proposed optimization algorithm is validated with both rigid and non-rigid image data sets.

Chapter 6: Conclusion and Future Scopes

Conclusions drawn on various issues are presented in this chapter and the scope for future work is also outlined here.

Chapter 2

Image Registration using Mutual Information based Similarity Measure

This chapter describes about registration of brain images of different modalities achieved by the maximization of suitable information theoretic similarity measures within a given class of geometric transformations. The thrust of this chapter is that many of the existing methods for multi-modal registration that use mutual information is extended to more accurate intensity-based similarity measures incorporating the spatial information. To this end, we perform a computation of the variations of a hierarchy of information theoretic measures. The proposed method extends to the case of spatially computed similarity measures for brain image registration.

2.1 Introduction

The problem of establishing correspondences between two or more images is fundamental in computer vision, which is one of the building blocks for some challenging problems such as template matching, 3D reconstruction, camera motion estimation and camera calibration. When images have been acquired through similar sensors, they can be realigned by a direct comparison of their intensities. The registration algorithms that mainly look for the geometric transformation between two images which optimizes the similarity measure between their intensity values. There are several situations in which the hypothesis of the invariance of the intensity is no longer valid. One may consider for instance varying illumination conditions, or sensors with different spectral sensitivities. The same situation is encountered in brain imaging, where several acquisition modalities must be realigned to allow for an accurate fusion of complementary information and cover both structural and functional aspects of the anatomically studied form. Today, to locate a tumor, to plan a surgical act or to understand a physiological process, physicians use information acquired with different modalities. CT scanner provides structural information whereas SPECT or MRI or FMRI give functional information. The combination of different image modalities facilitates much greater understanding of the underlying condition of the brain, resulting in improved patient care.

The focus of this chapter is the registration of spatial information, which requires spatial alignment of the involved images. The images must be aligned geometrically and must represent the same anatomical form. Several intensity-based similarity measures have already been used for this purpose. The traditional cross correlation and the sum of squared difference based methods fail to register properly [39]. Mutual information overcomes the problems and has been popularly used in last decades [12, 40, 41]. For multi-modal images, entropy, relative entropy, and mutual information have been used as matching criteria for clinical image alignment [13]. Pluim *et al.* presented literature on mutual information based medical image registration [41]. Wells *et al.* proved the robustness of mutual information as compared to the traditional correlation where the edge or gradient-magnitude based method fails to register accurately [39]. In [42], Pluim *et al.* included spatial information to develop rigid and affine unimodality image registration.

During brain image acquisitions, the contrast tissue changes locally sometimes due to neurodegeneration procedure, which modifies the tissue volume integrity. In such cases, the MI fails to map. Also, MI is time-consuming due to joint histogram computation. So, Viola *et al.* proposed Parzen window kernel density estimation to evaluate the joint probability distribution between the probability masses [40]. In [43,44], a novel extension of MI was proposed considering the regions of corresponding pixels to provide faster

and significant reduction in errors. A new similarity metric combining the anatomical features along with intensity distribution has been presented for automated MRI/ SPECT image registration in [45]. Loeckx *et al.* proposed a novel similarity measure for non-rigid image registration. They estimated the 3D joint histogram considering image intensities of input images with a given spatial distribution [4]. However, all these matching criteria are found to be time-consuming as well as lack the qualitative information of images. Luan *et al.* incorporated the qualitative information into the measure of mutual information, and proposed a quantitative-qualitative measure of information (QMI) in [38]. In this chapter, an attempt has been made to propose a new mutual information-based similarity measure with more qualitative information along with quantitative information of the images which could register the brain images with better accuracy.

The main contribution in this chapter is the proposition of a new information theoretic based efficient similarity measure named as Enhanced Mutual Information (EMI), for the brain image registration in rigid registration framework (translation, rotation and scaling). The relative information signifies qualitative and quantitative information of the mutual information. The performance of the proposed approach relies on mean registration error.

The rest of the chapter is organized as follows. Section 2.2 describe basic concept of intensity based registration, similarity measure. All the information theoretic based similarity measures are described in this chapter. The formulation and justification of proposed similarity measure are explained in Section 2.3. Section 2.4 presents the performance analysis with experimental results of proposed method and those in existing literature [13], [42], [43] and [38]. Finally, the summary is drawn in Section 2.5.

2.2 Materials and Methods

This section describes the details about intensity based registration framework, different similarity measures such as statistical, information theoretic and spatial dependency measures.

2.2.1 Intensity-based Image Registration

Registration methodologies based on voxel intensity are commonly known as intensity-based. As the method does not utilize segmentation, feature detection, intensive user interaction, can be achieved fully automatic. In this framework, a similarity measure is defined by transformation of raw image content and is used as a criterion for optimal registration. Several well established intensity-based similarity measures have been used in the biomedical image registration domain [46–48]. The block diagram of this registration framework is shown in Fig. 2.1. The components of the same are as follows:

- The spatial mapping of intensities throughout the alignment process is achieved with a transform component.
- An interpolation component is used to evaluate intensities at non-discrete locations. The similarity metric component calculates a measure of alignment accuracy.
- Optimization of the similarity measure within a search space defined by transform parameters is achieved with an optimization component.

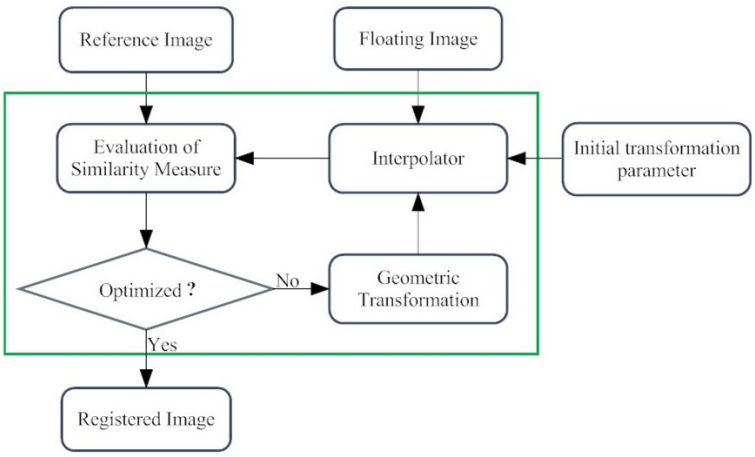

Figure 2.1: Block diagram of intensity based image registration framework

2.2.2 Similarity Measures

The similarity measure is a significant task in intensity-based image registration. The purpose of an image similarity metric is to quantify how well a given transformation aligns two images. It serves as a cost function to be maximized or minimized (depending on the metric) to achieve accurate alignment. For intensity based registrations, these parameters are generally calculated from all overlapping pixels in aligned images. There are some possible metrics to use, each of which is suited to a different type of registration problem.

The registration problem is expressed in terms of similarity measure associated with transformation parameters as

$$t^* = arg \quad \max_t(SM(R(x), F(T_t(x))) \tag{2.1}$$

where T_t is the transformation with parameter t, t^* is the optimum or final transformed parameter, SM is the similarity measure, R is the reference image, F is the floating image and x is the associated pixel value of the images.

Intensity-based similarity measures are categorized into three groups: statistical measures i.e. calculation of intensity difference of same contrast images, information theoretic measures that focus on the entropy of an image, and spatial dependency measure where neighboring pixels/voxels are taken into account.

The statistical measure used for image registration are cross correlation (CC), and sum of squared difference (SSD). Many researchers successfully employed the cross-correlation of intensities as a similarity measure for image registration [49–51]. It is used to register translated images with only slight rotations and scalings. It has been also used for alignment of X-ray images and biomedical volume data by Russakoff *et al.* [46]. The basic cross-correlation of intensities of both input images is computed as:

$$CC(R,F) = \frac{\sum_{x=1}^{I}\sum_{y=1}^{J} R(x,y)F(x-u,y-v)}{\left[\sum_{x=1}^{I}\sum_{y=1}^{J} |F^2(x-u,y-v)|\right]^{\frac{1}{2}}} \tag{2.2}$$

where R and F are reference and floating image, I and J are the number of pixel rows and columns, x and y are discrete pixel coordinates, while u and v represent the components of transformation respectively. Although popular, correlation-based metrics are sensitive to the presence of outliers and are limited to the alignment of images from the same modality and affine transformation. Also the computational cost is unmanageable with higher degree of transformations.

Another similarity measure based on the intensity difference is the sum of squared differences (SSD). Hajnal *et al.* and Woods *et al.* have successfully computed the SSD metric as a similarity measure with identical intensities of corresponding structures of reference and floating image [52, 53]. The lower value of SSD signifies the better alignment of floating image F with respect to the reference image R. SSD is evaluated as

$$SSD(R,F) = \frac{1}{N}\sum_{x_R \in \Omega_{RF}} \mid R(x_r) - F(T(x_f)) \mid^2 \tag{2.3}$$

where x_r, x_f are the pixel positions and Ω_{RF} is the overlapping domain of R and F.

These methods are based on the proposition of independence and stationarity of the intensities from pixel to pixel. Information theoretic based similarity measures overcome the problems associated with SSD. For last two decades, mutual information (MI) has been the accustomed similarity measure for brain image registration [41].

2.2.3 Information Theoretic based Similarity Measure

A Mutual Information

According to information theory, the concept of mutual information (MI) between two variables is to measure the amount of information that one variable contains about

the other. Mutual information makes few assumptions regarding the relationships that exist between two images, i.e. statistical dependence. It determines the uncertainty of one of the images when the other one is known. It was independently computed for mono-modal and multi-modal brain image registration by the researchers [12, 39, 40]. By maximizing MI, the marginal entropies becomes higher with a lower joint entropy. The popular interpretation of MI is based on the dispersion of the joint histogram, i.e. the less dispersed the joint histogram, the better the two images are registered.

Entropy is a measure of dispersion of a probability distribution. For uniform distribution, entropy becomes maximum. It is computed by estimating the probability distribution of image intensities. The joint probability distribution is estimated by the normalized joint histogram of the gray values. Shannon measure of entropy is popular in information theory. The Shannon entropy of a discrete distribution is invariant to rotation and translations, which makes the problem tractable [54].

Let $R = r_1, r_2, r_3, ...r_N$, $r_n > 0, \sum_{n=1}^{N} r_n = 1$ be a discrete probability distribution. Then Shanon's entropy is given by

$$H(R) = -\sum_{n=1}^{N} r_n log r_n \tag{2.4}$$

Considering R as the probability distribution of a set of N number of events with the predicted probability distribution on the basis of experiment $F = f_1, f_2, f_3, ...f_N$, $f_n > 0, \sum_{n=1}^{N} f_n = 1$, then Kullback's measure of relative information is given by

$$D\,(R/F) = -\sum_{n=1}^{N} r_n log \frac{r_n}{f_n} \tag{2.5}$$

Considering R and F be the reference image and floating image with pixel intensities r and f respectively, the associated joint probability distribution function is $p(r, f)$. The marginal probability distribution functions are $p(r)$ and $p(f)$, which can be thought of as the projection of the joint PDF onto the axes corresponding to intensities in image R and F respectively. The marginal entropies $H(R)$ & $H(F)$ vary during the registration process and is defined as

$$\begin{aligned} H(R) &= -\sum_{r} p(r) log p(r) \\ H(F) &= -\sum_{f} p(f) log P(f) \end{aligned} \tag{2.6}$$

The joint entropy $H(R, F)$ is defined as

$$H(R, F) = -\sum_{r,f} p(r, f) log p(r, f) \tag{2.7}$$

According to the information theory, mutual information (MI) is related to the

entropies as follows:

$$\begin{aligned} MI(R,F) &= H(R) + H(F) - H(R,F) \\ &= \sum_{r \epsilon R} \sum_{f \epsilon F} p(r,f) log \frac{p(r,f)}{p(r)p(f)} \end{aligned} \tag{2.8}$$

The above mutual information related variables are considered throughout the thesis.

Steps of mutual information based registration algorithm are described as follows:

1. Initialize the parameters for transformation of floating image.
2. Compute marginal entropies and joint entropy of reference and floating image using Equations 2.6 and 2.7.
3. Compute mutual information (MI) using Equation 2.8.
4. Apply geometric transformation to floating image F.
5. Evaluate new mutual information of transformed floating image and reference image, MI_{new}.
6. **If** $\varepsilon = MI_{new} - MI \leq 0.01$,
   then the image is registered with optimum transformation parameters,
   else go to Step 2 and repeat.

Viola *et al.* applied an information theoretic approach to find the pose of an object in an image [40]. He experimented on MR and CT image to align the 3D object model to real scenes by maximizing the mutual information. MI has gained popularity in multi-modal image registration [12]. But, the registration function using MI is ill-defined due to local maxima that occur for various reasons, i.e. low resolution of images, less information content, a small region of overlap or interpolation method, etc. To overcome the sensitivity of MI to the above factors, Studhlome *et al.* introduces Normalized Mutual Information (NMI) [13].

B Density Function Estimation

Step 2 of the MI-based registration algorithm as described earlier is to compute the entropy, i.e. registration of an image using the density function. However, in a typical registration problem, direct access to the probability density information is not available and hence they have to be estimated from the image data. There are several techniques available to estimate the density function, such as: histogram approach [12] and Parzen window approach [40].

B.1 Histogram Approach

Histogram based density function estimation is presented by Collignon *et al.* [55]. It calculates the density function using the equation:

$$p\left(r,f\right)=\frac{1}{N}h\left(x,y\right) \tag{2.9}$$

where N is the number of samples. x and y are the associated pixel intensities of reference and floating image. It is used to calculate the mutual information as presented in Equation 2.8. Joint intensity histogram is obtained by binning the intensity pair (r, f) of the overlapping parts of the reference image R and floating image F. Then, the joint floating probability $p(r, f)$ is estimated by normalizing the joint intensity histogram.

B.2 Parzen Window approach

Emanuel Parzen invented this approach, which is widely applied to pattern recognition, classification, image registration, tracking, image segmentation and image restoration [56]. Parzen window (PW) density estimation is essentially a data interpolation technique. With a given instance of the random sample $\mathbf{x}$, parzen windowing estimates the probability density function (PDF), from which the sample is derived. It essentially superposes kernel functions placed at each observation, so that each observation x_i contributes to the PDF estimate [56]. PW based density estimation was successfully applied for image registration [35].

Let w be a function with unit integral $\int_{-\infty}^{\infty} w(\zeta)d\zeta = 1$. Let x_i be a set of samples of a random variable X with PDF $p(x)$. Then, the Parzen estimation of p is

$$p_{N(x)}=\frac{1}{N}\sum_{i=1}^{N}\frac{w((x-x_i)/\gamma(N)}{\gamma(N)} \tag{2.10}$$

where γ is the scaling factor, which controls the Parzen window width w. Using Equation 2.10, the joint discrete Parzen histogram is defined as

$$h(x,y;\mu)=\frac{1}{\gamma_r\gamma_f}\sum_{x_i\epsilon\Omega}w(x/\gamma_r-F(T(x_i;\mu))/\gamma_r).w(y/\gamma_f-R(x_i)/\gamma_f) \tag{2.11}$$

where $x\epsilon X_R$, $y\epsilon X_F$ and γ_r, γ_f are corresponding scaling factor of X_R, X_F respectively. X_R and X_F are discrete set of intensities associated to reference image R and floating image F respectively. $T(x;\mu)$ is the geometric transformation associated with parameter μ. The discrete Parzen probability becomes,

$$p(x,y;\mu)=\rho(\mu).h(x,y;\mu) \tag{2.12}$$

where $\rho(\mu)$ is the normalization factor.

C Normalized Mutual Information

The registration accuracy depends on the optimization of the similarity measure. The mutual information is assumed to be maximum with proper alignment of floating image with respect to the reference image R. Despite an increasing MI value, the quality of registration falls due to overlap regions of the pixels of R and F. To overcome this dependence on volume of overlap, normalization of the combined information in the overlapping region has been considered and Normalized Mutual Information (NMI) in [13] by Studholme *et al.*, which is represented by

$$NMI(R,F) = \frac{H(R) + H(F)}{H(R,F)} \tag{2.13}$$

Though NMI solved the problem of the overlapping region occurred in MI but fails to take care of the ignored neighborhood pixels of the gray values, that are dependent on each other. Russakoff *et al.* introduced the regional information as spatial information and proposed a new variation of mutual information [43].

D Regional Mutual Information

The estimation of the probability density is the crucial step in normalized mutual information. The method only considers the image content in histogram excluding any spatial information such as anatomical structure, which hampers the registration quality in the presence of outliers or artifacts. According to Viola *et al.*, maximization of mutual information between two images find the complex overlapping regions by maximizing individual entropies and minimizing the joint entropy [39]. NMI does not take the geometry into account as it considers only pixel values instead of pixel positions. An extension of MI is done considering neighborhood regions of corresponding pixels for utilization of spatial information named as Regional Mutual Information (RMI) [43]. RMI is equivalent to projecting the data onto each of the axes of the new, uncorrelated basis and summing up the entropies. Here, each pixel along with its neighboring pixel constitutes a block. Then for each block marginal probabilities and joint distributions were calculated. The joint distribution is formed by extracting the spatial feature information and transformed to a decorrelated space. The spatial and intensity estimations were calculated by mean and covariance matrix of the image. Considering a pixel with (3×3) neighborhood gives 9D histogram for marginal probabilities and 18D histogram for joint distribution. A $(d \times N)$ matrix is formed by making a d dimensional vector of the joint distribution, where $d = 2(2r+1)^2$, r is specified square radius, $N = (m-2r)(n-2r)$ and $(m \times n)$ is size of image. Here, N represents the number of points distributed in d dimensional space.

The entropy of normally distributed set of points in $\Re^d$ with covariance matrix Σ_d

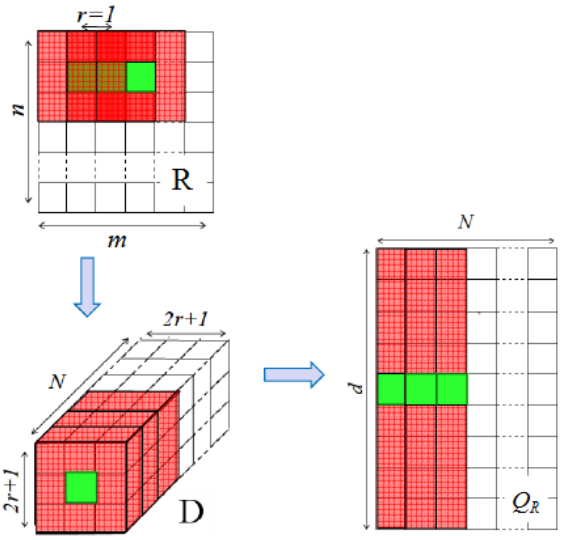

Figure 2.2: Illustration of relationship between an image region with its neighborhoods and joint distribution

is

$$H_s\left(\Sigma_d\right) = log\left((2\pi e)^{\frac{d}{2}}\, det\left(\Sigma_d\right)^{\frac{1}{2}}\right) \tag{2.14}$$

RMI is calculated by estimating the marginal entropies and the joint entropy as follows:

$$RMI(R,F) = H_s(\Sigma_R) + H_s(\Sigma_F) - H_s(\Sigma_{R,F}) \tag{2.15}$$

Extensions of RMI have been proposed for brain image registration to assess the quality [44, 57]. Though RMI is more efficient and robust than traditional MI and NMI, the computational cost due to high-dimensional joint distribution is more. Hence, several weighted information has been introduced as spatial information into MI [42].

E Spatial Mutual Information

The different imaging techniques do not depict the same tissue transition in both of the images. Image locations with a high gradient are assumed to express a change of tissues, with high information value. Many researchers applied the gradient information in the registration problem [58, 59]. As gradient information plays a dramatical role for better performance, calculation of gradient is necessary. The spatial information is incorporated by applying mutual information to gradient images. The registration function would probably have a narrow attraction range, and a lot of information from the gray value of images will be discarded with this. Therefore, a combination of mutual information along with gradient information is evaluated as the similarity measure [42]. Gradient-based similarity measure is also known as spatial mutual information and is calculated by

$$SMI(R,F) = G(R,F) * MI(R,F) \tag{2.16}$$

where $G(R,F)$ is the gradient information of both images. However, multi-modal images with same anatomical structures, might have same or different orientation of gradient. Pluim *et al.* considered the magnitude as well as the orientation of the gradient [42], where the gradient vector included the angle function weighted with a minimum gradient magnitude. The gradient information is expressed as

$$G(R,F) = \sum_{x,x^{'}\epsilon(R,F)} w(\alpha_{xx'}) min(|\nabla_x|, |\nabla_{x'}|) \tag{2.17}$$

where x is a sample point in the reference image. $x^{'}$ is the corresponding point of floating image obtained by geometric transformation of x. w is the weighting function which is a function of $\alpha_{xx'}$, where $\alpha_{xx'}$ is the angle between gradient vector. The angle is calculated by

$$\alpha_{xx'} = arccos \frac{\nabla_x . \nabla_{x'}}{|\nabla_x||\nabla_{x'}|} \tag{2.18}$$

where ∇_x is the gradient vector of point x, $|.|$ is the magnitude.

F Qualitative-quantitative Mutual Information

All the above MI based registration methods consider the pixels of the images equally. The pixels having the same intensity should be utilized differently because of their different characteristics and utilities while used for image registration. MI only defines the quantitative aspects of information based on the probability of events. But the occurrence of events causes different influences and effects. Hence, to justify the information of events, qualitative aspect is necessiable for consideration of the effects of their occurrence. The qualitative aspect is also known as utility or salient point, which is a non-negative large real base number. Let us consider R as probability distribution of a set of N events, where $R = \{(r_1, r_2, ..., r_N), r_n > 0, \sum_{n=1}^{N} r_n = 1\}$ be a discrete probability distribution and $W = \{(w_1, w_2, ..., w_N), w_n > 0\}$ be the set of utility. Let w_n be the utility of n^{th} event corresponding to probability r_n. Bellis *et al.* proposed an utility based weighted information measure [60], which is defined as

$$H_1(R;W) = -\sum_{n=1}^{N} w_n r_n log r_n \tag{2.19}$$

Motivated by this information measure, Luan *et al.* incorporated the saliency information as utility along with mutual information and proposed qualitative−quantitative mutual information (QMI), which was successfully applied for image registration [38]. QMI similarity measure is defined as

$$QMI(R,F;W) = \sum_{r\epsilon R} \sum_{f\epsilon F} w(r,f) p(r,f) log \frac{p(r,f)}{p(r)p(f)} \tag{2.20}$$

where $w(r, f)$ is a joint utility for each intensity pair (r, f). Each joint utility $w(r, f)$ is updated from its initial value $w_0(r, f)$ to final value through the registration process. The pixel with higher utility value contribute more towards the goal. Finally, all pixels contribute equally for the alignment of the floating image F with reference to the reference image R.

2.3 Proposed Registration Framework

During acquisition of brain images, relative changes found with relatively short periods between scan, which needs corrections for a small amount of subject motion during imaging. Also, the anatomical structures appear with more contrast in one image than other. These structures in various modalities are convenient to have more information about them. Brain images of magnetic resonance imaging are more sensitive to contrast changes [61]. It becomes difficult to distinguish any injuries or malignant with same contrast in different regions of the organ. To quantify the specified region of interest sharp intensity changes contribute more efficient match. Hence, a weighting factor or utility factor is needed for qualitative information measure. Researchers over the past years have proposed several weighted information measures, by integrating the probabilistic, objective and quantitative measure of information with the non-stochastic, subjective and qualitative measure of utility [60, 62, 63].

The proposed registration framework consists of three steps. (1) Evaluation of similarity measure, (2) transformation using interpolation and (3) optimization. In this chapter, the focus is towards implementation of a new similarity metric using rigid registration framework. The transformation parameters are initialized in the first step. The notion of utility or saliency of each pixel is incorporated into mutual information to evaluate the new similarity measure between the reference and floating image. The new similarity measure provides a qualitative-quantitative measure of relative information of floating image and the reference image, which enables to register with improved accuracy. Consequently, the proposed similarity measure is maximized by updating the new transformation parameters using Powell's optimization technique. The bi-cubic interpolation method is used during the update process. The procedure iterates until the proposed similarity measure is maximized and the subsequently floating image is aligned to the reference image with a less mean registration error.

2.3.1 Information Measure

In information theory, the occurrence of an event depends on two aspects, (i) the quantitative; is related to the probability of occurrence, (ii) the qualitative; is related to utility for the fulfillment of the goal. Considering R as probability distribution of

a set of N events, where $R = \{(r_1, r_2, ..., r_N), r_n > 0, \sum_{n=1}^{N} r_n = 1\}$ be a discrete probability distribution and $F = (f_1, f_2, ..., f_N), f_n > 0, \sum_{n=1}^{N} f_n = 1$ is the set of estimated probability distribution of events. The Kullback-Leibler distance, also known as relative entropy can be expressed as a measure of how close F approaches R [64].

$$H(R/F) = \sum_{n=1}^{N} r_n log \frac{r_n}{f_n} \tag{2.21}$$

Different pixels have their own efficiency towards the gratification of the elementary target, which may be self-reliant of their probability of occurrence. Therefore, both intensity distributions and effectiveness are essential to characterize a pixel. In 2006, Munteanu and Tarniceriu considered a new set of axioms and proposed a new weighted measure of information [65] as follows:

$$H_2(R; W) = -\sum_{n=1}^{N} r_n log r_n + \sum_{n=1}^{N} w_n r_n \tag{2.22}$$

Considering $w_n = 0$ for each n, the information measure will be equivalent to Equation 2.4. According to Taneja *et al.* [62], the quantitative-qualitative measure of relative information is expressed as

$$H_3(R/F; W) = \sum_{n=1}^{N} w_n r_n log \frac{r_n}{f_n} \tag{2.23}$$

In 2008, Srivastav *et al.* developed the quantitative-qualitative measure of relative information [66], which is defined as

$$H_4(R/F; W) = \sum_{n=1}^{N} r_n log \frac{r_n}{f_n} + \sum_{n=1}^{N} w_n r_n \tag{2.24}$$

The bounds of this weighted information measures using the Lagrange's multiplier method and well known inequalities were proved in [67]. They proved that the new weighted entropy measure $H_2(R; W)$ in Equation 2.22 is more significant in a maximum than the weighted measure $H_1(R; W)$ in Equation 2.19.

2.3.2 Proposed Similarity Measure: Enhanced Mutual Information

All variants of mutual information-based similarity measures only define the quantitative aspects of information based on the probability of pixels. Whereas the occurrence of pixels causes different weights and effects. For justification of the information of each pixel, a qualitative aspect is substantial for the consideration of the effects of their occurrence. The qualitative facet is the salient point, with a non-negative large real base number is the utility of the pixel and is independent of the probability of occurrence of that pixel.

In this part of work, a new information theoretic based similarity measure named as Enhanced Mutual Information (EMI) is proposed. Motivated by the information measure proposed by [62,67], and using the weighted entropy information $H_4(R/F;W)$ given in Equation 2.24, a new mutual information is proposed as the similarity measure for image registration. Here, the weighted information or the utility of each pixel is calculated according to the regional saliency value computed by scale-space mapping [68]. Voxels with higher saliency value contributes more towards the calculation of the similarity measure. The utility factor is incorporated which considers the useful relative information rather than the self information. The proposed mutual information adopting the new weighted information is termed as Enhanced Mutual Information (EMI) and is defined as

$$EMI(R,F;W) = \sum_{r\epsilon R}\sum_{f\epsilon F} p(r,f) log \frac{p(r,f)}{p(r)p(f)} + w(r,f)p(r,f) \tag{2.25}$$

where $w(r,f)$ is the joint weighted information or utility measure of R and F. In this measure, the saliency is incorporated to mutual information measure so that the saliency measure exhibits a relative character rather than a non−negative character. The maximum information gain of the proposed similarity measure has been proved and is presented in the **Appendix- A**.

Utility measure: Utility is determined by analyzing the entropy in the local regions. Here, self-similarity based saliency measure helps in finding the joint weighted information as utility of the images. First we calculate the probability distribution $p_i(s,x)$ of intensity i which is centered at pixel x in a circular region of radius s. Then, the local entropy $H_D(s,x)$ is defined as

$$H_D(s,x) = -\sum_i p_i(s,x) log_2 p_i(s,x) \tag{2.26}$$

The best scale s_p for the region centered at pixel x is found by maximizing the local entropy $H_D(s,x)$ with a condition $s_p = \{s : H_D(s-1,x) < H_D(s,x) > H_D(s+1,x)\}$. The saliency value $\delta(s,x)$ of each pixel is defined by a maximal local entropy value, weighted by the inter-scale saliency measure

$$\delta(s_p,x) = H_D(s_p,x) \times U_D(s_p,x) \tag{2.27}$$

where U_D is the self dis-similarity measure i.e

$$U_D(s,x) = \sum_i |\frac{\partial p_i(s,x)}{\partial s}|_{s_x} \tag{2.28}$$

After calculating the utility of each pixel, we compute the joint utility, which is the weight information of the QMI and EMI [69]. The joint weighted information for each

intensity pair is calculated by

$$w_n(r,f) = \sum_{i,j\varepsilon\varsigma} \delta_r(i).\delta_f(j). \tag{2.29}$$

where ς is the overlap region of both images. $\delta_R(i)$ and $\delta_F(j)$ are the weighted values of pixel i and j respectively in images R and F respectively. R_i and F_j are the respective intensity of the reference and floating image at locations i and j. Throughout the registration process, the joint weighted information is updated hierarchically. The weighted information changes with the registration steps l with a function

$$W_n(r,f) + \alpha(l).(1 - W_n(r,f)) \tag{2.30}$$

where $\alpha(l)$= 0 to 1

2.3.3 Image Registration using Enhanced Mutual Information

From Section 2.3.2, it is proved that the maximum information gain in the EMI measure is more than that of the QMI measure. Hence, by maximizing the proposed similarity measure EMI, the transformed floating image (F^*) will be aligned with respect to the reference image (R). The block diagram of the proposed registration framework is presented in Fig. 2.3.

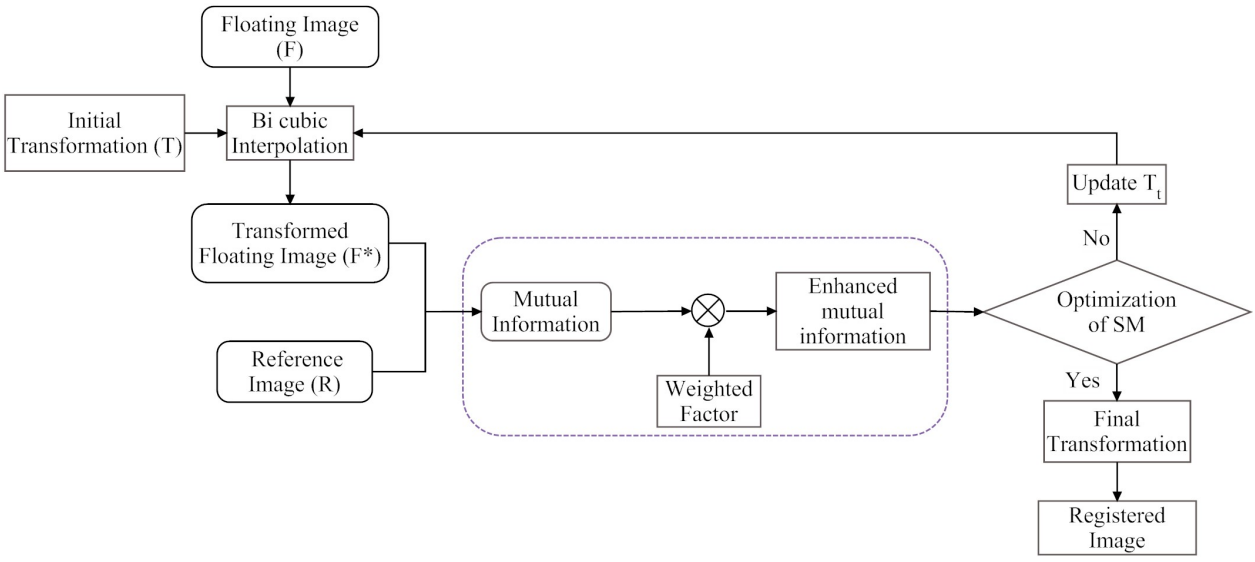

Figure 2.3: Block diagram of proposed image registration framework

Referring to Equation 2.1, the optimal transformed parameters are obtained by

$$t^* = arg \quad \max_t(EMI(R(x), F(T_t(x))) \tag{2.31}$$

where EMI between R and F^t with transformation parameter t^* is evaluated by

$$EMI(R,F;W) = \sum\sum p(R,F^t) log \frac{p(R,F^t)}{p(R)p(F^t)} + w(R,F^t)p(R,F^t) \tag{2.32}$$

The algorithm of the proposed scheme is as follows. $diff(f_c)$ is the difference of the cost function.

Algorithm 1: EMI based registration algorithm

Input: I_r, $T(I_f)$
Output: t^* with high cost function
1 Initialize geometric transformations
2 **for** *each transformation-step=1* **to** n **do**
3 Calclate the cost function as given by Equation 2.32
4 **repeat**
5 Use Powell technique to solve the optimization problem as in Equation 2.1
   Update the joint utility using Equation 2.29
6 Go to Step 3
7 **until** ;
8 The $diff(f_c)$ in three consecutive transformation steps is ≤ 0.01
9 **end**

Optimization Optimization is important to find a set of transformation parameters for which the similarity measure, i.e., the cost function is maximized. In the case of rigid transformation, there is six dimensional space of possible parameters to search, which is not feasible to manage with an exhaustive search. Hence, we used a standard approach i.e. initial estimation of transformation parameters and an iterative search of that. At each iteration, the optimized cost function is evaluated for the current parameter estimate and depending on its value; a new estimate is constituted. The optimization stops on achieving some convergence criterion.

The optimization algorithm we have chosen here is the Powell optimization technique. This method is demonstrated for registration of MR and CT images in Maes *et al.* [12]. Convergence of optimization is declared when the fractional decrease of the optimized function is smaller than some threshold. The threshold is set to 10^3. This method repeatedly iterates the dimensions of the whole search space, performing one-dimensional optimization for each dimension until the convergence is reached. But, this approach is not efficient in case of multi-scale approach. Hence, evolutionary optimization techniques are adopted for the registration procedure, which are described in Chapter 5.

2.4 Simulation and Results

Extensive experiments have been carried out to evaluate the performance of the proposed similarity measure based registration technique. Multi-modal brain images such as simulated brain MR images of T1, T2 and PD weighted have been taken from the database (http://brainweb.bic.mni.mcgill.ca/brainweb/). MR images are with 128×128

pixels, in plane, and of pixel size $1.25mm \times 1.25mm$. Real MR and CT images of the same subject are taken from internet source (http://medind.nic.in). The CT images are of size 256×256 pixels. Some of the real images are taken from Ispat General Hospital (IGH), Rourkela, India. The scale difference in multi-modal images is due to different pixel size. Here, we highlight the registration function for a different problem, comparing the behavior of information theoretic based similarity measure and statistical dependencies or weighted information-based similarity measure. We evaluated the accuracy and robustness of the proposed similarity measure for multi-modal images by comparing the performance measures as described in the following section.

In this work, the simulation based experimentation on registration has been performed with five different cases (reference image with floating image).

- **Case I**: MR T2-weighted image with translated T1-weighted image
- **Case II**: MR T1-weighted image with translated T2-weighted image
- **Case III**: MR T2-weighted image with rotated PD-weighted image
- **Case IV**: MR PD-weighted image with translated and rotated T1-weighted image
- **Case V**: MR image with CT image

2.4.1 Performance Evaluation Measures

The optimized transformed parameters t^* with a higher similarity measure value indicates the alignment of the transformed floating image and reference image. The time required to optimize the similarity measure referred as a measure of computation time. The performance measures used to demonstrate the efficacy of the proposed scheme are listed below.

Mean registration error (MRE): It is measured by calculating the difference of pixel distance of the registered image with respect to the reference image or ground truth image. The mean distance between the two surfaces is calculated by averaging the distance between corresponding points (x_{ij}^r, y_{ij}^r) on reference image and $(x_{ij}^{r^*}, y_{ij}^{r^*})$ on the registered image surface. The corresponding points are projected from four selected corner points of the surface of the object. The lower value of MRE indicates better alignment of the images.

Target registration error (TRE): It is defined as the distance between corresponding points other than those used to estimate the transformation parameters [70].

Peak signal-to-noise ratio (PSNR): Mean squared error (MSE) and PSNR are widely used simplest quality metric, computed by averaging the squared intensity differences of floating and reference image. For given two images $r = (r_i | i = 1, ..., N)$

and $f = (f_i|i = 1, ..., N)$ the MSE and the related PSNR is used to assess the image quality.

$$MSE(r, f) = \frac{1}{n}\sum_{1}^{N}(f_i - r_i)^2$$

and

$$PSNR(r, f) = 10log_{10}\left(\frac{L^2}{MSE(r, f)}\right) \tag{2.33}$$

where L^2 is representing the image dynamic range.

Normalized Cross Correlation (NCC): The NCC of given images is used to compare the performance of the registration algorithm using the following relationship

$$NCC = \frac{\sum_i \sum_j (I_{r_{ij}} - \overline{I_r})(I_{f_{ij}} - \overline{I_f})}{\sqrt{\left(\sum_i \sum_j (I_{r_{ij}} - \overline{I_r})^2\right)\left(\sum_i \sum_j (I_{f_{ij}} - \overline{I_f})^2\right)}} \tag{2.34}$$

where $I_{r_{ij}}$ and $I_{f_{ij}}$ are the reference and floating image intensities at point (i, j) in image I_r and I_f and $\overline{I_r}$ and $\overline{I_f}$ are the average intensities of I_r and I_f.

Universal Quality Index (UQI): The universal quality index is modeled by considering the three factors such as contrast distortion, luminance distortion, and loss of correlation.

$$Q = \frac{4\sigma_{rf}\overline{r}\,\overline{f}}{(\sigma_r^2 + \sigma_f^2)[(\overline{r})^2 + (\overline{f})^2]} \tag{2.35}$$

where $\overline{f} = \frac{1}{N}\sum_{i=1}^{N} f_i$ and $\overline{r} = \frac{1}{N}\sum_{i=1}^{N} r_i$

$\sigma_r^2 = \frac{1}{N-1}\sum_{i=1}^{N}(r_i - \overline{r})^2$ and $\sigma_f^2 = \frac{1}{N-1}\sum_{i=1}^{N}(f_i - \overline{f})^2$

$\sigma_{rf} = \frac{1}{N-1}\sum_{i=1}^{N}(r_i - \overline{r})(f_i - \overline{f})$

Structure Similarity (SSIM): To assess the image quality, universal assessment method structure similarity (SSIM) is widely used. SSIM considers the luminance, contrast and structure comparison of images. SSIM is calculated as

$$SSIM = \frac{(2\overline{I_f I_f} + C_1)(2cov(I_r I_f + C_2)}{(2\overline{I_f}^2 + \overline{I_f}^2 + C_1)(\sigma_r^2 + \sigma_f^2 + C_2)} \tag{2.36}$$

where C_1 and C_2 are the variables to stabilize the division with weak denominator.

2.4.2 Registration Function

An ideal registration function that measures the similarity of two images should be smooth and convex with respect to different transformation parameters. Also, the global maximum of the registration function should be close to the correct transformation parameters that align two images perfectly. Moreover, the capture range around the

global maximum should be as small as possible, and the number of local maxima of the registration function should be as small as possible. These criteria will be used to evaluate the registration functions generated by the proposed measure and other existing measures respectively. All the registration functions are obtained by using the Parzen window-based joint density estimation.

The simulated floating images for the four different cases are generated by following specific geometrical transformations with respect to the reference image, i.e. (i) translation along x-axis, (ii) translation along y-axis, (iii) rotation about the x-axis. The registration algorithm is validated with different similarity measures i.e. NMI [40], SMI [42], RMI [43], and QMI [38]. From the result, we found that NMI could not handle the case with a wide range of transformation parameters. It is because NMI only considers the self-intensities of the pixels, not the neighborhood pixel, whereas RMI considers 3×3 neighborhood with the 18D histogram for the joint histogram evaluation. Although RMI considers the neighborhood information, the drawback is for high dimension space during calculation of the joint histogram. Similarly, SMI uses a local intensity gradient to optimize the pixel movements. But, this method may trap in local minima if brain tissues of the reference image are overlapped with other tissues (including background) of the floating image and vice versa. It is because the pixels may be driven towards the wrong direction. Different from RMI and SMI, qualitative-quantitative based similarity measure optimizes the registration process in a global manner by using utility factor which provides qualitative information content. Therefore utility based proposed new similarity measure is tested with all the 5 cases. Experimental results on these different registration cases are detailed below.

A Simulated T1-T2 weighted image data set

For evaluation of the proposed scheme, at first two sets of multi-modal simulated brain images are considered i.e Case I and Case II. In Case I, the simulated T2 weighted image is considered as the reference image whereas T1 weighted image is taken as the floating image which is translated along the x-axis. The input images and the paired image before registration are shown in Fig. 2.4 (a-c) respectively, and the registered images using NMI (Viola *et al.*), SMI (Pluim *et al.*), RMI (Russakoff *et al.*), QMI (Luan *et al.*), EMI (Proposed) are shown in Fig. 2.4 (d-h) respectively. The difference of paired image after registration have been presented in Fig. 2.4 (i-m). From this figure, it is observed that, the registered image using EMI aligns better than that of other existing methods.

Similarly, for Case II, the reference image is T1 weighted, and the floating image is T2 image translated along y-axis. The input images, along with paired image before registration and registered images using different information theoretic based similarity

measure are shown in Fig. 2.5 (a-c), and Fig. 2.5 (d-h) respectively. In Fig. 2.5 (i-m), the difference of paired image after registration using different similarity measure based registration scheme are shown. To validate the proposed technique with the above two cases, we have also done the quantitative evaluation. The SM value along with different performance measures are tabulated in Table 2.1. The SM value is found to be higher in case of proposed EMI based registration scheme as compared to other existing schemes. It demonstrates that the proposed registration method using EMI outperforms the other methods including SMI and QMI, which uses spatial information for the registration framework. Also, EMI based scheme significantly reduces the mean registration error (MRE) of different tissues as compared to QMI and SMI based schemes. This shows that improvement in registration accuracy that mainly comes from the saliency or utility factor that is embodied with EMI.

B Simulated T2-PD weighted image data set

In Case III, the PD-weighted image is rotated about the x-axis with 15 degrees considered as floating image and T2 weighted image is taken as a reference image. The images are multi-modal due to different tissue characteristics, but the structures are same containing detailed anatomical information. So, the utility of the corresponding location is found easily. The respective registered images along with the difference paired images using EMI and other similarity measure based registration schemes are shown in Fig. 2.6. Similarly, for Case IV, the input images are shown in Fig. 2.7 (a,b), where PD-weighted image is the reference image and T2 weighted image is rotated about the x-axis and translated along the x-axis. The registered images and the paired images using all schemes as discussed earlier are shown in Fig. 2.7 (d-h) and (i-m) respectively. The corresponding SM value and all the performance measure values are tabulated in Table 2.1.

C Real MR-CT image data set

In Case V, a set of real brain MR and CT images of the same subject are considered as the reference and floating image for evaluation of registration function. As the images are of different sizes, the CT image is scaled according to the size of MR image. The registered images along with the difference paired images are shown in Fig. 2.8 (d-h) and (i-m) respectively. The corresponding SM values and other performance measures are tabulated in Table 2.1. From the table, it is observed that the proposed similarity metric EMI has higher similarity measure value of 2.59. Also, the MRE of the scheme is 5.49, which is lower than those of other existing similarity measure based registration schemes. Similarly, the SSIM index, NCC, and PSNR values for the proposed scheme are found to be 0.83, 0.84 and 16.81 respectively, which are higher than those of other

Table 2.1: Performance Measures for all Cases

Case	Methods	SM value	MRE	SSIM	NCC	PSNR	UQI
	MI (Maes)	1.76	5.95	0.55	0.62	16.94	0.5
	NMI (Viola)	1.80	5.91	0.59	0.68	17.04	0.48
	RMI (Russakoff)	1.84	5.89	0.61	0.72	17.14	0.45
I	SMI (Pluim)	1.95	5.73	0.69	0.78	17.43	0.42
	QMI (Luan)	2.05	5.42	0.75	0.86	17.63	0.34
	EMI (Proposed)	**2.15**	**5.05**	**0.81**	**0.91**	**17.68**	**0.32**
	MI (Maes)	1.64	6.40	0.61	0.60	15.94	0.6
	NMI (Viola)	1.70	6.31	0.65	0.65	16.01	0.58
	RMI (Russakoff)	1.76	6.24	0.71	0.71	16.49	0.52
II	SMI (Pluim)	1.82	6.15	0.74	0.76	16.65	0.46
	QMI (Luan)	1.92	5.92	0.79	0.83	16.86	0.41
	EMI (Proposed)	**2.09**	**5.88**	**0.81**	**0.89**	**16.98**	**0.37**
	MI (Maes)	1.55	7.5	0.5	0.62	17.42	0.73
	NMI (Viola)	1.60	7.44	0.53	0.66	17.64	0.68
	RMI (Russakoff)	1.65	7.37	0.59	0.68	17.60	0.65
III	SMI (Pluim)	1.79	7.28	0.63	0.72	17.69	0.59
	QMI (Luan)	1.88	7.13	0.70	0.81	17.82	0.45
	EMI (Proposed)	**1.99**	**6.98**	**0.78**	**0.86**	**17.89**	**0.41**
	MI (Maes)	1.92	6.85	0.55	0.52	15.04	0.61
	NMI (Viola)	1.99	6.41	0.59	0.58	15.54	0.58
	RMI (Russakoff)	2.03	6.13	0.65	0.61	16.09	0.51
IV	SMI (Pluim)	2.11	6.05	0.71	0.66	16.55	0.45
	QMI (Luan)	2.20	5.90	0.78	0.73	16.66	0.40
	EMI (Proposed)	**2.39**	**5.84**	**0.85**	**0.79**	**16.78**	**0.35**
	MI (Maes)	2.02	5.89	0.58	0.58	16.44	0.65
	NMI (Viola)	2.19	5.81	0.63	0.63	16.52	0.59
	RMI (Russakoff)	2.23	5.73	0.68	0.67	16.59	0.52
V	SMI (Pluim)	2.31	5.65	0.74	0.72	16.65	0.48
	QMI (Luan)	2.40	5.58	0.79	0.79	16.72	0.42
	EMI (Proposed)	**2.59**	**5.49**	**0.83**	**0.84**	**16.81**	**0.37**

schemes. At the same time, the UQI measure is only 0.37, which is the lowest in case of EMI based registration scheme as compared to the other schemes.

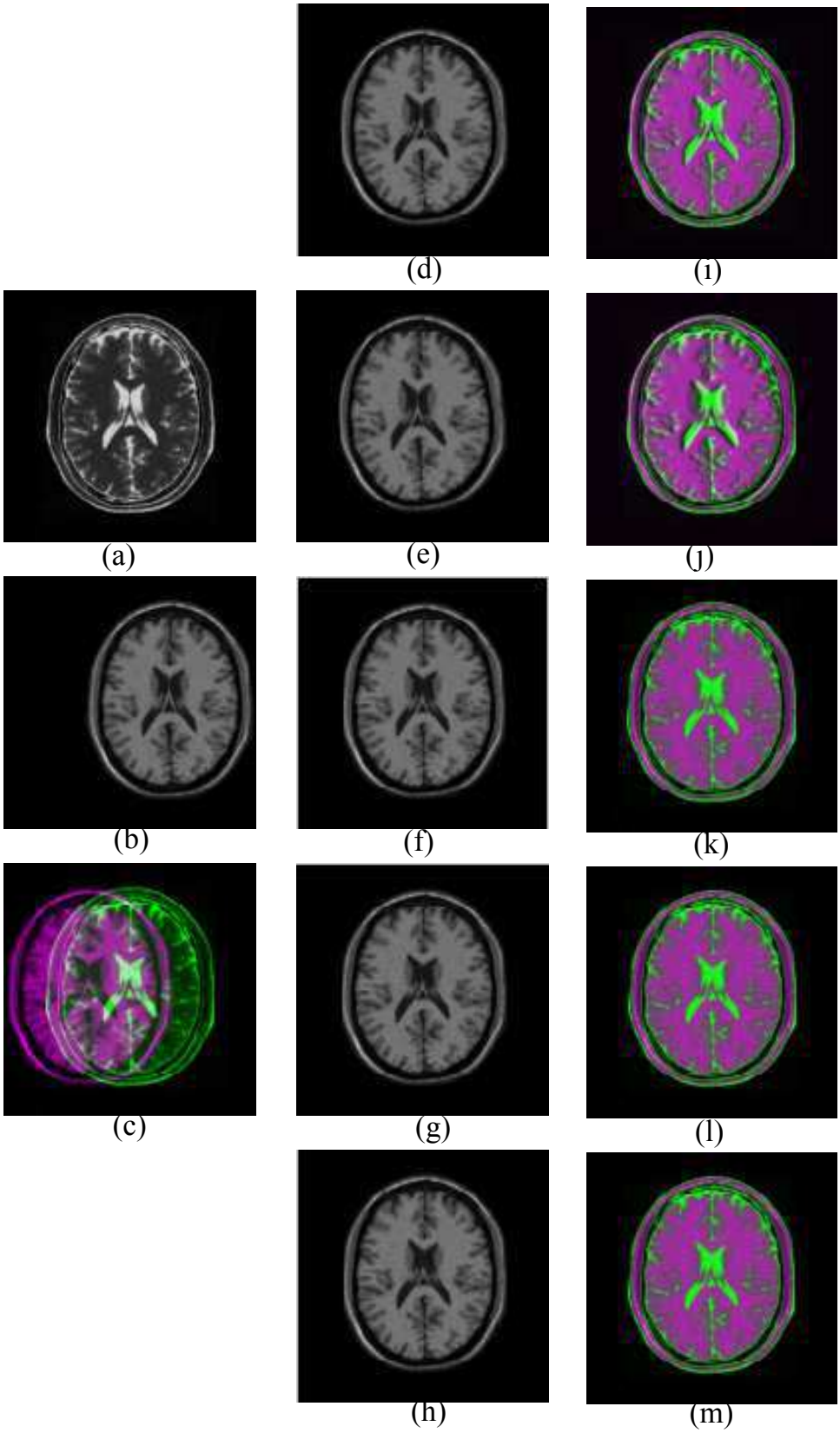

Figure 2.4: (a) Reference image, (b) Floating image translated along x axis, (c) Paired image before registration, (d-h) Registered image and (i-m) Paired image after registration using NMI (Viola), SMI (Pluim), RMI (Russakoff), QMI (Luan) and EMI (proposed) scheme respectively for Case I

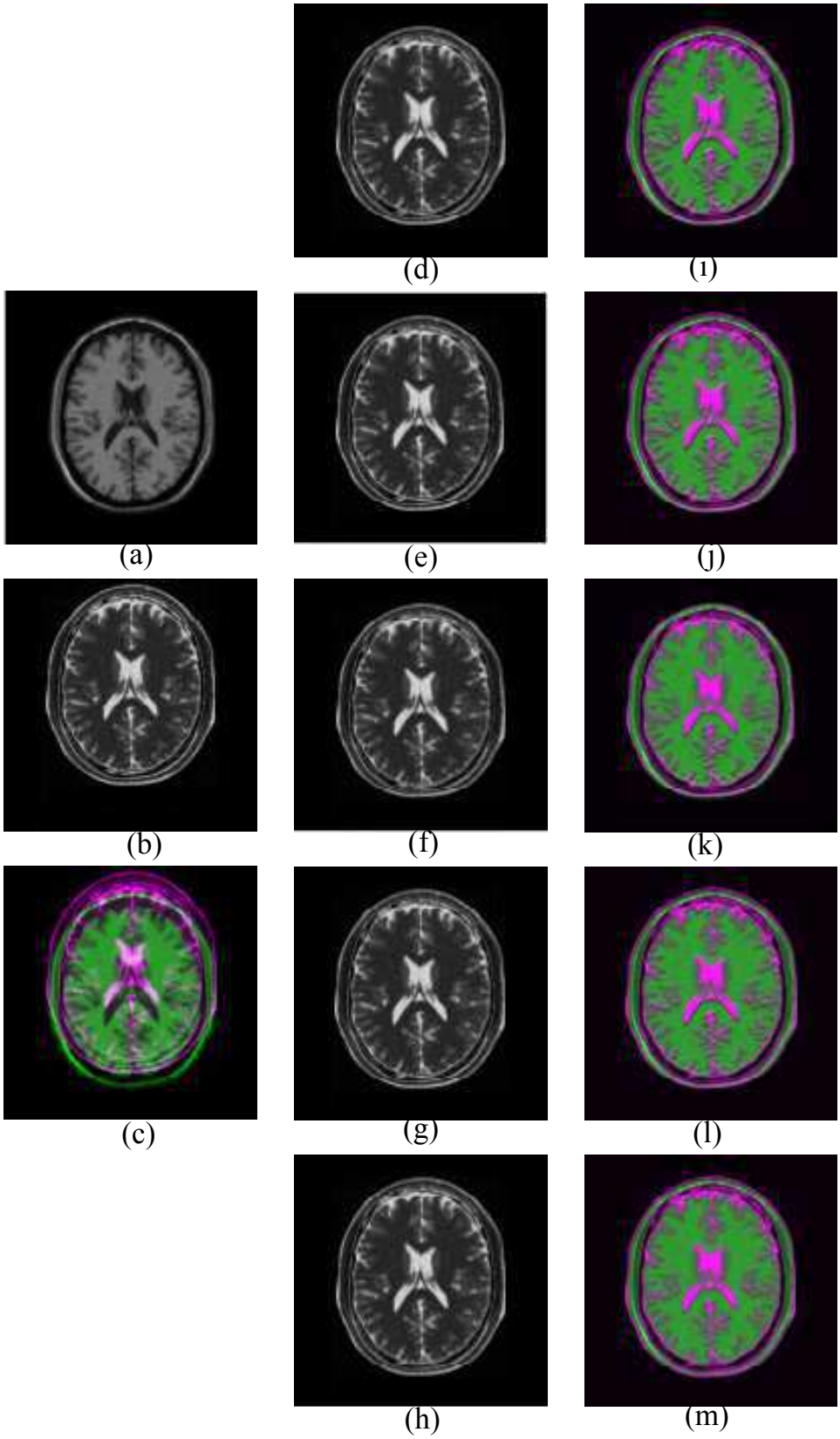

Figure 2.5: (a) Reference image, (b) Floating image translated along y axis, (c) Paired image before registration, (d-h) Registered image and (i-m) Paired image after registration using NMI (Viola), SMI (Pluim), RMI (Russakoff), QMI (Luan) and EMI (proposed) scheme respectively for Case II

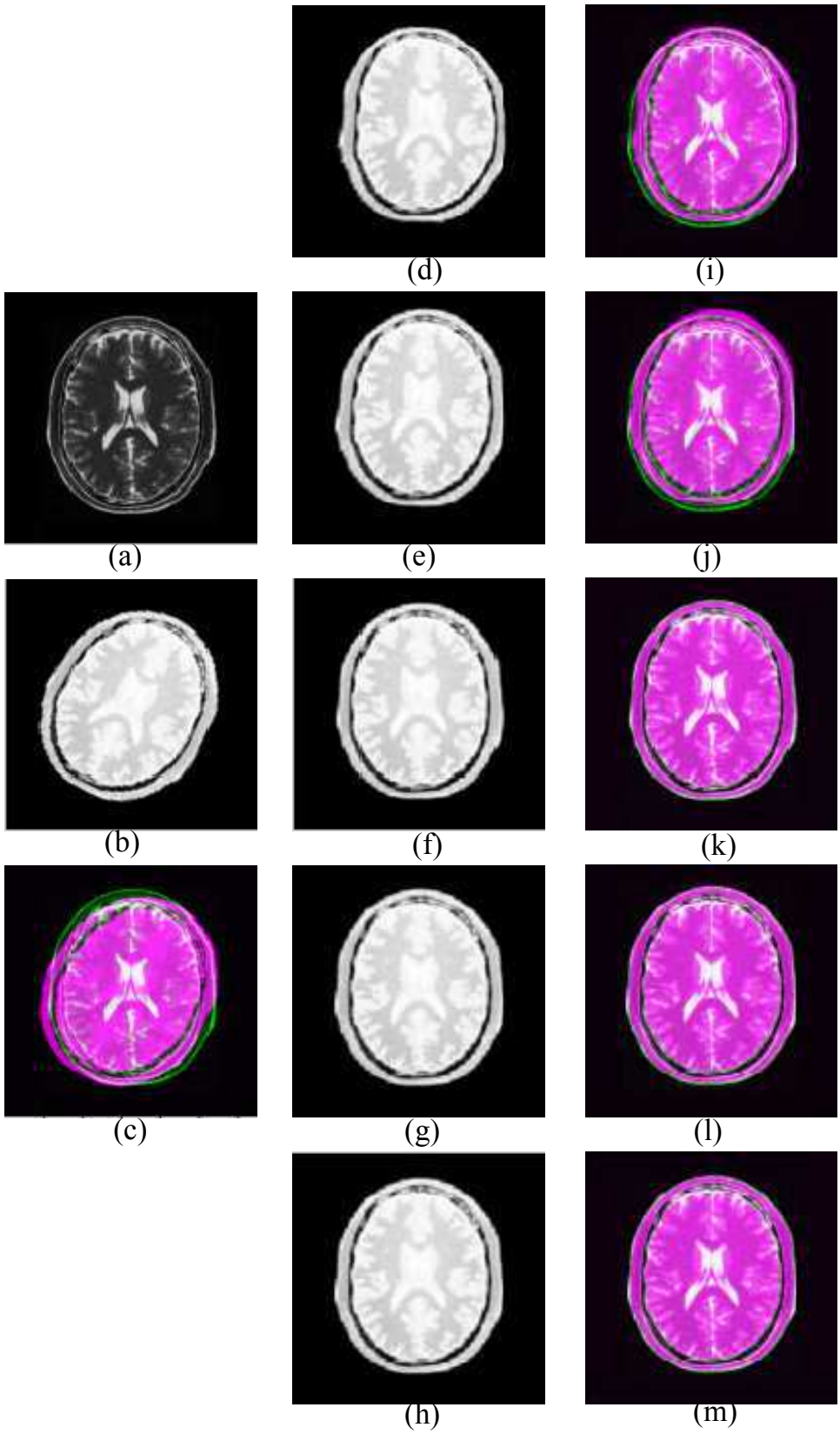

Figure 2.6: (a) Reference image, (b) Floating image rotated about x axis, (c) Paired image before registration, (d-h) Registered image and (i-m) Paired image after registration using NMI (Viola), SMI (Pluim), RMI (Russakoff), QMI (Luan) and EMI (proposed) scheme respectively for Case III

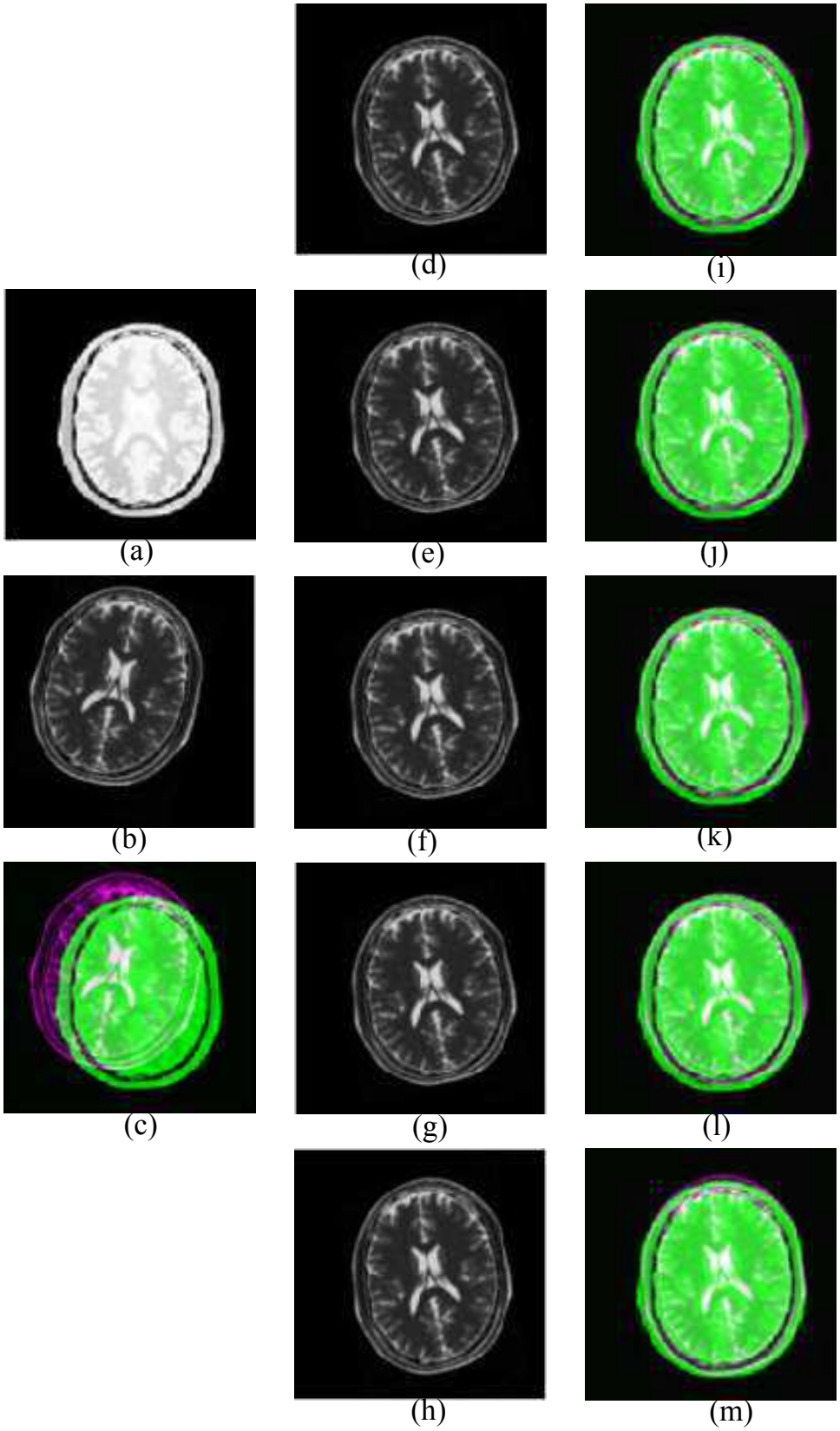

Figure 2.7: (a) Reference image, (b) Floating image translated and rotated about x axis, (c) Paired image before registration, (d-h) Registered image and (i-m) Paired image after registration using NMI (Viola), SMI (Pluim), RMI (Russakoff), QMI (Luan) and EMI (proposed) scheme respectively for Case IV

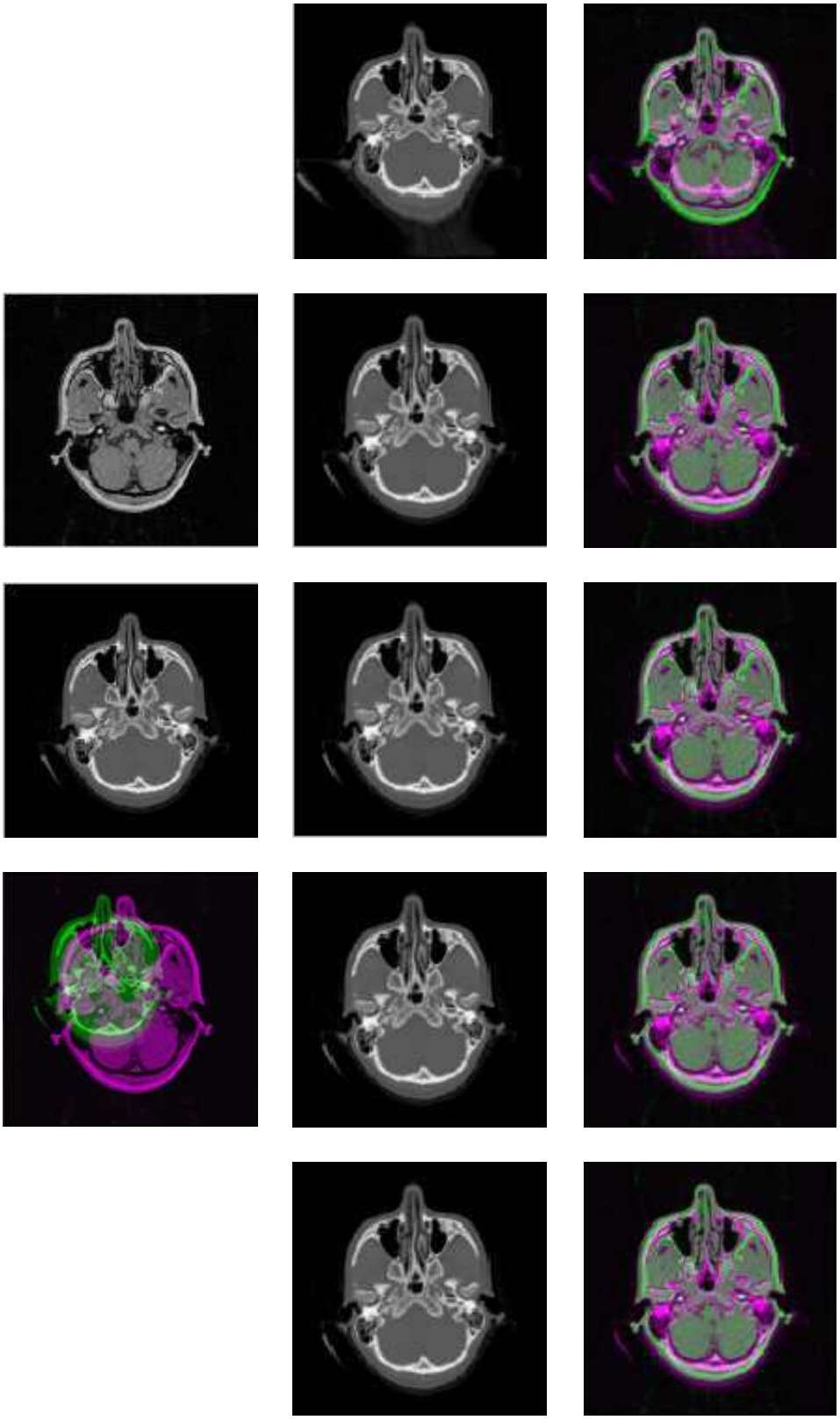

Figure 2.8: (a) Reference image, (b) Scaled floating image, (c) Paired image before registration, (d-h) Registered image and (i-m) Paired image after registration using NMI (Viola), SMI (Pluim), RMI (Russakoff), QMI (Luan) and EMI (proposed) scheme respectively for Case V

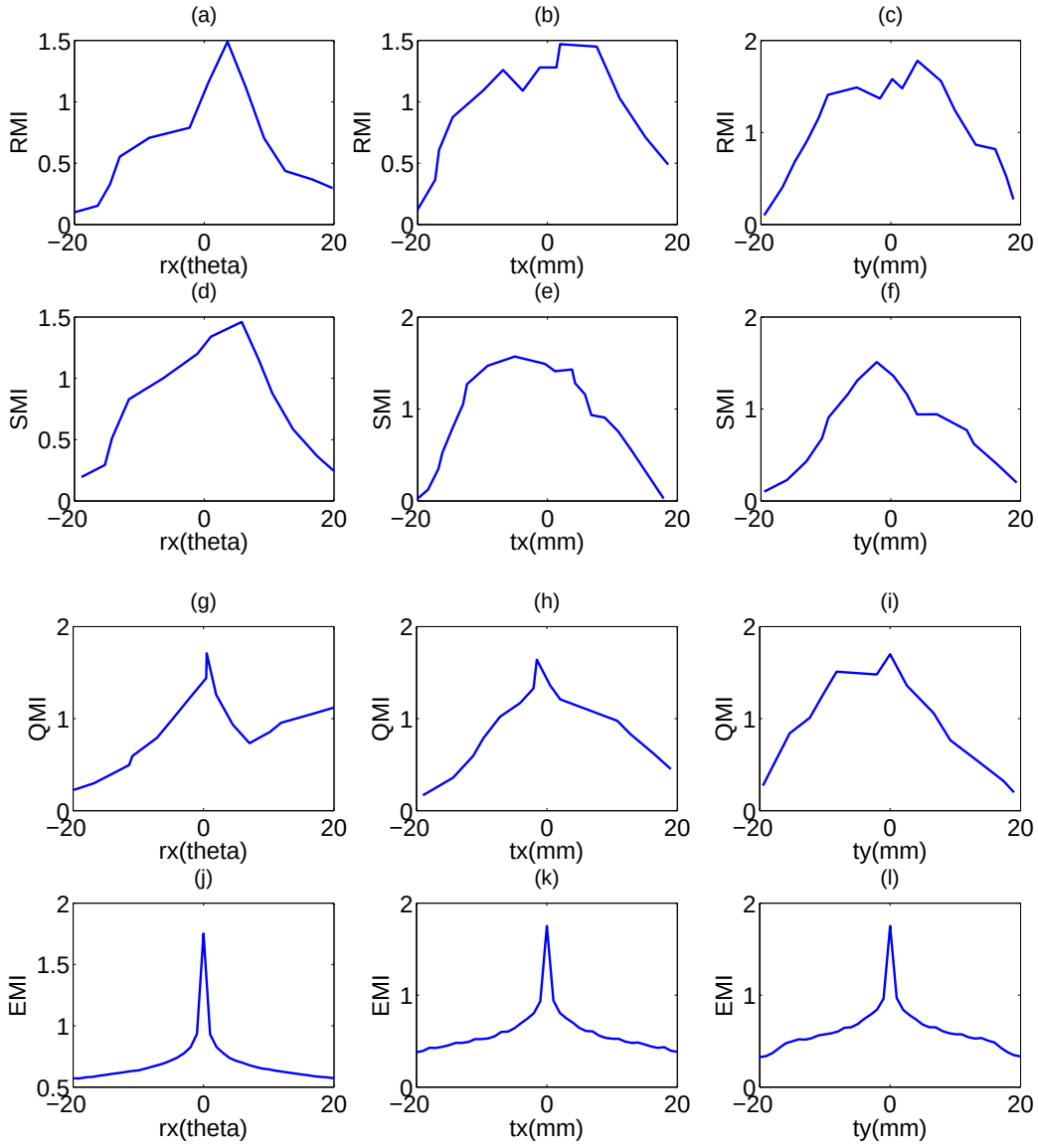

Figure 2.9: Similarity measures with respect to geometrical transformation for Case III: using RMI (a) Rotation along x axis r_x, (b) Translation along x-axis t_x, (c) Translation along y-axis t_y; using SMI (d) Rotation about x axis r_x, (e) Translation along x-axis t_x (f) Translation along y-axis t_y; using QMI (g) Rotation about x axis r_x, (h) Translation along x-axis t_x, (i) Translation along y-axis t_y; using Proposed EMI (j) Rotation about x axis r_x, (k) Translation along x-axis t_x, (l) Translation along y-axis t_y

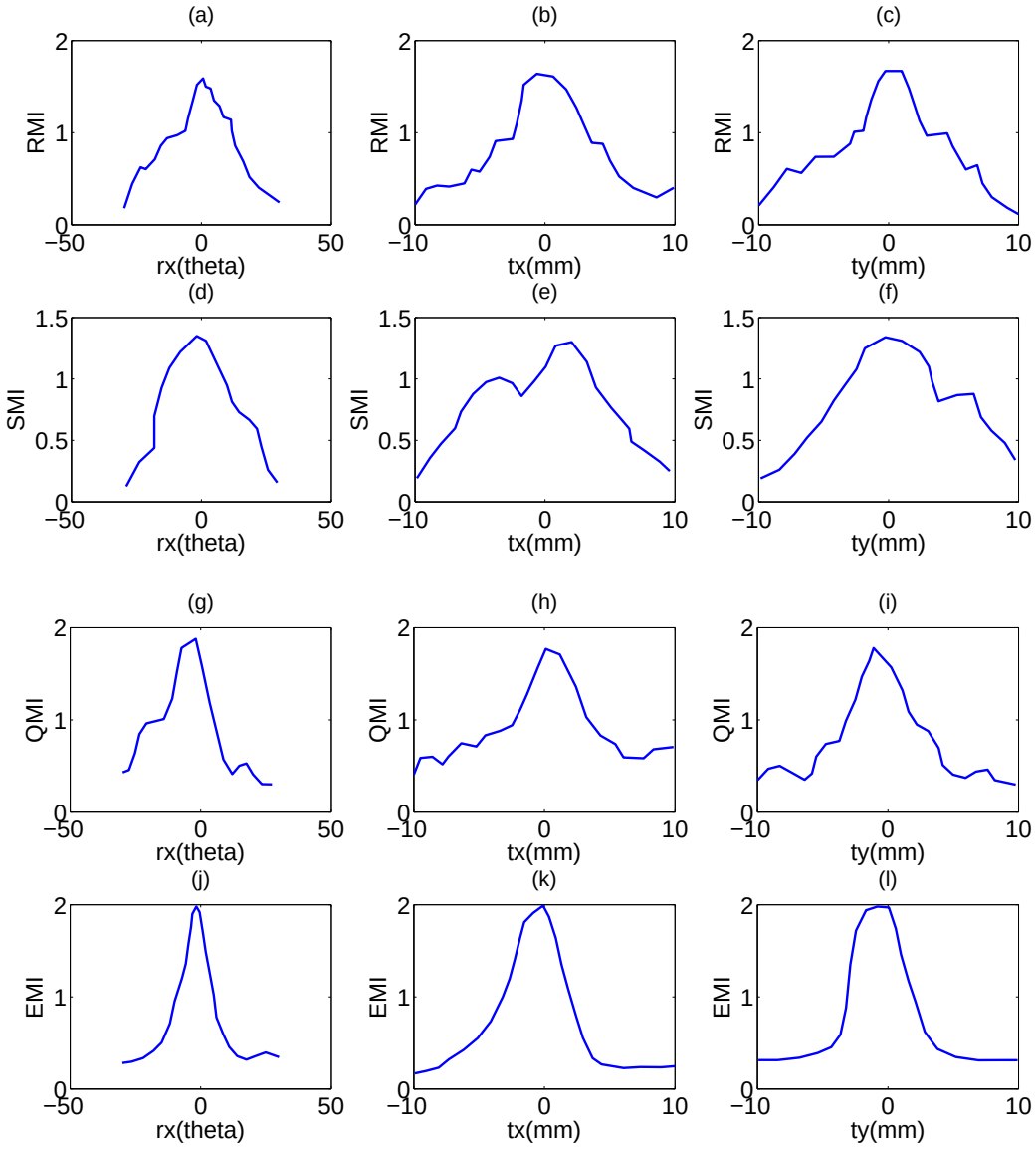

Figure 2.10: Similarity measures with respect to geometrical transformation for Case IV: using RMI (a) Rotation along x axis r_x, (b) Translation along x-axis t_x, (c) Translation along y-axis t_y; using SMI (d) Rotation about x axis r_x, (e) Translation along x-axis t_x, (f) Translation along y-axis t_y; using QMI (g) Rotation about x axis r_x (h) Translation along x-axis t_x (i) Translation along y-axis t_y; using Proposed EMI (j) Rotation about x axis r_x (k) translation along x-axis t_x (l) translation along y-axis t_y

Table 2.2: Comparison of rigid transformation parameters, and computational time for Case (I-IV)

Case	Methods	Parameters			Difference			Computation Time (sec)
		θ	t_x	t_y	θ	t_x	t_y	
I Brain MR image T2-T1	MI (Maes)	10	1.0	5.0	1.8	0.46	1.46	66
	NMI (Viola)	10	1.0	5.0	1.63	0.41	1.42	69
	RMI (Russakoff)	10	1.0	5.0	1.52	0.39	1.32	75
	SMI (Pluim)	10	1.0	5.0	1.45	0.36	1.25	78
	QMI (Luan)	10	1.0	5.0	1.21	0.31	1.13	81
	EMI (Proposed)	**10**	**1.0**	**5.0**	**1.09**	**0.25**	**1.02**	**82**
II Brain MR image T1-T2	MI (Maes)	15	2.0	5.0	3.21	0.71	1.86	69
	NMI (Viola)	15	2.0	5.0	2.89	0.65	1.78	74
	RMI (Russakoff)	15	2.0	5.0	2.65	0.59	1.51	82
	SMI (Pluim)	15	2.0	5.0	2.55	0.49	1.4	84
	QMI (Luan)	15	2.0	5.0	2.32	0.41	1.20	91
	EMI (Proposed)	**15**	**2.0**	**5.0**	**1.98**	**0.32**	**1.04**	**99**
III Brain MR image T2-PD	MI (Maes)	20	1.0	10	2.59	0.39	2.31	71
	NMI (Viola)	20	1.0	10	2.46	0.35	2.22	78
	RMI (Russakoff)	20	1.0	10	2.38	0.32	2.14	84
	SMI (Pluim)	20	1.0	10	2.25	0.29	2.02	89
	QMI (Luan)	20	1.0	10	2.18	0.23	1.89	93
	EMI (Proposed)	**20**	**1.0**	**10**	**2.0**	**0.18**	**1.81**	**97**
IV Brain MR image PD-T1	MI (Maes)	30	5.0	10	3.9	2.21	2.36	61
	NMI (Viola)	30	5.0	10	3.66	2.16	2.32	68
	RMI (Russakoff)	30	5.0	10	2.96	2.12	2.24	74
	SMI (Pluim)	30	5.0	10	2.5	1.99	2.2	81
	QMI (Luan)	30	5.0	10	1.98	1.89	2.01	95
	EMI (Proposed)	**30**	**5.0**	**10**	**1.76**	**1.80**	**1.91**	**98**

2.4.3 Robustness of Registration Scheme

A robust registration algorithm should be able to recover the true transformation of the floating image under registration, even if the initial misalignment between the reference and floating image is large. To validate the robustness of the EMI based registration algorithms, simulation is done with various amounts of initial misalignment between T1, T2 and PD-weighted brain MR images. Four sets of tests have been performed, with initial misalignment of rotation transformation in degree and translation transformation in mm. Here, Case III is taken into consideration for the validation, where the PD weighted image is the reference image and translated, rotated T1 image is floating image. The image is translated 1 mm along x axis, 10 mm along y axis and 20 degree rotated ablout x axis. The different ranges of rotation and translation along x and y

axis i.e., $[-20, 20]$, and $[-20, 20]$ are randomly chosen. The registration is considered as successful for each test, if the difference between the estimated transformation is less than a pre defined threshold. The threshold for each transformation parameters are selected as 2 degree for rotation about x-axis, 0.2 mm for translation in x-axis and 2mm for translation in y-axis respectively.

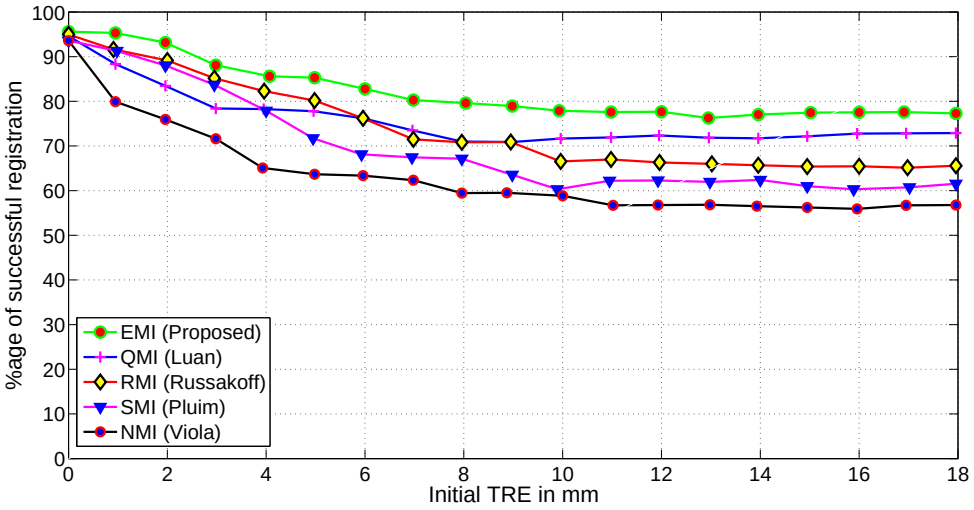

Figure 2.11: Percentage of successful registration for initial transformation with TRE values for Case III

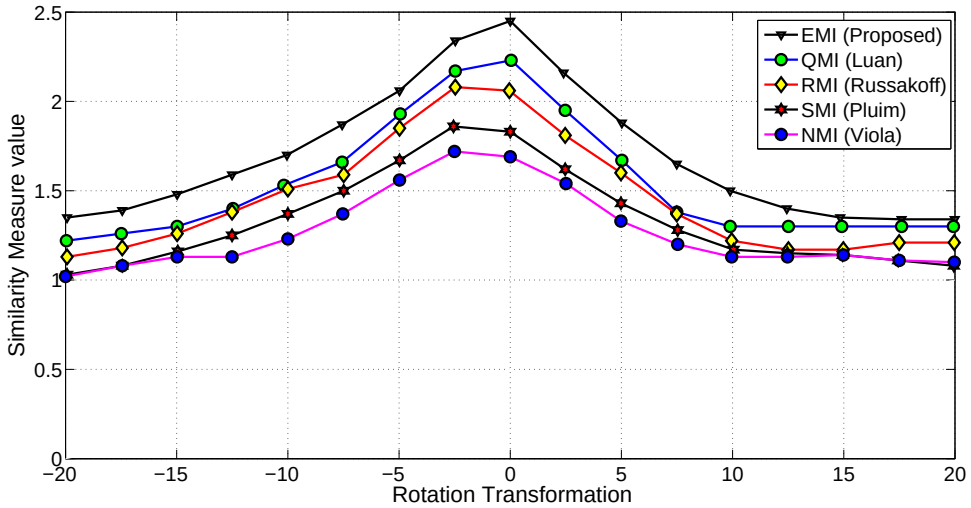

Figure 2.12: Comparison of Similarity measures for Case III

The respective number of successful registration for the four cases with different rotation and translation ranges, using the EMI and other similarity measure based registration algorithms are summarized in Table 2.2. These results indicate that the EMI based registration algorithm produces a much higher success rate, and thus it is more robust than QMI and other similarity based registration algorithm. For

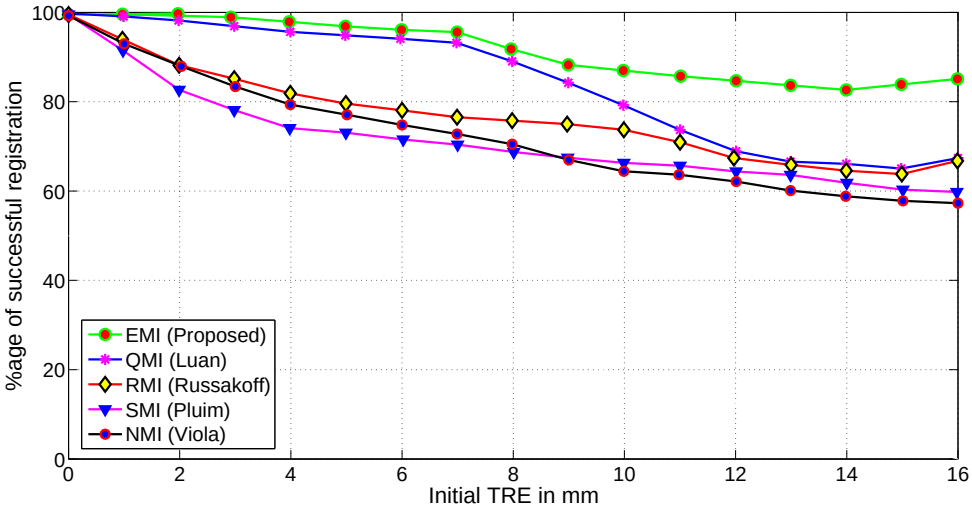

Figure 2.13: Percentage of successful registration for initial transformation with TRE values for Case IV

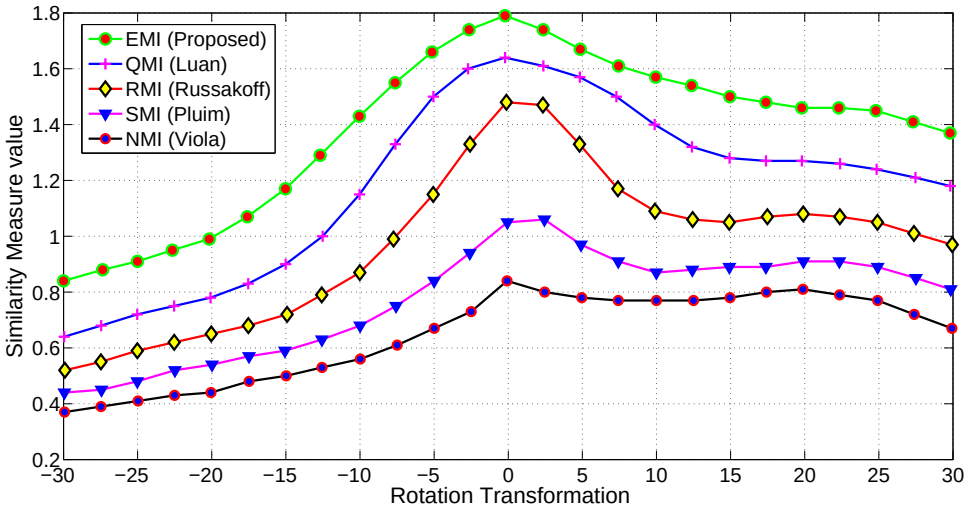

Figure 2.14: Comparison of Similarity measures for Case IV

visual inspection, EMI and other schemes, the similarity measure value with respect to transformation function are shown in Fig. 2.9. The registration functions of EMI versus the rotation about x-axis (r_x), the translation along x-axis (t_x), and the translation along y-axis (t_y) are shown in Fig. 2.9 (j-l) respectively. Similarly Fig. 2.9 (a-c), (d-f), (g-i), show the variation of registration function of RMI, SMI and QMI along all transformations respectively. By comparing the figures, it is observed that the smoothness and optimum global SM value of proposed EMI are better than those of QMI, SMI, and RMI. This property is due to the integration of joint utility through relative information into EMI calculation. Similarly, for case IV, the registration functions of EMI versus the rotation about x-axis (r_x), the translation along x-axis (t_x), and the translation along y-axis (t_y) are plotted in Fig. 2.10, where Fig. 2.10 (j-l) show

EMI based registration function, which is more smoother than that of other existing state of the art.

In both cases, we can observe that the registration function of EMI drops quickly with the increase in rotation and translations. It signifies that the amount of saliency measure using relative information in the overlap region of two images decreases quickly in comparison to the saliency measure using joint information. Therefore, the capture range using EMI is found to be smaller than that of QMI, SMI, and RMI with respect to geometrical transformations.

The transformed parameters, and computation time for all methods are tabulated in Table 2.2. Though the computation time for the proposed method is high as compared to other methods, the lower transformation difference after registration shows the efficacy of EMI based registration method. The percentage of successful registration for case III is shown in Fig. 2.11. The initial transformation is characterized by computing the target registration error (TRE) for the transformation of a group of (0-2, 2-4, ..., 16-18 mm). The registration is successful if TRE $<$ 2.5 mm or unsuccessful if TRE $>$ 2.5 mm. Fig. 2.12 shows the maximum similarity measure value obtained with a set of rotation transformation parameters. It is observed from the plot; the proposed EMI based registration scheme is aligned at zero degree with a higher similarity measure value as compared to other similarity measure based registration schemes. In all cases, images are aligned with a maximum value that is closer to zero degree.

Also, for case IV, the percentage of the successful registration of the proposed EMI based registration method is found to be more than 80%, whereas, in all other cases, it is less than 80%, as shown in Fig. 2.13. The maximum information gain of the proposed scheme, i.e SM value is higher within a group of rotation transformation parameter, which is shown in Fig. 2.14. It is observed that the obtained similarity measure value is maximum at zero degree, whereas in all other cases, the SM value is maximum nearer to zero degree. It indicates the proper alignment of the floating image with respect to the reference image with maximum information gain.

2.5 Summary

In this chapter, the proposition of a new information theoretic based similarity measure is the main focus for efficient registration of multi-modal brain images in intensity based registration framework. The registration method is addressed in rigid transformation domain. Motivated by the work of [38], on weighted entropy measure of relative information, a new similarity measure, i.e. Enhance Mutual Information (EMI) is proposed. EMI is proposed using a qualitative-quantitative measure of relative information of both reference and floating images. The qualitative measure is incorporated into weighted entropy information or utility factor whereas quantitative measure is incorporated into mutual information. The maximum information gain using proposed EMI is found to be more than that of QMI. A new registration algorithm is proposed using EMI for enhancing the efficacy of multi-modal brain image registration. For validation of the proposed method, the experimental analysis has been performed on various multi-modal brain images with translation, rotation and scaling transformations. The combination of the qualitative and quantitative measure of weighted relative information is found to be suitable similarity measure than the existing state of the art for brain image registration. The performance analysis shows that the EMI based registration algorithm outperforms the similar existing algorithms regarding MRE, TRE, SSIM, NCC, PSNR, and UQI.

Though the incorporation of qualitative information through the utility factor enhances the similarity measure but, this utility factor is a scale invariant feature. It can perform well in case of rigid transformation. It may fail to register properly in case of affine transformation. To overcome this, an attempt has been made to develop an affine invariant utility factor for efficient registration, which is discussed in the next chapter.

Chapter 3

Image Registration using Affine Invariant Saliency based Similarity Measure

The evaluation of utility factor or saliency measure is one of the important job in the similarity measure step of brain image registration. When the scale of both input images are different, the sensitivity of each pixel information for the same soft tissues becomes challenging task for analysis. Though this problem can be solved by using a scale invariant saliency, this saliency generally affects the registration when the images are having projective and perspective transformations. In this chapter, an affine invariant saliency measure, is taken into consideration for evaluation of the proposed similarity measure in the registration procedure.

3.1 Introduction

Fast and accurate registration of low quality medical image is a challenging task due to low contrast, intensity inhomogeneity as well as unhealthy image caused due to various pathology. Intensity based methods incorporate the whole image information for the calculation of a global similarity measure. These methods are closely related to the background changes, image quality and initial misalignment, but fails when the overlap region is not large enough and the intensity variance is large.

In the previous chapter, the utility or saliency used for similarity measure is a scale invariant weighting factor, which fails to register properly in case of affine transformation. To overcome this difficulty, an attempt has been made to incorporate an affine invariant saliency into the similarity measure. In addition to it, the scale invariant saliency is computed for each pixel pair intensities which enormously increases the computational burden. Hence, an attempt has also been made here to reduce the computation time.

In computer vision system, salient image regions make the computation burden easy permitting the nonuniform allocation of an image. The selection of a proportional set of salient regions forms the first step in the computer vision algorithm. Salient points and region facilitate interest point detection [71] and image matching [72], as they permit immediate attention on object of interest in an image. The study on human visual perception system suggests that the saliency is referred to uniqueness, rarity and attractiveness of a scene, which is represented by visual features such as color, motion, texture and shape etc. Recently, a lot of research attempt have been made to design various algorithms to compute the saliency for static images [73, 74]. Liu *et al.* found multi-scale contrast by linearly combining contrast in a Gaussian image pyramid [73]. Saliency models is roughly divided into two kinds: local contrast and global contrast. Local contrast based methods estimate saliency of a particular patch based on their dissimilarity with its neighbors. Itti *et al.* proposed central-surrounded differences based on a set of pre-attentive image feature [75]. Many techniques have been developed to define the saliency of image, i.e., using edge gradient, local phase, salient regions [76], corner and keypoints [77].

The constitution of salient region and importance of that over other feature selection method was proposed and described in [68]. The authors also discussed about the algorithm with both feature space and scale space. Previously they used a circular window to control the radius [76]. Luan *et al.* obtained the saliency through entropy of the intensity distribution within its neighborhood [38]. But those saliency have some limitations. Also the problem is choice of scale. To overcome this problem, Kadir *et al.* proposed affine invariant salient image detector [78]. For those cases, the features

are considered salient if their feature space properties vary rapidly with an incremental change in radius. Huang *et al.* extended the region extraction criteria to hybrid image registration based on scale invariant salient region [69].

Motivated by the work of Kadir *et al.*, in this chapter, affine invariant salient region (SR) is incorporated into the computation of saliency measure. The SR based saliency further helps in computation of the similarity measure for accurate registration of multi-modal brain images. The proposed affine invariant SR based similarity measure is named as SR-EMI. The proposed registration method not only helps in reducing computation time but also makes the registration robust against affine transformation.

The rest of the chapter is organized as follows. Section 3.2 describes basic concept of saliency, different types of saliency measures. The saliency measure using information theory is discussed in this section. The formulation and justification of proposed registration algorithm using salient region is explained in Section 3.3. Section 3.4 presents the performance analysis with experimental results of proposed method and those in existing literature [38, 79, 80]. Finally, summary is drawn in Section 3.5.

3.2 Materials and Methods

The word saliency refers to the quality of being salient. A given entity is salient if it stands out from other ones in the same domain. The definition is directly applied to image analysis. An image region is visually salient if it is distinguishable from the rest of elements in the image, in terms of intensity, orientation or any other property.

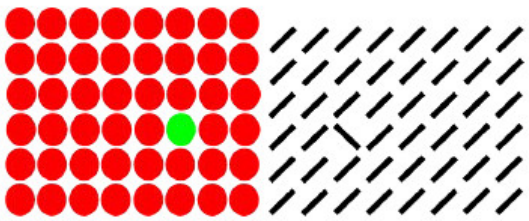

Figure 3.1: Example of visual saliency

In this section we will briefly define the term local visual saliency and we will also introduce the Scale Saliency algorithm proposed by Kadir and Brady [76]. The distinct part which is discriminative, prominent in image regions are referred to as salient. It is the spatial region which attracts the attention in the visual field. The notion of saliency has been studied in computer vision literature. A good saliency region is robust to background changes, intensity variance to pathologies. In Fig. 3.1, the intensity of the green circle makes it salient with respect to the rest of circles in the left side image, where as in the right side image, the salient element is the one with different orientation. Both elements may be considered globally (because they are salient with respect to the

rest of elements of the image) and locally (because they are salient with respect to their neighborhood) salient.

3.2.1 Visual Saliency

Several computational models of selective visual attention have been suggested in [81]. The visual attention models is grouped into two classes, i.e. bottom-up approach and top-down approach. In the top-down approach, a saliency map is computed from the basic visual features such as colour, orientation, spatial frequency, brightness and direction of movement. The saliency map is usually represented as a two-dimensional (2D) grey-scale image, in which the brightness of a pixel is proportional to its saliency. The top-down attention mechanism is volitionally controlled subjective and task dependent model. It is generally used with prior knowledge to completely understand the content and context of the image. This mechanism is mainly used to search for similar objects or patterns in the images. A bottom-up computational model for visual saliency map is introduced based on intensity chromatic channels and orientation. Itti *et al.* [75] computed the similarity measure from local feature contrast between surround and center scales in multi resolution framework using the bottom-up approach.

The approach of Liu *et al.* is based on learning low, medium and high level image features combined with eye fixation location, collected from human observers through eye trading [73]. Unsupervised approach for saliency detection is described in [82], where both low level or pixel features and intermediate region features determine the saliency of each pixel in the image. Mohapatra *et al.* used neurobiology based saliency measure to improve the performance of QMI for rigid registration [83]. They have applied the saliency map for 4D registration of renal perfusion MR images. They applied a soft threshold function to get normalized saliency. Ou *et al.* developed a similar mutual saliency map for outlier rejection in 3-D non-rigid image registration [84]. Chen *et al.* presented a hybrid saliency detection method which predicts the saliency region integrating the low level features and high level cues [85].

In order to extract useful features from images, Kadir *et al.* focused on the detection of locally salient regions (in terms of intensity), i.e. regions with a locally distinguishable intensity distribution. Those regions were supposed to remain salient under several transformations, like for instance scale variations or affine distortion [78]. This property is required by high-level vision tasks that rely on this kind of features.

Gilles was the first researcher to relate saliency in the context of visual image feature extraction to information theory [86]. In information theory, Shannon entropy is an adequate tool to estimate image saliency. It refers to the amount of information contained in an message. It is a measure of the unpredictability associated with a

random variable. The less predictable the value of a random variable is, the more information it provides. Gilles defined salient regions in gray-scale images as piecewise regions that were locally unpredictable, i.e. the set of highest-informative regions in an image (high-entropy regions).

Given a pixel x, with its local neighborhood R_x, and a descriptor d that takes value from $D = d_1, ..., d_n$, where D ranges from 0 and 255 for a 8 bit gray level image, the saliency is estimated by means of Shannon entropy [54] is

$$H_{D,R_x} = -\sum_i P_{D,R_x}(d_i) log_2 P_{D,R_x}(d_i) \tag{3.1}$$

where $P_{D,R_x}(d_i)$ is the probability of D considering the value d_i in the local region R_x. Low entropy values correspond to predictable or low informative random variables, that is, random variables in which the probability of a given random value is much higher than that of the rest of values. On the contrary, higher entropy values correspond to unpredictable random variables, in which the probability of all their possible random values is similar. From information theory, it is observed that highest entropy regions of the image should be detected by using the feature extraction algorithm.

The feature extraction algorithm proposed by Gilles works as follows: firstly, the size and shape of R_x is set. A square region with a fixed radius measured in pixels is assumed. This radius is called as scale. Then, the entropy is estimated for each pixel using Equation 3.1. All pixels with entropy below a given threshold are discarded. The result is a binarized image containing blobs. Finally, the algorithm selects the local entropy maxima in these blobs. These points correspond to the most salient regions in the image.

Although entropy-based saliency estimation is intuitive and simple, the algorithm suffers some limitations [76]. The most evident one is the fixed scale constraint, due to the fact that scale is a preset parameter, the saliency search is constrained to a narrow range of scales. The algorithm is also very sensitive to small noise. Finally, highly textured regions with high intensity variations are usually labeled as salient regions, even if these regions are part of a larger textured region and are not salient from a perceptual point of view.

3.2.2 Scale Saliency

Kadir and Brady proposed their Scale Saliency algorithm in order to deal with the limitations of the Gilles algorithm [78]. This algorithm detects salient regions not only in the image-space but also in the scale-space. Scale limitation is solved by applying the entropy measure to each pixel while isotropically increasing the size of R_x. The output of the algorithm is a set of circular salient regions of different size. Kadir and Brady stated that saliency in a wide range of scales is a consequence of fractal or random

images, or self-similarity measure. In the Scale Saliency algorithm a salient region must be distinguishable both in the feature space and scale space.

The algorithm works as follows: Firstly, the range of scales is set between a minimum scale s_{min} and a maximum scale s_{max}. Then, the entropy of each pixel x at each scale s is estimated from its intensity pdf

$$H_D(s,x) = -\sum_{d\epsilon D}(P_{d,s,x})(log_2 P_{d,s,x}) \tag{3.2}$$

where $P_{d,s,x}$ is probability density as a function of scale s, position x and descriptor d, which takes on values from D. Next, the algorithm detects entropy peaks in the scale-space, that is, local maxima of the entropy function:

$$S_p = s : H_D(s-1,x) < H_D(s,x) > H_D(s+1,x) \tag{3.3}$$

The entropy of x in scales $s\epsilon S_p$ is weighted by means of a measure of self-dissimilarity in the scale-space. The self-dissimilarity measure allows the computation of direct saliency value between pixels at different scales and penalizes those features that are salient in a wide range of scales. The inter scale saliency measure, $W_D(s,x)$ is defined as

$$W_D(s,x) = \frac{s^2}{2s-1}\sum_{d\epsilon D}|Pd,s,x - Pd,s-1,x| s : H_D(s-1,x) < H_D(s,x) > H_D(s+1,x) \tag{3.4}$$

The saliency of a region in terms of weighted entropy is computed for those scales $s\epsilon S_p$ as

$$Y_D(s_{p,x}) = H_D(s_{p,x})W_D(s_{p,x}) \tag{3.5}$$

The output of the Kadir and Brady algorithm is an array $Y(S;X)$ that stores the saliency for every pixel $x\epsilon X$ in the selected scales. The salient region of the image are the maxima in $Y(S;X)$. Being K as neighborhood and V_{th} as variance, two preset parameters, the steps of the feature clustering process are:

- Choose the highest salient region in $Y(S;X)$
- Find its k nearest neighbors
- Calculate the variance V of their center points, the mean scale s_{mean} and the mean location x_{mean}.
- Find distance D in R^3 (image row, image column, scale) from the selected region to salient regions already clustered

- Create a new salient region with scale s_{mean} and location x_{mean} if $D > s_{mean}$ and $V < V_{th}$.
- Repeat from the second step with the next highest salient region until a percentage of elements in $Y(S; X)$ is processed.

3.3 Proposed Registration Framework

The main problem of the Scale Saliency algorithm is the inefficiency towards view point changes in the image and computation of joint utility or saliency [87]. Even if histograms are reused along the scale-space, the bottleneck of the algorithm is the estimation of Shannon′s entropy in Equation 3.2 for every pixel at every scale in the range $[s_{min}, s_{max}]$. In this work, a new image registration technique is proposed based on salient region based saliency measure instead of pixel based saliency measure for obtaining the similarity measure. A well-defined region saliency measure is adopted that consists of both local adaptive variance and gradient field entropy to extract the salient region (SR) in each image. Further, local saliency measure is computed to get more information from the neighborhood regions with less computation time. Then, the new similarity measure EMI as proposed in the previous chapter is computed. The rigid registration (translation, rotation, scaling) is performed to compute the new similarity measure between the floating image with respect to the reference image. Finally, the two images are registered by adopting a global transformation model with locally well-aligned region centers as control points.

The block diagram of the proposed scheme is shown in Fig. 3.2.

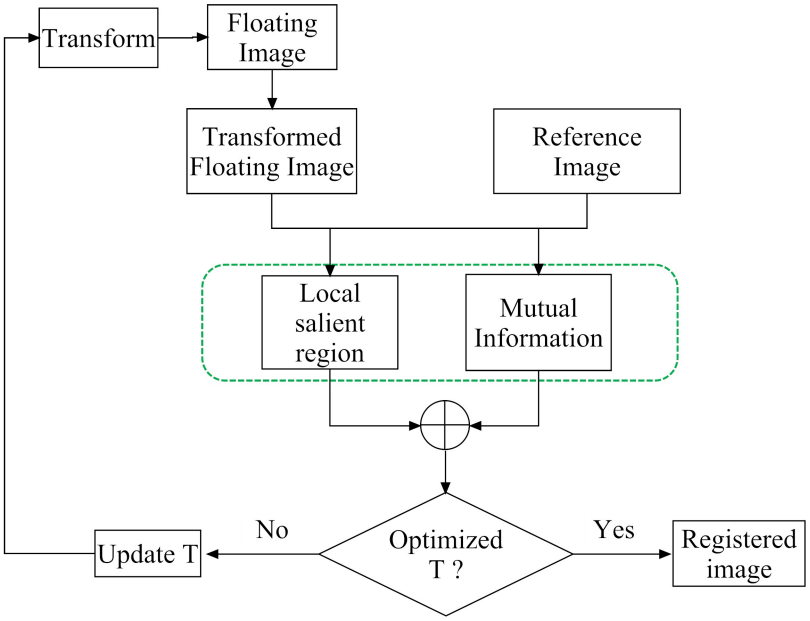

Figure 3.2: Block diagram of proposed image registration scheme

3.3.1 Salient Region (SR)

Self information is the more appropriate metric than entropy, is presented by Bruce *et al.* [88]. Also Kadir *et al.* proved this in [76]. They described the image region saliency in the following two aspects: local intensity variance saliency and local structural saliency. For intensity variance saliency, the coefficient of variation is an effective evaluation criterion. The local intensity variance saliency of region R is defined in terms of adaptive variance $(Av(R))$:

$$Av(R) = \frac{\sigma}{\mu} \tag{3.6}$$

where σ is the standard deviation of R and μ is the mean value of R. The $Av(R)$ characterizes the intensity variance saliency of region R and guarantees the invariability of SRs to local linear scale change in pixel intensities. According to information theory [54], entropy is appropriate for measuring local structural saliency. In this work, local gradient field entropy is used. Here, the 2-D direction angle $\pi/2, 3\pi/2$ is divided into 36 bins uniformly. For a given pixel X_i, the index of 2-D direction angle is denoted as direction (X_i), and is computed as:

$$direction(X_i) = \begin{cases} \left\lceil \frac{\arctan(g(X_i))+\frac{\pi}{2}}{\frac{2\pi}{36}} \right\rceil, & g_x(X_i) \geq 0. \\ \left\lceil \frac{\arctan(g(X_i))+\frac{3\pi}{2}}{\frac{2\pi}{36}} \right\rceil, & g_x(X_i) < 0. \end{cases} \tag{3.7}$$

where $\lceil . \rceil$ denotes the ceil operator and $g(X_i) = (g_x(Xi), g_y(Xi))$ denotes the gradient vector of pixel X_i. The local gradient field entropy of region R, denoted as $Lge(R)$, is computed as:

$$Lge(R) = -\sum_{i=1}^{36} p_i(R) log_2 p_i(R) \tag{3.8}$$

where

$$p_i(R) = \frac{\int_{R_i} |g(X_i|) dX_i}{\int_R |g(X|) dX} \tag{3.9}$$

and

$$R_i = \{X_j | X_j \in R \wedge direction(X_j) = i\} \tag{3.10}$$

To reduce the effect of pixels with low gradient magnitude, that are influenced by intensity variance and background changes, a magnitude weighted strategy is adopted. Combining the variance and local gradient field entropy, the local saliency measure of region R is formulated as $Ls(R)$,

$$Ls(R) = Av(R) Lge(R) \tag{3.11}$$

3.3.2 Proposed Affine Invariant Similarity Measure

The main issue of scale-invariant saliency methods is that their scale-space representation is based on isotropic Gaussian kernels. They detect isotropic (circular) interest regions. But, similarity invariant also includes geometric transformation along with photometric shifts. Circular regions can not cope with certain affine transformations, like those generated by viewpoint variations. Hence, an affine-invariant saliency is needed for this salient region extraction. An affine invariant saliency is presented in [78]. This saliency extracts anisotropic (elliptical) regions by means of a non-uniform scale-space representation, which is shown in Fig. 3.3.

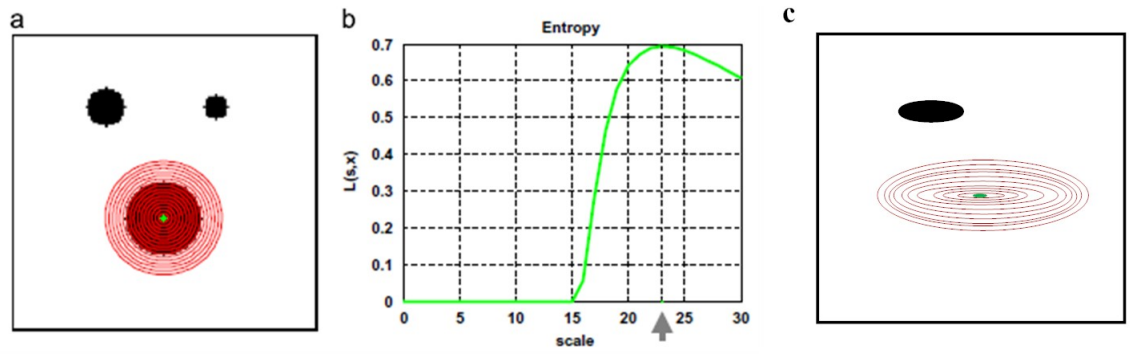

Figure 3.3: Example of finding salient regions with ellipse

The region R in affine saliency is parameterized by three parameters (s, ρ, θ). where s is the scale factor, ρ is the axis ratio and θ is the orientation of the ellipse. It increases the search space of previous saliency measure, from a scale to set of parameters. Hence, complexity increases. It starts with the set of points and scales generated from scale saliency then iteratively approximates the suboptimal parameters. The example of extracted salient regions using affine invariant saliency measure is shown in Fig. 3.4.

In this chapter, an affine invariant saliency measure using SR is encoded into Enhanced Mutual Information (EMI). Motivated by the saliency measure proposed by [78, 80], and using the SR $Ls(R)$ given in Equation 3.11, a new similarity measure is proposed for image registration. Here, the saliency or the utility of each pixel is calculated according to the regional saliency value. Voxels with higher saliency value contributes more towards the calculation of similarity measure. After calculating the local saliency region of both images as in Equation 3.11, the joint utility or saliency, which is the weight information to EMI is computed. The joint weighted information is calculated as

$$w_n(r, f) = \sum_{i,j \varepsilon \varsigma} Ls_r(i).Ls_f(j) \tag{3.12}$$

where ς is the overlap region of both images. $Ls_R(i)$ and $Ls_F(j)$ are the weighted values of pixel i and j respectively in images R and F respectively.

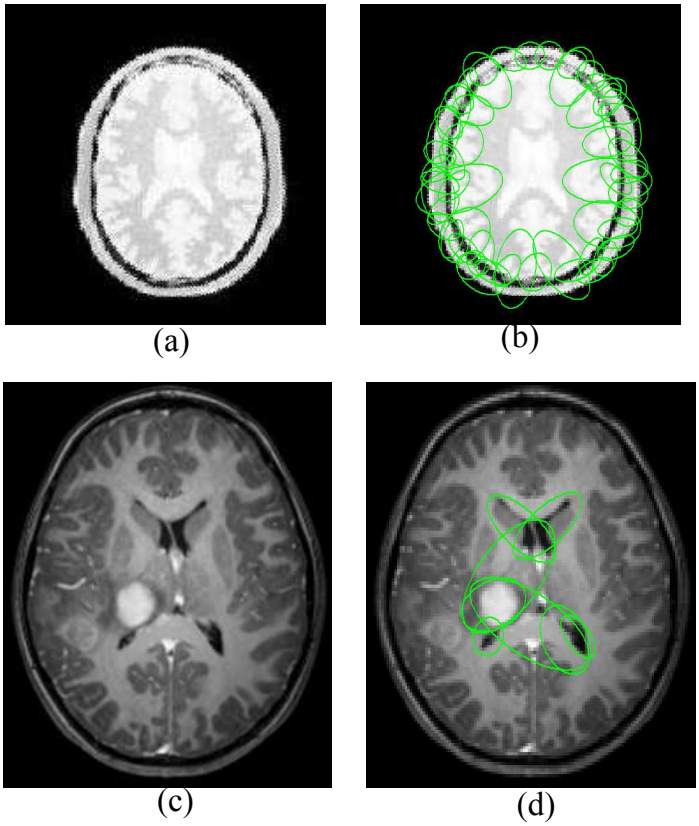

Figure 3.4: (a,c) PD image, Pre operative brain MR image respectively, and (b,d) Extracted salient regions with affine invariant saliency

The proposed similarity measure adopting the SR based saliency measure is defined as

$$SR-EMI(R,F;W)=\sum_{r\epsilon R}\sum_{f\epsilon F}p(r,f)log\frac{p(r,f)}{p(r)p(f)}+w(r,f)p(r,f) \tag{3.13}$$

where $w(r,f)$ is the joint saliency region. This similarity measure is termed as salient region based enhanced mutual information (SR-EMI).

3.3.3 Image Registration using SR-EMI

In Chapter 2, it is found that the information gain in EMI measure is more than that of QMI measure due to utility or saliency. Maximizing the similarity measure during registration procedure, enables proper alignment of transformed floating image (F^*) with respect to reference image (R). The optimal transformed parameters are obtained by Equation 2.1. Adopting the proposed scheme as presented in Fig. 3.2, the proposed similarity measure SR-EMI between R and F^* with transformation parameter t^* and new weighed parameter as saliency is evaluated by

$$SR-EMI(R,F;W)=\sum\sum p(R,F^t)log\frac{p(R,F^t)}{p(R)p(F^*)}+w(R,F^t)p(R,F^t) \tag{3.14}$$

The algorithm of the proposed scheme is as follows:

Algorithm 2: SR-EMI based registration Algorithm

Input: I_r, $T(I_f)$
Output: t^* with high cost function

```
Initialize geometric transformations
for each transformation − step = 1 to n do
    Calclate the cost function as given by Equation 3.14
    repeat
        Use Powell technique to solve the optimization problem as in Equation 2.1
        Update the joint utility using Equation 3.12
        Recalculate the cost function
    until ;
    The Diff(f_c) in three consecutive transformation steps is ≤ 0.01
end
```

$Diff(f_c)$ is the difference of the cost function.

3.4 Simulation and Results

Several number of experiments have been carried out to evaluate the performance of the proposed salient region based similarity measure for the registration technique. The T1, T2 and PD weighted images that are taken for simulation are mentioned in 2.4. Two sets of Pre and Post operative brain MR images are also considered for the validation of the proposed scheme, which are taken from internet source (http://medind.nic.in). Those images are of size 256×256 pixels. The scale difference in multi-modal images is due to different pixel size.

In this work, the simulation based experimentation on registration have been performed with five different cases (reference image with floating image).

- **Case I**: MR T2 weighted image with translated T1 weighted image.
- **Case II**: MR T1 weighted image with translated T2 weighted image.
- **Case III**: MR T2 weighted image with rotated PD-weighted image.
- **Case IV**: Pre and post operative brain MR image data set of same subject.
- **Case V**: Pre and post operative brain MR image data set of same subject.

Here, we highlight the registration function for different cases, comparing the behavior of scale and affine invariant saliency measure incorporated into EMI and SR-EMI based similarity measure. The saliency of the images using scale and affine invariant saliency measures are shown in Fig. 3.5. We evaluated the efficacy of the

proposed similarity measure for multi-modal images by comparing different performance measures with those of other state-of-art methods.

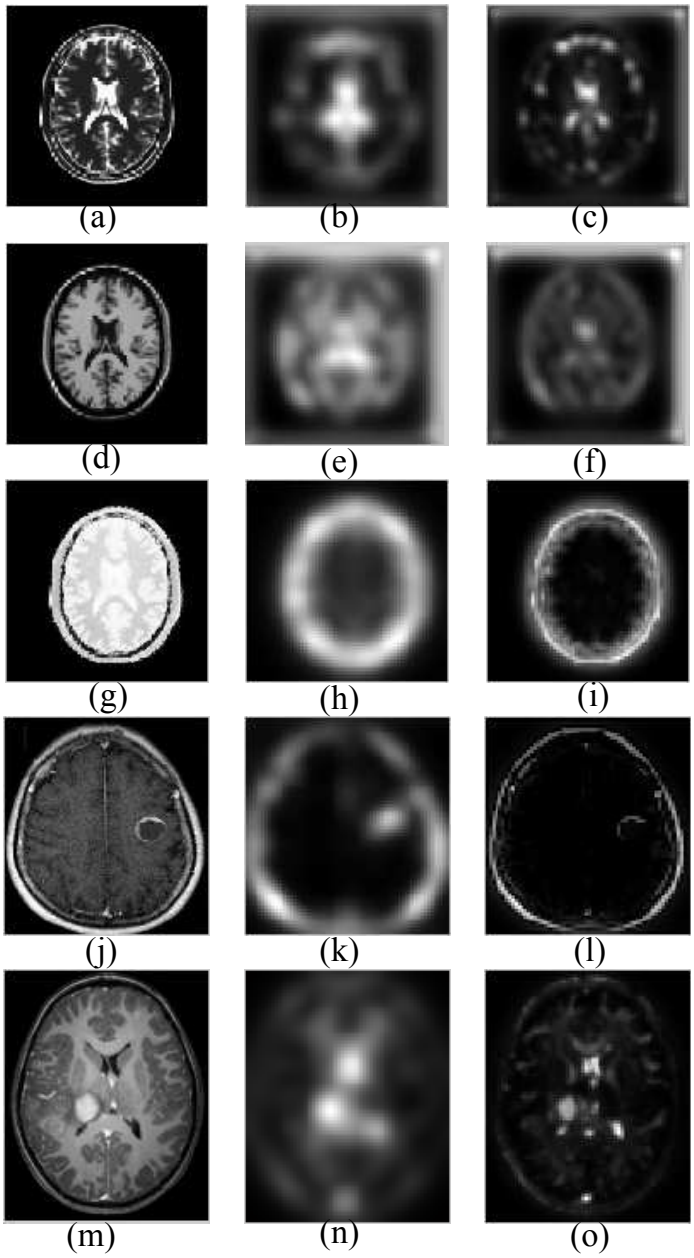

Figure 3.5: (a,d,g,j,m) Input images, (b,e,h,k,h) Saliency using scale invariant saliency, and (c,f,i,l,o) Saliency using affine invariant saliency

3.4.1 MR T1, T2 and PD weighted image data set

For evaluation of the proposed scheme, three sets of MR images are chosen i.e Case I, Case II and Case III. For all set of images, the axis ratio is considered as 1/5, and θ defines the orientation of the image. As discussed in Section 3.3.2, the major and minor axis of the ellipse are considered as $s/\sqrt{\rho}$ and $s.\sqrt{\rho}$ respectively. In Case I, the simulated T2 weighted image is considered as the reference image whereas T1 weighted image is taken as the floating image which are shown in Fig. 3.6 (a,b) respectively. The floating image is rotated around X-axis, then translated along x and y axis respectively. In the previous chapter, we found that our proposed EMI based registration method outperforms the other state of the art methods. Therefore, in this chapter we have considered EMI and QMI based similarity measures for performance comparison analysis of the proposed scheme. The checker board image (CBI) after registration using the proposed SR-EMI, EMI and QMI based similarity measure, with the three types of transformations (rotation around X-axis, translation along X and Y axis) are shown in Fig. 3.6 (c-e), (f-h), and (i-k) respectively. From this, it is observed that, the registered image using SR-EMI is accurately aligned rather than that of the EMI and QMI based registration scheme. Similarly, for Case II, the reference image is T1 weighted and the floating T2 weighted image is transformed with rotation and translation parameters. The floating image is rotated about X axis with 15 degree and registered with respect to the reference image using SR-EMI, EMI and QMI based registration schemes. The corresponding CBI after registration are shown in Fig. 3.7 (c-e). Similarly, the floating image is translated along X axis with 15 mm, and the CBI after registration using the proposed SR-EMI along with EMI and QMI based registration schemes are shown in Fig. 3.7 (f-h). Fig. 3.7 (i-k) shows the CBI after registration of the floating image that is translated along Y axis with respect to the reference image. For the above two cases, the proposed scheme is compared with EMI and QMI based registration method using different performance measure such as MRE, PSNR, NCC, and computation time, which are recorded in Table 3.1.

Similarly, for Case III, PD weighted image is rotated around X axis with 30 degree, is considered as floating image and T2 weighted image is taken as the reference image. Though the structures are similar containing detailed anatomical information, the images are multi-modal due to different tissue characteristics. The saliency of the corresponding location helps to register the images with maximum information gain. To evaluate the proposed SR-EMI based registration technique, we have performed a quantitative validation for this case considering different transformation parameters. The SM value along with the performance measures are tabulated in Table 3.1. The SM value is found to be 1.79 in case of SR-EMI based registration method, whereas in case of EMI and QMI it is 1.63 and 1.42 respectively. Also, the MRE of SR-EMI is 3.54, which

is lower than those of EMI and QMI based registration scheme. Similarly, the PSNR and NCC value of SR-EMI are higher as compared to other methods. It demonstrates that the proposed method outperforms both EMI and QMI based registration schemes. The enhancement of the SM value is due to the incorporation of salient region based utility into EMI based similarity measure. The recorded computation time for the proposed SR-EMI based registration scheme is 107 sec, but in case of EMI and QMI, the computation time is 94 sec and 88 sec respectively. Though the computation time is more in case of SR-EMI scheme, it significantly reduces the mean registration error (MRE) of different tissues as compared to EMI and QMI based schemes.

Table 3.1: Performance Measures for all Cases

Case	Methods	SM value	MRE	PSNR	NCC	Time (s)
I	**SR-EMI**	**1.88**	**1.42**	**16.58**	**0.83**	**89**
T1-T2 rotated	EMI	1.73	2.63	12.59	0.58	85
about x-axis	QMI	1.62	3.89	12.09	0.54	80
II	**SR-EMI**	**1.67**	**1.54**	**17.33**	**0.72**	**88**
T1-T2 rotated	EMI	1.55	2.24	16.75	0.57	84
about x-axis	QMI	1.31	2.81	16.19	0.49	78
III	**SR-EMI**	**1.79**	**3.54**	**13.63**	**0.58**	**107**
T1-T2 rotated	EMI	1.63	4.34	11.75	0.50	94
about x-axis	QMI	1.42	4.61	11.49	0.47	88
IV	**SR-EMI**	**1.92**	**3.05**	**14.97**	**0.39**	**98**
Pre-post operative	EMI	1.60	3.36	12.95	0.34	74
Brain MR image	QMI	1.15	3.56	12.84	0.33	70
V	**SR-EMI**	**2.12**	**2.09**	**16.27**	**0.46**	**105**
Pre-post operative	EMI	1.90	3.16	15.86	0.38	89
Brain MR image	QMI	1.75	3.40	14.74	0.32	85

3.4.2 Pre and post operative brain MR image data set

For Case IV, a set of pre and post operative brain MR image of same subject is also considered for the validation of the proposed scheme. The reference and floating image for evaluation of the proposed salient region based similarity measure for the registration framework are shown in Fig. 3.8 (a,b) respectively. Fig. 3.8 (c) shows the checker board image (CBI) before registration. The registered image using SR-EMI, EMI and QMI based registration schemes are shown in Fig. 3.8 (d-f) respectively. Corresponding CBI as well as difference images after registration are shown in Fig. 3.8 (g-i) and (j-l) respectively. The related SM values and the performance measure values are tabulated in Table 3.1. From the table, it is observed that, the SM value for proposed SR-EMI is 1.92, whereas for EMI and QMI based registration scheme it is found to be 1.60 and 1.15 respectively. This signifies the augmentation of the similarity value in case of SR-EMI due to the incorporation of affine invariant salient region based utility factor. The

elliptical window used for saliency measure could be able to extract more qualitative information than the circular window based scale invariant saliency. This SR based weighted relative entropy measure (SR-EMI) enables to align more accurately than that of a weighted entropy and weighted relative entropy (EMI) measure. The recorded computation time for the proposed scheme is 98 sec, which is more as compared to other methods. Though, the computation time is more, mean registration error (MRE) is reduced significantly in case of SR-EMI based scheme because of the above factors. Similarly, the PSNR and NCC values are higher for the proposed scheme.

For Case V, another set of pre and post operative brain MR images is experimented for the evaluation of the proposed scheme. The SM value along with the performance measures are tabulated in Table 3.1. The SM value in case of SR-EMI is found to be 2.12, which is higher than EMI and QMI based registration schemes. The MRE of SR-EMI is 2.09, whereas for EMI and QMI MRE is 3.16 and 3.40 respectively. The reduced MRE signifies the efficiency of SR-EMI based registration scheme. Similarly the PSNR and NCC value of SR-EMI is 16.27 and 0.46 respectively, which are more as compared to EMI and QMI based registration schemes. The computation time for SR-EMI is 105 sec. which is more as compared to EMI and QMI. Though the affine invariant based salient region enhanced the similarity measure value, with improved PSNR, and NCC measure, the computation time is more due to the computation of the set of parameters (s, ρ, θ) for affine invariant saliency.

The comparison of recorded similarity measure value and MRE for Case (I-V) are plotted in Fig. 3.9 and Fig. 3.10 respectively. For all the cases, the SM value is maximum in case of SR-EMI based registration scheme as compared to the EMI and QMI based registration scheme. Also, the observed MRE for our proposed scheme is lower for the five cases as compared to the other state of the art methods.

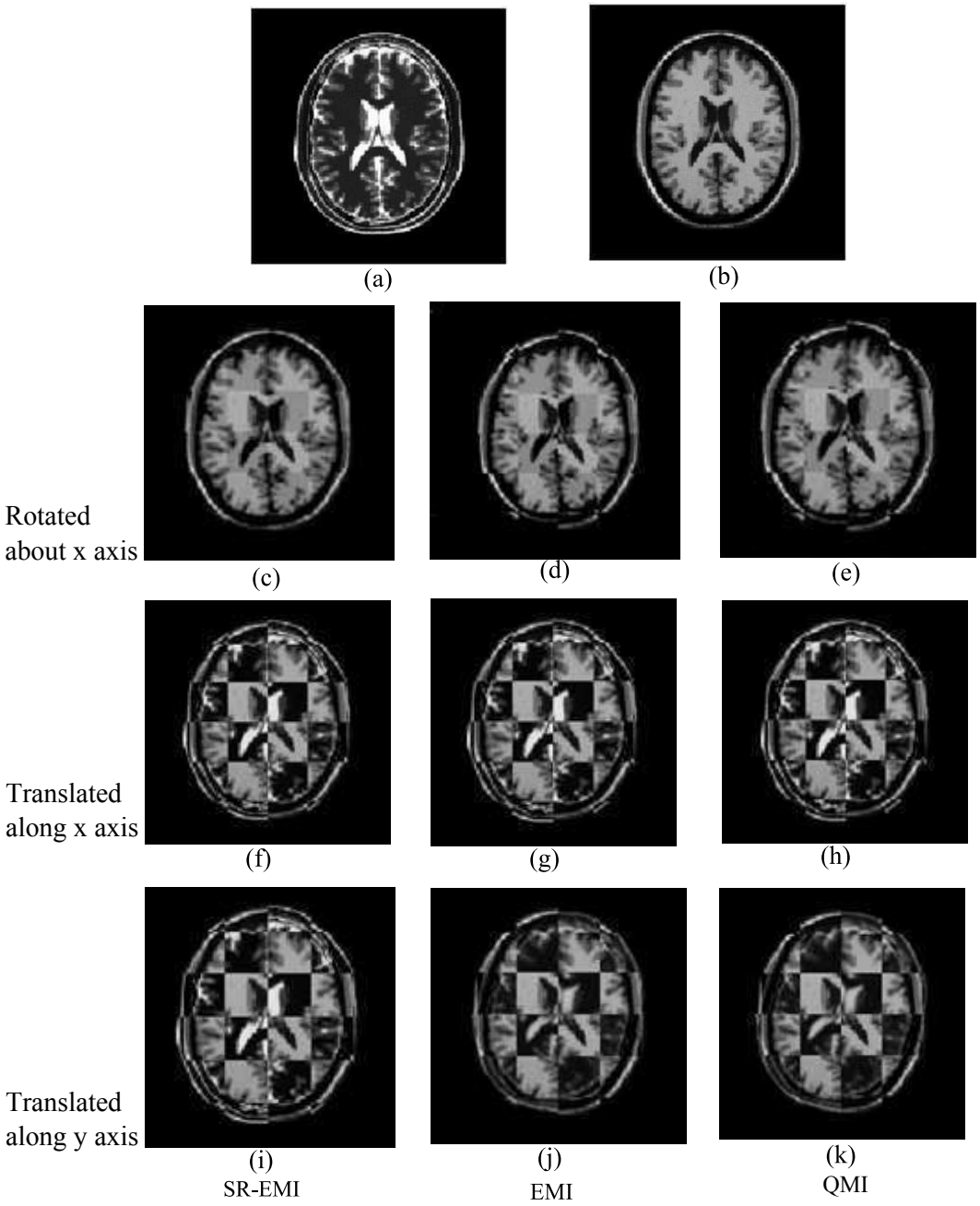

Figure 3.6: (a) Reference image, (b) Floating image;
CBI image after registration using SR-EMI, EMI and QMI based registration scheme respectively for transformation: (c-e) Rotated about x-axis, (f-h) Translated along x axis, and (i-k) Translated along y-axis for Case I

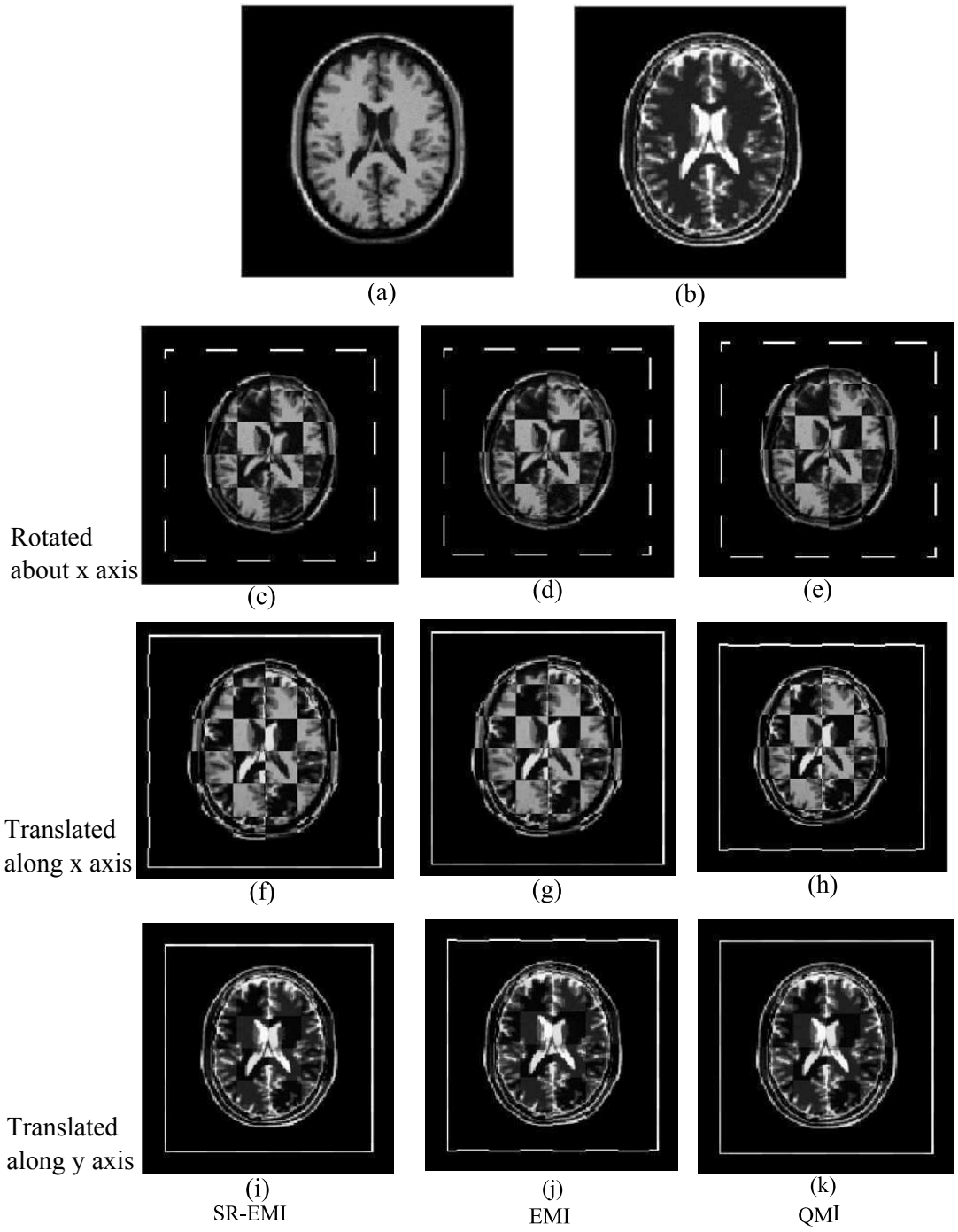

Figure 3.7: (a) Reference image, (b) Floating image;
CBI image after registration using SR-EMI, EMI and QMI based registration scheme respectively for transformation: (c-e) Rotated about x-axis, (f-h) Translated along x axis and (i-k) Translated along y-axis for Case II

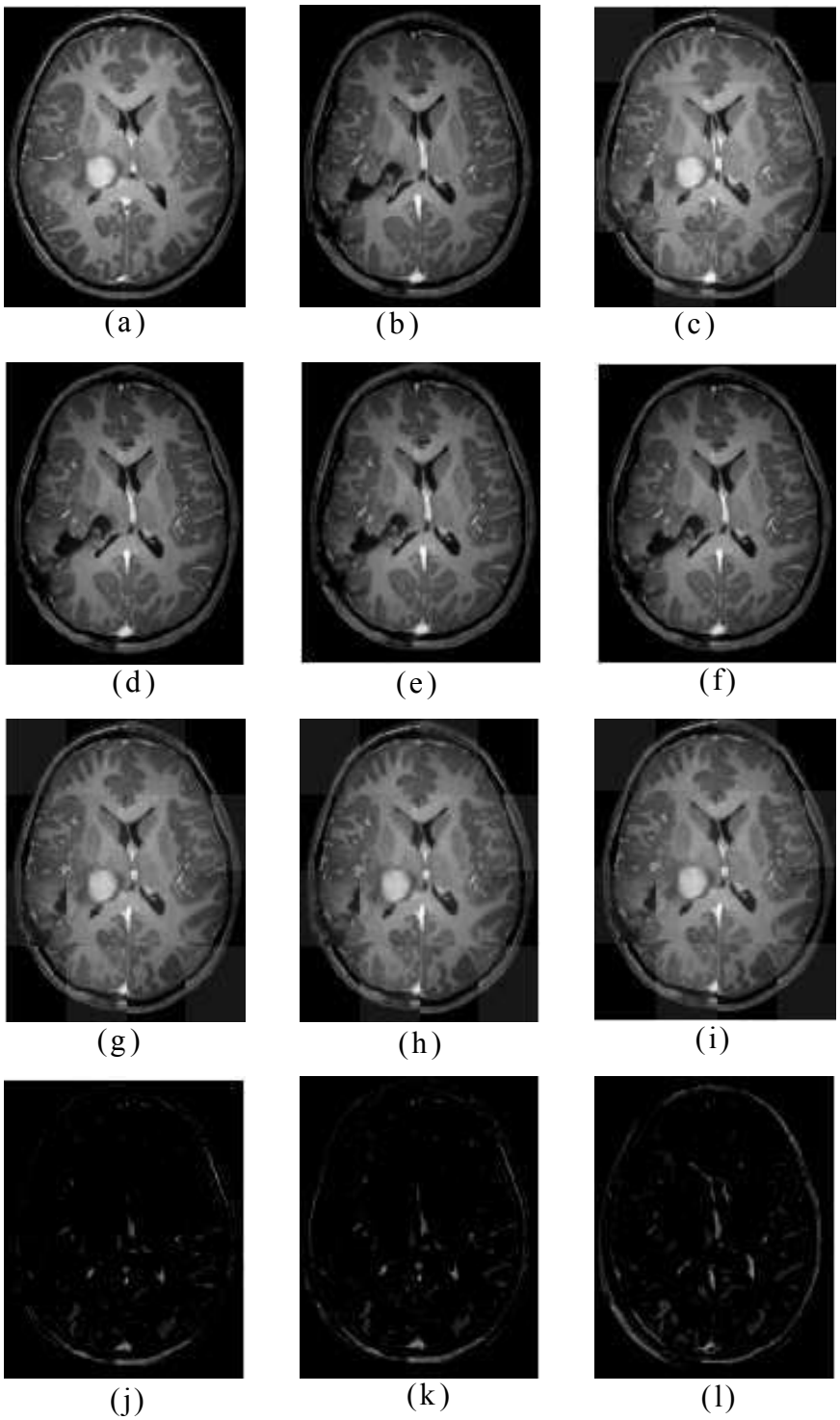

Figure 3.8: (a) Reference image, (b) Floating image, (c) CBI before registration, (d-f) Registered image, (g-i) CBI after registration, (j-l) Difference image after registration using SR-EMI, EMI and QMI based registration scheme respectively for Case IV

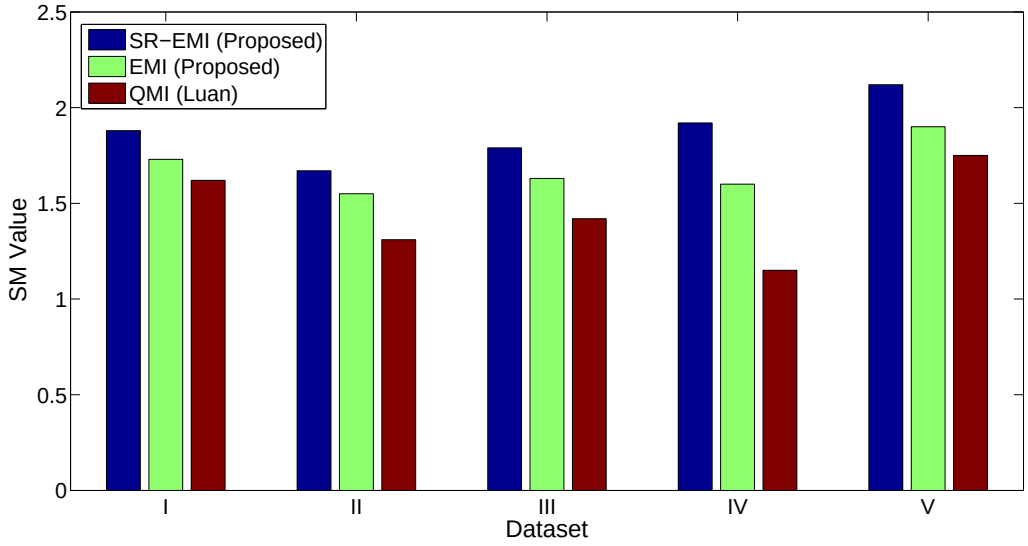

Figure 3.9: Comparison of SM value using proposed SR-EMI, proposed EMI and QMI based registration for all Cases

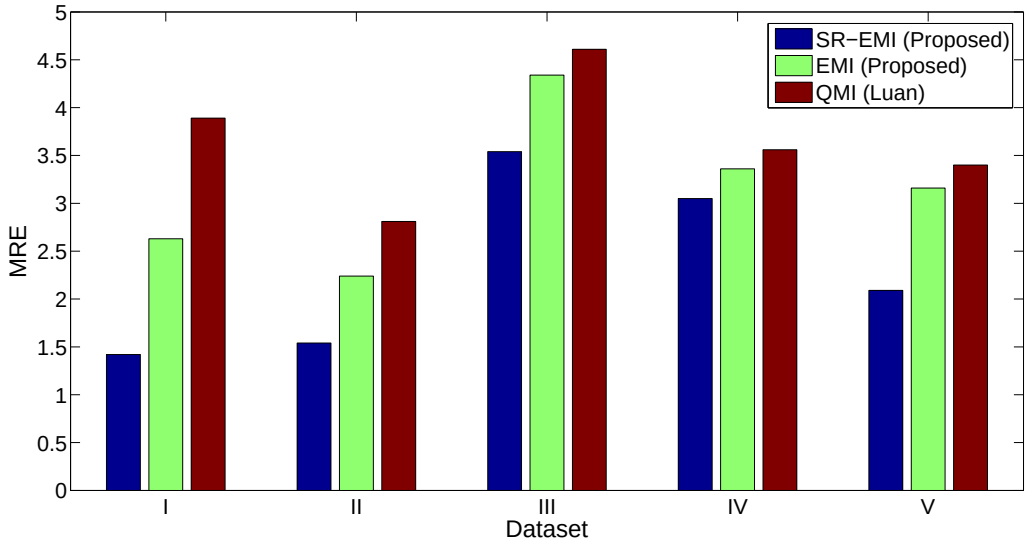

Figure 3.10: Comparison of MRE using proposed SR-EMI, proposed EMI and QMI based registration for all Cases

3.5 Summary

In the previous chapter, the utility used in the proposed similarity measure is a scale invariant weighting factor, which fails in case of affine transformation. To overcome this bottleneck, in this chapter an attempt has been made to propose an affine invariant similarity measure for accurate alignment of multi-modal brain images in case of affine transformation. In our proposition, new saliency measure i.e. salient region (SR) is incorporated as utility factor to EMI. The joint probability of the images are found through region based similarity measure. The combination of SR and the joint probability enhances the qualitative-quantitative measure of relative information and is found to be a better similarity measure than EMI and other existing state of art for intensity based image registration. Five number of multi-modal brain image data sets were considered for experimentation and performance evaluation. The SM value is increased where as MRE is decreased significantly in case of the proposed SR-EMI based registration scheme. The performance analysis shows that the SR-EMI based registration algorithm outperforms the similar existing algorithms.

Though the incorporation of a saliency measure as the utility factor enhances the similarity measure but it suffers when the images are geometrically deformed. Again the registration problem becomes intractable when pre and post operative brain MR images are taken for radiological analysis through image registration. To overcome this challenge, an attempt has been made to develop non-rigid transformation based image registration, which is discussed in the following chapter.

Chapter 4

Non-rigid Image Registration using Spline based Interpolation

In the previous chapters, we were dealing with registration of images with rigid transformations i.e. rotation, translation and scaling and affine. Images of different patients may be very dissimilar due to a normal variability of organs, i.e. human brain. Therefore, rigid-body transformations is not sufficient to match the shape and soft tissue structures of the organs. Affine transformations consisting of rigid-body + scaling + shear can accommodate for this normal variability. But may not be sufficient for the cases where local matching is required for utilization of non-linear deformations. In this chapter, non-rigid transformation is considered for registration framework and the spline interpolation method is proposed for efficient registration of multi-modal brain images.

4.1 Introduction

Image registration is an important tool in atlas matching, image fusion, brain mapping and intra operative image guided surgery for the last two decades. It is the process of finding the optimal transformation of the deformed image with respect to the reference image, which may be divided according to the type of transformation, i.e. affine and non-rigid transformation. Many researchers experimented on affine transformation for image registration [89]. But geometrically deformed images fail to transform with affine transformation based registration. To overcome this problem, non-rigid registration technique is accustomed for transformation of deformed images [47]. As the brain anatomy is deformable in nature, and the analysis depends on various imaging modalities, multi-modal non-rigid brain image registration is an important task for the researcher.

The important applications of non-rigid registration are:

- Alignment of an image or a set of images with an image template for statistical analysis of functional or anatomical variability both at normal and abnormal condition.
- Alignment of a model of anatomy with a particular image for the purpose of segmentation and interpretation.
- Construction of normal and disease-specific atlases and normative images.

Non-rigid transformations are important not only for applications to non-rigid anatomy, but also for inter-patient and intra-patient registration of rigid anatomy when there are non-rigid distortions in the image acquisition procedure. In all cases, it is preferable to choose transformations and the choice is made on the basis of convenient mathematical properties. In most cases, the transformed position of pixel or voxel in the deformed image will not necessarily coincide exactly with a grid point of the reference image. Therefore interpolation method is needed to obtain the intensity value of that point. Interpolation estimates the intensity value of that point from its neighborhood points with integral coordinates. The interpolation methods differ according to their relative quality and computational complexity of the estimation. The simplest method is the nearest neighbor approach while other includes bilinear interpolation, trilinear interpolation, and cubic interpolation.

As interpolation influences the transformations at nongrid point, that can cause a sudden change in the value of the similarity measure, resulting in a pattern of local extrema. The occurrence of such patterns has been described in several literature [35, 55, 90]. In [91], different patterns created by linear and partial volume interpolation

(PVI) are extensively studied. Likar and Pernu overcome this artefact problems in the registration functions of subimages, by random re-sampling of the image grids [92]. Chen et al. developed a new scheme for joint histogram estimation named generalized partial volume estimation (GPVE) and compared with PVI [12,93]. In GPVE, a kernel function is employed in each of the x and y directions to estimate the joint histogram of two images. To find the local details of deformed image with flexible matching, spline based non-rigid registration has been proposed, which overcomes artifacts problem caused by PVI and GPVE [94].

Due to the properties such as smoothness, faster and compact support, B-spline interpolation have been popularly used for non-rigid registration [94]. Thevenaz et al. and Mattes et al. used B-spline interpolation for 3D multi-modal non-rigid registration [35, 95]. However, deformation with high degree of freedom leads to unrealistic transformation result. Hence, regularization is needed to overcome the folding effect of transformation based on spline bases. Rueckert et al. penalized the bending energy of deformation field for registration to get the smooth transformation [21]. Similarly Chun et al. used jacobian penalty method to penalize the deformation transformation at each grid point of the image [28]. Motivated by the same, we applied penalty to the B-spline bases at each grid point of the deformed floating image.

The main contribution in this chapter is to develop an interpolation scheme for non-rigid registration based on free form deformation (FFD) transformation. The Penalized spline (P-spline) based transformation model is proposed for the non-rigid registration framework. EMI is used as a similarity measure; second derivatives of similarity measure were adopted as the smoothness function, and iterated with gradient descent optimization method. Though P-spline based transformation enhanced the efficiency for reformation with weighted information, it suffers with computation burden. So, an adaptive Penalized spline (AP-spline) interpolation scheme is proposed which reform the local transformation of the grid points at finer level. The proposed transformation function using adaptive P-spline interpolation provides smoother cost function than that of other existing transformation function.

The rest of the chapter is organized as follows. Section 4.2 describes basic concept of FFD based transformation. Different types of transformation models are also described in this section. The formulation of proposed P-spline and AP-spline based transformation model are explained in Section 4.3. Section 4.4 presents the performance analysis with experimental results of proposed method and those in existing literature [20, 27, 31, 93]. Finally, summary is drawn in Section 4.5.

4.2 Materials and Methods

Rigid body transformations are used when there is no changes in the shape of the structure being imaged. In rigid transformation, only rotation and translation transforms are allowed where as affine transformations allow skew and scaling in addition to rotation and translation. To define free-form mappings, deformable transformations are used with regularization constraint to limit the allowable solution space, also known as non-rigid registration. Non-rigid registration technique is also known as local registration, where the deformations perform through

- image features such as anatomical structures that utilize the geometrical information
  or
- intensity values where the intensity values are taken to find the transformation of interest
  or
- both geometrical information and intensity value.

4.2.1 Transformation Model

The transformation model defines the procedure to transform the deformed image with a set of parameters or degrees of freedom to match the reference image. It is performed by a transformation function, which contains information about geometric differences between the images. This information is sometimes crucial in understanding the contents of the underlying image, as the presence of sharp geometric differences may be due to the local motion or deformation of the image. Hence, deformable registration techniques are more complex and difficult to validate. Non-rigid transformations are categorized into the parametric and non-parametric approach [96]. The parametric transformations depend on a set of parameters. This approach is well posed due to small degree of freedom and is important in clinical applications including inter-subject brain registration and dynamic contrast breast MRI registration. Non-parametric image registration methods estimate the transformation as an unknown function within the variational calculus [97]. The non-parametric approach allows to model complex local deformations with exhaustive computational burden.

4.2.2 Free Form Deformation based Transformation

The goal of free form deformation (FFD) is modeling of arbitrary deformations applied to the image, which are manipulated geometrically. In FFD, the image is manipulated by a regular grid of control points that are distributed across the image at an arbitrary

mesh resolution. Control points are moved and the position of individual pixels between the control points is computed from those of surrounding control points. The techniques based on free-form deformations are attractive for smoothness property that are enforced using suitable basis functions [5,47]. The control points are placed at variable distances, giving a flexible way of controlling deformation precision. The spacing between the control points are used to control the local transformation. That means, more number of control points gives accurate transformation.

The problem becomes ill posed in intensity based registration methods. As the pixel in the deformed image is mapped to any point within a homogenous intensity region without changing the similarity metric, there will be ambiguous in the transformation since the correspondence between the transformation and the similarity measurement is not unique. In order to choose one deformation from transformations space, an extra constraint is added to make the transformation regular and smooth as well. The regularization constraint is an energy which is related to the change of the displacement field. The smaller change in displacement field gives lower regularization energy. Different kinds of regularization energies are used to smooth the control grid that are, first order and second order regularization [98]. Here, the second order regularization is used. It makes the control grid to be second order continuous.

4.2.3 Spline based Image Transformation

A B-spline based Interpolation

Interpolation is a strategy which evaluates the intensity value of the pixel at a new position after transformation to a non integer position. Mostly used interpolation techniques are nearest neighborhood, bilinear interpolation and cubic interpolation [19]. Cubic interpolation gain more popularity in case of medical imaging analysis [9, 28]. The letter B in B-spline refers to Basis. B-splines are the piecewise polynomial curves that have a parametric representation. B-spline parametrization uses a mesh of control points and interpolates with the B-spline basis functions. The shape of the B-spline basis functions and the sparseness of control points limit the admissible transformations. Cubic B-splines are most popular parametric non-rigid transformation parametrization [99]. It is expressed as

$$f_t^c(x) = \sum_{i \epsilon I_b} f_1 \beta_n(x - i) \tag{4.1}$$

where β_n is the tensor product of B-splines of degree of n, that is $\beta_n(x) = \Pi_{k=1}^{N} \beta_n(x_k)$, with $x = (x_1, ..., x_N)$, f_t^c is the image under the B-spline based deformation, f_1 is the pixel intensity at the neighboring 4×4 points around the point x, and c is the B-spline control grid. Fig. 4.1 (c) shows an example of interpolation of transformed grid on to

reference grid, where Fig. 4.1 (a) is the reference image grid and Fig. 4.1 (b) is the transformed floating image grid.

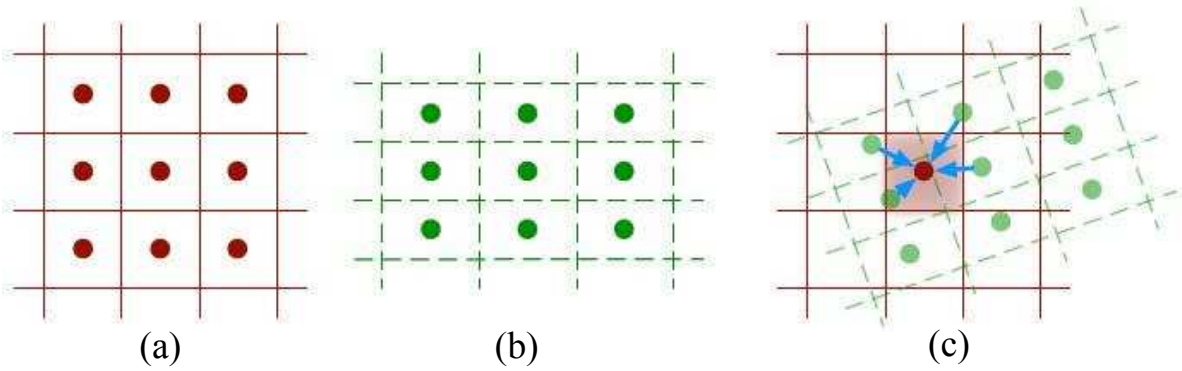

Figure 4.1: (a) Reference image grid, (b) Floating image grid, (c) Interpolation of transformed floating image to reference image

B B-spline based Deformation

The key advantage of cubic B-splines is, these are twice differentiable and continuous at the joints. They can model localized deformations with low computational complexity. Due to its wide popularity in medical image analysis, cubic B-spline is used as transformation model [20, 100]. To control the deformation field in brain images, 3^{rd} order B-spline is used. Medium number of control points are used to control the B-spline based deformation.

Considering a domain of imaging as $\Omega = (x, y, z)|0 \leq x < X, 0 \leq y < Y, 0 \leq z < Z$. Θ as a mesh of n_x, n_y, n_z control points φ_{ijk} with uniform spacing Δ. B-spline based deformation is defined by the tensor product of n dimensional B-spline, which is expressed as follows:

$$T_{local}(x, y, z) = \sum_{k=0}^{3} \sum_{m=0}^{3} \sum_{n=0}^{3} B_n(u_x) B_m(v_y) B_k(w_z) \varphi_{i+n,j+m,l+k} \tag{4.2}$$

where $i = [x/n_x] - 1, j = [y/n_y] - 1, l = [z/n_z] - 1$, $u_x = x/n_x - [x/n_x], v_y = y/n_y - [y/n_y], w_z = z/n_z - [z/n_z]$ and $B_n(u_x), B_m(v_n), B_k(w_z)$ represent the n^{th}, m^{th}, k^{th} basis functions along x,y,z direction respectively.

The displacement field at a point is controlled by the control vectors and is calculated by B-spline based interpolation. The control vectors are located with a spacing of n_x, n_y, n_z of grid points.

C NURBS

NURBS stands for **Non-Uniform Rational B-spline**.

- **Non-Uniform** refers to the parametrization of the curve which allows the use of the needed multiple knots to represent Bezier curves.
- **Rational** refers to the mathematical representation of shapes. It allows for both free form shapes and exact conic representation in NURBS.
- **B-splines** are the piecewise polynomial curves that have a parametric representation.

NURBS based analysis has been done on human brain surface [32]. Motivated with this, Wang et al. developed non-rigid registration of brain MRI using NURBS [33]. NURBS are defined by a set of control points, basis functions, knots, degrees, and weights that are associated with every control point. These five components are evaluated mathematically at a range of parameters to produce NURBS curves and surfaces. The set of control points are used to characterize the general shape of the curve or surface. Moving one of the control points is one of the easiest ways to change the shape of a NURBS curve or surface. The desirable locality property of NURBS will limit the effect of a single control point to the area of the curve in the vicinity of the point [101]. An investigation of NURBS based deformable image registration is depicted in [31].

NURBS generalizes the non-rational parametric form. They are infinitely smooth in the interior of a knot span provided the denominator is not zero, which enables them to satisfy different smoothness requirements. The properties of NURBS are:

- It includes weights as extra degrees of freedom which influence the local shape. The spline is attracted toward a control point more if the corresponding weight is increased and less if the weight is decreased.
- It offers a common mathematical framework for implicit and parametric polynomial forms. This powerful modelling flexibility is achieved through the specific combinations of control points and weights.

A NURBS curve $C(u)$ is vector-valued tensor-product function in the following form

$$c(u) = \frac{\sum_{i=0}^{n} N_{i,p}(u) w_i P_i}{\sum_{i=0}^{n} N_{i,p}(u) w_i} for \;\; a \leq u \leq b \tag{4.3}$$

where P_i are the control points that form the control polygon, w_i are values of weighting functions associated with P_i, and i^{th} $N_{i,p}$ are the p^{th} degree B-spline non-rational basis functions given by the Cox-de Boor recurrence relation

$$N_{i,0}(u) = \begin{cases} 1 & if \quad u_i \leq u \leq u_{i+1} \\ 0 & otherwise, \end{cases} \tag{4.4}$$

and

$$N_{i,p}(u) = \frac{u-u_i}{u_{i+p}-u_i} N_{i,p-1}(u) + \frac{u_{i+p+1}-u}{u_{i+p+1}-u_{i+1}} N_{i+1,p-1}(u) \tag{4.5}$$

defined over the non-periodic knot vector U for degree p,

$$U = \left\{ \underbrace{a, ...a,}_{p+1} u_{p+1}, ..., u_{m-p-1}, \underbrace{b, ..., b}_{p+1} \right\} \; subject \; to \;\; x_i \leq x_{i+1} \tag{4.6}$$

4.2.4 Non-rigid Image Registration using B-spline Interpolation

Let $F_r(x)$ and $F_t(x)$ represent the reference and floating image respectively. For a given set of B-spline control vector, the multi-modal non-rigid cost function is defined in terms of energy with parameters c. The registration scheme is the process to find the B-spline control grid which can minimize the cost function. The cost function consists of two parts. First is similarity energy E_{sim} and the second is regularization energy E_{reg}. The optimal parameter for optimum B-spline deformation grid is expressed as

$$c^{opt} = arg \quad \min_{c \epsilon C} (E_{sim}(c) + \lambda . E_{reg}(c)) \tag{4.7}$$

Mutual information is used as the similarity measure. Since MI reaches a maximum value with proper alignment, to find the minimum cost function, the similarity energy of the registration scheme is defined as negative MI. That is

$$E_{sim} = -MI(f_r(x), f_t^c(g(x))) \tag{4.8}$$

where

$$MI(f_r(x), f_t^c(x)) = \int \int p(i_r, i_s) log \frac{p(i_r, i_s)}{p(i_r)p(i_s)} \tag{4.9}$$

The probability density in mutual information is derived by a discrete form of the joint histogram or by approximating the density using the parzen window. For multi-modal image registration, the partial derivative of MI has been calculated with respect to the displacement field [12]. Here, the partial derivative of MI is calculated with respect to B-spline controlling vector.

4.3 Proposed Registration Framework

In non-rigid registration, the concept of minimization of an energy function drives the registration process by maximizing the similarity between the images where the control points are dynamically updated, resulting new transformation function in each iteration. In this chapter, the transformation $g(\psi; \mu)$ is modeled based on cubic B-spline using FFD. The 3D transformation at any point $\psi = [x, y, z]^T$ in the floating image is interpolated using a linear combination of a cubic B-spline convolution kernel as

$$T(\psi;\mu) = \sum_{ij} \eta_{ijk} \beta^3 \left(\frac{\psi - \varphi_{ijk}}{\Delta} \right) \tag{4.10}$$

where $\psi = [x, y, z]^T$ is the transformation at any point in the floating image, Δ is the uniform spacing between the mesh control points, $B^3(\psi) = B^3(x)B^3(y)B^3(z)$ is the separable cubic spline convolution kernel, η_{ijk} are the deformation coefficients associated to the control points φ_{ijk}. The block diagram of non-rigid image registration is shown in Fig. 4.2.

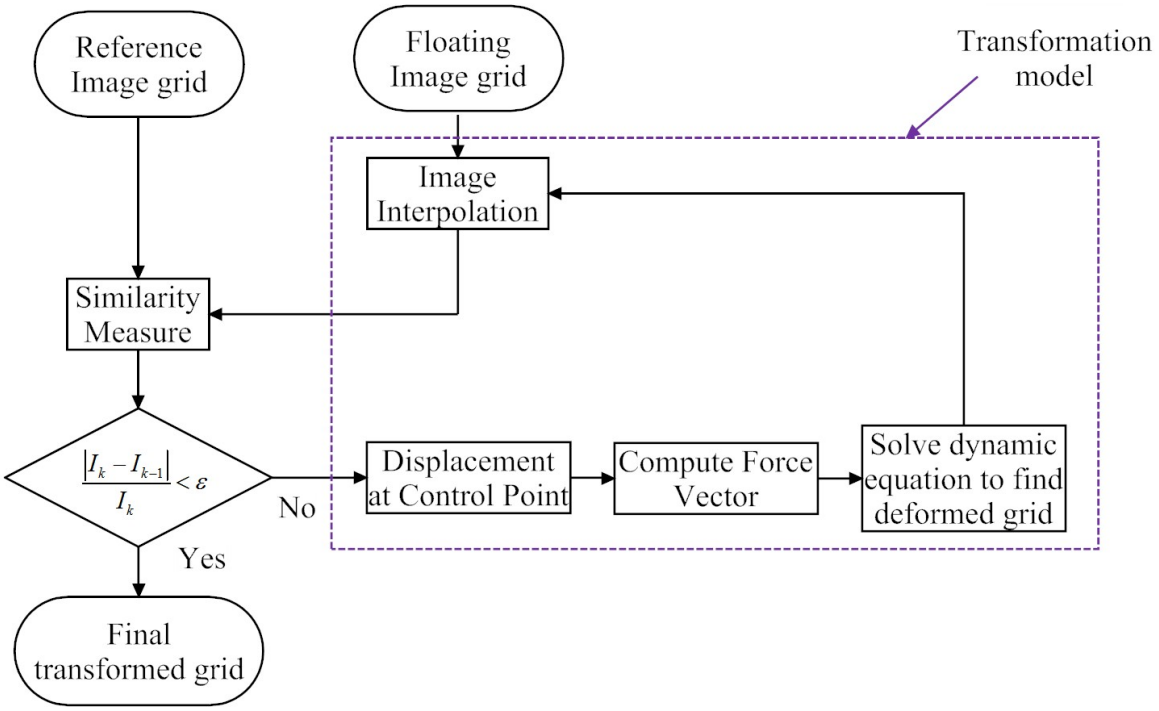

Figure 4.2: Block diagram of non-rigid image registration

4.3.1 Smoothing Spline

The B-spline approach requires knowledge of the location and number of knots. This information may not be possible in general and the placement of proper number of knots is a complex nonlinear optimization problem. Since B-spline functions are inherently smooth, an additional regularization term is needed in order to avoid the singularity or folding effect in the deformation field. Penalized spline proposed by Ruppert and Carroll allow the penalty to act differently for each spline basis, where the smoothing parameters are selected using a multivariate generalized cross validation [102, 103]. To circumvent this problem, the penalized spline smoothing approach is adopted [104]. The penalty is constructed from the difference between neighboring spline coefficients [30].

4.3.2 Proposed P-spline Interpolation based Image Registration

Motivated by Eilers and Marx [104], in our proposition a regularization or penalty term is incorporated at each grid point of the image during B-spline based interpolation for non-rigid registration. This penalty term helps in smooth reformation of the deformed images. The two steps to achieve the smoothness are:

1. Use of rich regression basis for purposely overfit of smooth coefficient vector with a modest number of equally spaced B-splines and
2. Ensuring proper amount of smoothness through a difference penalty on adjacent B-spline coefficients.

The proposed Penalized spline (P-spline) model is represented as:

$$\Phi = B\theta$$

where B: b-spline bases, θ: unknown coefficient. P-spline approach places penalties on the coefficients to control the function. Let P_1, P_2 be penalties for the marginal bases B_1, B_2 respectively, then the resultant penalty is

$$P = \lambda_1(P_2 \otimes I_{k1}) + \lambda_2(I_{k2} \otimes P_1) \tag{4.11}$$

where λ_i : smoothing parameters, I_k : identity matrix. The transformation model using P-spline is written as,

$$T(\psi;\mu) = \sum_{ij} \eta_{ijk}\beta^3\left(\frac{\psi - \varphi_{ijk}}{\Delta}\right) + P \tag{4.12}$$

where P is the penalty for the marginal bases. We have considered up to second order marginal bases.

4.3.3 Knot Selection

Knot vectors have the significant role to smooth the curve during interpolation of data points [105]. Considering three points p_{i-1}, p_i and p_{i+1} $i = 0, 1, 2, ..., n$ for curvature approximation, Li et al. presented local deflection of $a_i \leq \frac{\pi}{6}$, where a_i is angle between L_{i+1} and L_i. where

$$L_i = p_i - p_{i-1} \tag{4.13}$$

With this condition, the interpolated points are approximated. The rule for approximation of knot placement is, if points corresponding to the knots can satisfy above condition, the reconstructed curve will be a good approximation to the given data points.

4.3.4 Proposed Adaptive P-spline Interpolation based Image Registration

Medical images with large deformations dealt with non rigid registration. Some regularization constraints needs to impose on deformation to ensure the smoothness of the solution and proper convergence to obtain a desired result. The choice of knots has considerable effect on the shape of an object. Uniform grid refinement has been applied in brain image registration. Pradhan *et al.* have successfully applied the P-spline interpolation method for brain image registration [106]. In P-spline interpolation, penalty term is used globally i.e. each grid point of the whole image is penalized. However, the penalty differs from region to region, which depends on local deformation. Many adaptive grid refinement detect large deformation areas and locally refine these regions [107]. Adaptive mesh refinement scheme using hierarchical B-spline have been proposed by [100, 108].

Here, the large deformations are reformed using dynamic computation of fewer control points, which is efficient and faster as compared to uniform grid refinement. A multilevel technique, which makes it more efficient and flexible. Equation 4.5 represents the i^{th} B-spline function of polynomial order $p+1$. It is defined on a knot vector $u_1, ..., u_m$ in the u direction.

Let $N_{j,3}(u)$ be the cubic B-splines in the u direction with an open knot vector $\xi^u = u_1, u_1, u_1, u_1, u_2, ..., u_{m-1}, u_m, u_m, u_m, u_m,$ and $N_{k,3}(v)$ are the cubic B-splines in the v direction with an open knot vector $\xi^v = v_1, v_1, v_1, v_1, v_2, ..., v_{m-1}, v_m, v_m, v_m, v_m$. Then the global basis functions $\phi_i(x)$ are expressed by

$$\phi_i(x) = N_{j,3}(u)N_{k,3}(v) \tag{4.14}$$

where $x = (u, v), j = 1, ..., m+p+1, k = 1, ..., n+q+1$, and $i = 1, ..., (m+p+1)(n+q+1)$. The maximization of the cost function in Equation 2.1 to solve the optimal control points for the spatial transformation is written as

$$C^k = C^{k-1} - \varepsilon \delta p^* \tag{4.15}$$

where δp^* is the differential of the energy function, C^k and C^{k-1} are the control points calculated by the k^{th} and the $(k-1)^{th}$ iteration steps, and ε is the time step chosen manually.

A Proposed Algorithm

The algorithm starts from two given images, the reference image $I_r(x)$ and the floating image $I_f(x)$. The goal is to find a spatial transformation $T(x)$, aligning $I_r(x)$ with $I_f(x)$ such that $I_f(T(x)) \approx I_r(x)$. The registration process is divided into a multilevel procedure, using coarser levels for large deformation and finer levels for more detailed

deformation. The steps of the algorithm are described as follows:

1. Based on the chosen initial control points, the initial spatial transformation $T_1^1(x) = \sum_{i=1}^{N1} C_{1i}^1(x)$ is built, then interpolation is performed to obtain $I_f^1(T_1^1(x))$.

2. For different levels $l = 1, ..., z$, do the following

   (a) For different iterations $s = 1, ..., k$, do the following

      i. Substitute $I_f^1(T_1^1(x))$ into the cost function to obtain δE_l^k.

      ii. Substitute the control points C_l^k and the calculated δE_l^k into Equation 4.15, and then we obtain a new group of control points, $C_l^{k+1} = C_l^k - \epsilon \delta E_l^k$.

      iii. Using the newly calculated control points C_l^{k+1}, the corresponding spatial transformation is constructed using $f_l^{k+1}(x) = \sum_{i=1}^{Nl} C_{li}^{k+1} \phi_i(x)$. From the interpolation approximation, obtain $I_l^{k+1}(f_l^{k+1}(x))$.

   (b) Check the similarity ratio after each iteration. After certain iteration steps, if the similarity ratio increases slower or even decreasing. Then increase the number of control points. Reset the spatial transformation, i.e. $f_{l+1}^1(x) = \sum_{i=1}^{N_{L+1}} C_{(l+1)i}^{N_{l+1}} \phi_i(x)$, and perform the interpolation operation to yield $I_{l+1}^1(f_{l+1}^1(x))$.

3. The multilevel procedure continues until the cost function becomes stable without further improvement.

4.4 Simulation and Results

The deformable registration algorithm presented in this chapter is targeted at 2D-2D intensity-based registration problem. The algorithm in general is applied to mono-modal as well as multi-modal image registration. Free-form deformations and B-spline basis functions are used to model the non-rigid deformed brain images. Here, the transformation between the images contain localized non-linear stretching. Although deformable image registration is more flexible for deformed images, it requires significantly more computation time than rigid registration techniques, due to the computation of a very large number of parameters.

A number of experiments have been carried out to evaluate the performance of the proposed P-spline and adaptive P-spline interpolation based registration schemes. Multi-modal brain images such as simulated brain MR images of T1, T2 and PD weighted have been taken from database (http://brainweb.bic.mni.mcgill.ca/brainweb/). MR images are with 256×256 pixels, inplane, and of pixel size $1.25mm \times 1.25mm$. Those images are reformed with

some geometric transformations. A set of real brain MR image of same subject is also taken from internet source (http://medind.nic.in). Here, we highlight the registration function for different problem, comparing the final deformed grid using spline based transformation into the registration process. We evaluate the accuracy and robustness of the proposed transformation methods for multi-modal images.

In this work, the simulation based experimentation on non-rigid registration have been performed with four different cases. (reference image with floating image)

- **Case I**: MR T1 weighted image with deformed T1 weighted image
- **Case II**: MR T2 weighted image with deformed T1 weighted image
- **Case III**: MR T2 weighted image with deformed PD weighted image
- **Case IV**: Brain MR image of same subject

Following performance measures are evaluated for performance analysis of the proposed registration methods.

Mean squared error (MSE): The simplest quality metric is MSE. For given two images $r = (r_i|i = 1, ..., N)$ and $f = (f_i|i = 1, ..., N)$ MSE is computed using intensity differences to assess the image quality.

$$MSE(r, f) = \frac{1}{n}\sum_{1}^{N}(f_i - r_i)^2 \tag{4.16}$$

Universal Quality Index (UQI): The universal quality index is modeled by considering the three factors such as contrast distortion, luminance distortion, and loss of correlation.

$$Q = \frac{4\sigma_{rf}\overline{r}\,\overline{f}}{(\sigma_r^2 + \sigma_f^2)[(\overline{r})^2 + (\overline{f})^2]} \tag{4.17}$$

where $\overline{f} = \frac{1}{N}\sum_{i=1}^{N} f_i$ and $\overline{r} = \frac{1}{N}\sum_{i=1}^{N} r_i$

$\sigma_r^2 = \frac{1}{N-1}\sum_{i=1}^{N}(r_i - \overline{r})^2$ and $\sigma_f^2 = \frac{1}{N-1}\sum_{i=1}^{N}(f_i - \overline{f})^2$

$\sigma_{rf} = \frac{1}{N-1}\sum_{i=1}^{N}(r_i - \overline{r})(f_i - \overline{f})$

4.4.1 MR image data set

For evaluation of the proposed scheme, three sets of MR images are considered i.e Case I, Case II, and Case III. Four types of similarity measures are considered for registration framework, such as SMI, QMI, both proposed EMI and SR-EMI. For each case, the four similarity measures are taken into consideration, where four types of spline based

interpolation schemes, such as B-spline, proposed P-spline, NURBs, and proposed AP-spline schemes are incorporated into registration framework and evaluated.

In Case I, the simulated T1 weighted image is considered as the reference image where as deformed T1 weighted image is taken as the floating image which is geometrically deformed. As the images are having the same intensity, they are considered as mono-modal images. The input images and the difference image before registration are shown in Fig. 4.3 (a-c) respectively. The registered images, final transformed grids and the difference images after registration using B-spline, P-spline, NURBs and proposed AP-spline interpolation based schemes have been demonstrated and are shown in Fig. 4.3 (d-g), (h-k) and (l-o) respectively. From this figure, we observed that, the registered image using the AP-spline based scheme is accurately registered as compared to other aforementioned spline based registration schemes. The grids after transformation using AP-splines are found to be smoother as compared to the other schemes. The SM values of SMI, QMI, EMI and SR-EMI with the four interpolation based registration schemes are tabulated in Table 4.1. The table shows SM value of the proposed AP-spline using SR-EMI based similarity measure i.e. 2.29, which is higher than those of other interpolation techniques using SR-EMI based similarity measure. Also, the performance measures such as MSE, UQI and the computation time are tabulated here. The MSE and UQI value for the proposed AP-spline interpolation based registration framework is lower as compared to other existing state-of-arts. Consequently, the computation time using proposed P-spline interpolation is little bit higher as compare to B-spline and NURBs interpolation based registration schemes. For faster convergence of the transformed grids, the AP-spline based registration scheme is validated to reduce the computation time. Table 4.1 also demonstrates that, the computation time is comparatively reduced in case of AP-spline interpolation scheme, incorporated into SR-EMI similarity measure based registration scheme. The computation time is reduced due to the adaptive selection of the grid points with a penalty term.

The convergence plot for all types of transformation methods are plotted in Fig. 4.4. It is shown that, in case of (SR-EMI+ AP-spline interpolation) based registration scheme, MSE is minimized to 5.21 with minimum computation time of 80 sec., whereas in case of other interpolation based methods MSE is found to be higher than 5.21 and the computation time is more than 80 sec. The RMS error curve for all the interpolation based registration schemes are plotted in Fig. 4.5. From the graph, it is noticed that, the RMS error is lower for the proposed AP-spline based registration scheme. Also, after 10 iterations, the cost function of the registration framework has been converged with lower RMS value whereas in all other cases, the RMS value is more as compared to the AP-spline based registration scheme. It shows the efficacy of the proposed AP-spline based registration scheme as compared to other existing state of the art. The

Table 4.1: Performance Measures for Case I

Method	SM method	SM value	MSE	UQI	Comp time (s)
	SMI	1.81	5.92	0.89	94
	QMI	1.87	5.89	0.84	111
B-spline	EMI	1.94	5.83	0.78	127
Interpolation	**SR-EMI**	**2.01**	**5.76**	**0.72**	**149**
	SMI	1.87	5.88	0.85	133
	QMI	1.92	5.82	0.79	146
P-spline	EMI	2.13	5.79	0.74	155
Interpolation	**SR-EMI**	**2.22**	**5.73**	**0.69**	**170**
	SMI	1.88	5.85	0.82	65
	QMI	1.95	5.81	0.78	84
NURBS	EMI	2.17	5.76	0.72	105
Interpolation	**SR-EMI**	**2.26**	**5.71**	**0.67**	**123**
	SMI	1.92	5.70	0.79	46
Adaptive P-spline	QMI	1.98	5.56	0.73	58
Interpolation	EMI	2.19	5.38	0.69	68
Proposed	**SR-EMI**	**2.29**	**5.21**	**0.65**	**80**

regularization applied on the spline interpolation based schemes, reform the deformed floating image efficiently and smoothly. The adaptiveness incorporated in the proposed penalized spline is able to reduce computational burden of the registration scheme.

In Case II, the reference image is T2 weighted and the floating image is deformed T1 image. The input image and registered image using different spline based transformation schemes are shown in Fig. 4.6 (a,b) and (d-g) respectively. Fig. 4.6 (h-k) and (l-o) shows the final transformed grids and difference images after registration respectively. The SM value along with the performance measures are tabulated in Table 4.2. The convergence and RMS error curve for this set of images are demonstrated in Fig. 4.7 and Fig. 4.8 respectively. From Fig. 4.7, it is also observed that, the computation time of the proposed AP-spline is 110 sec., which is faster than those of B-spline, P-spline and NURBs transformation based registration scheme. It is also found that the MSE value for the proposed scheme is reduced after registration, which is lower than other existing transformation based registration methods. In Fig. 4.8, it is observed that, the RMS error for the proposed transformation based registration scheme is quite smaller than those of other state of the art and it also converges faster.

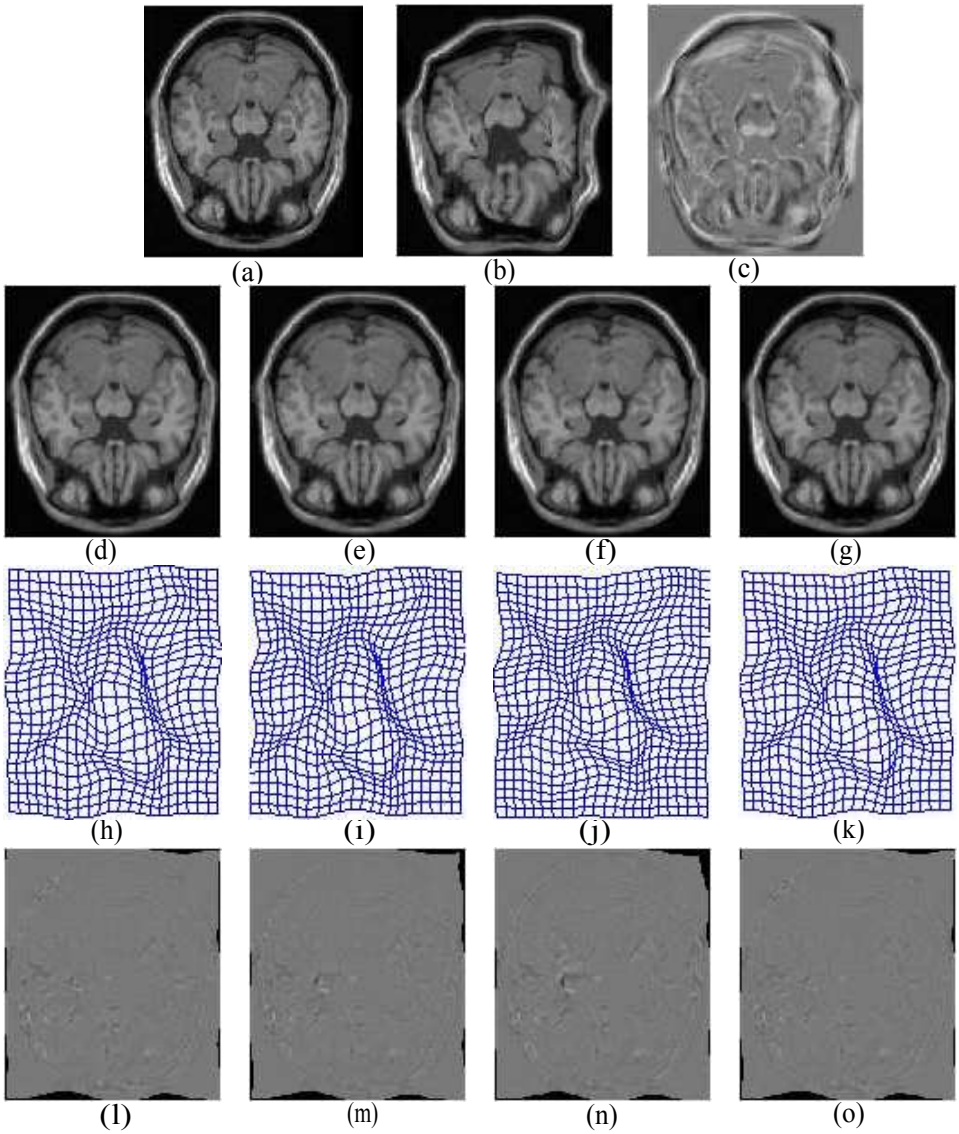

Figure 4.3: (a) Reference image, (b) Floating image, (c) Difference image before registration, (d-g) Registered image using B-spline, P-spline, NURBs and AP-spline transformation, (h-k) Corresponding final transformed grid, (l-o) Difference image after registration for Case I

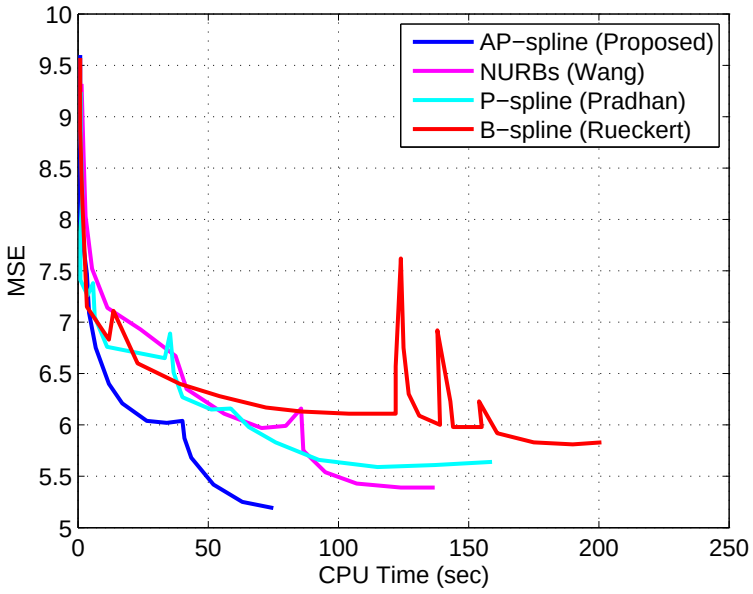

Figure 4.4: Convergence of different transformation method for Case I

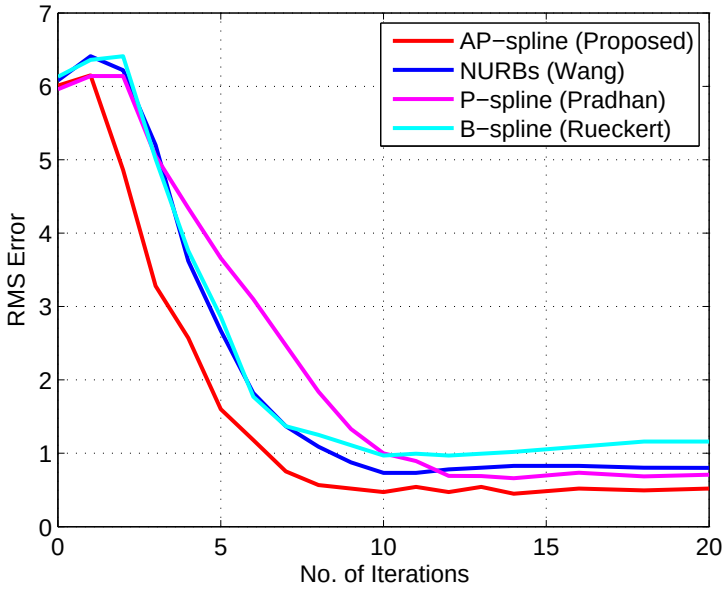

Figure 4.5: RMS error curve for different transformation method for Case I

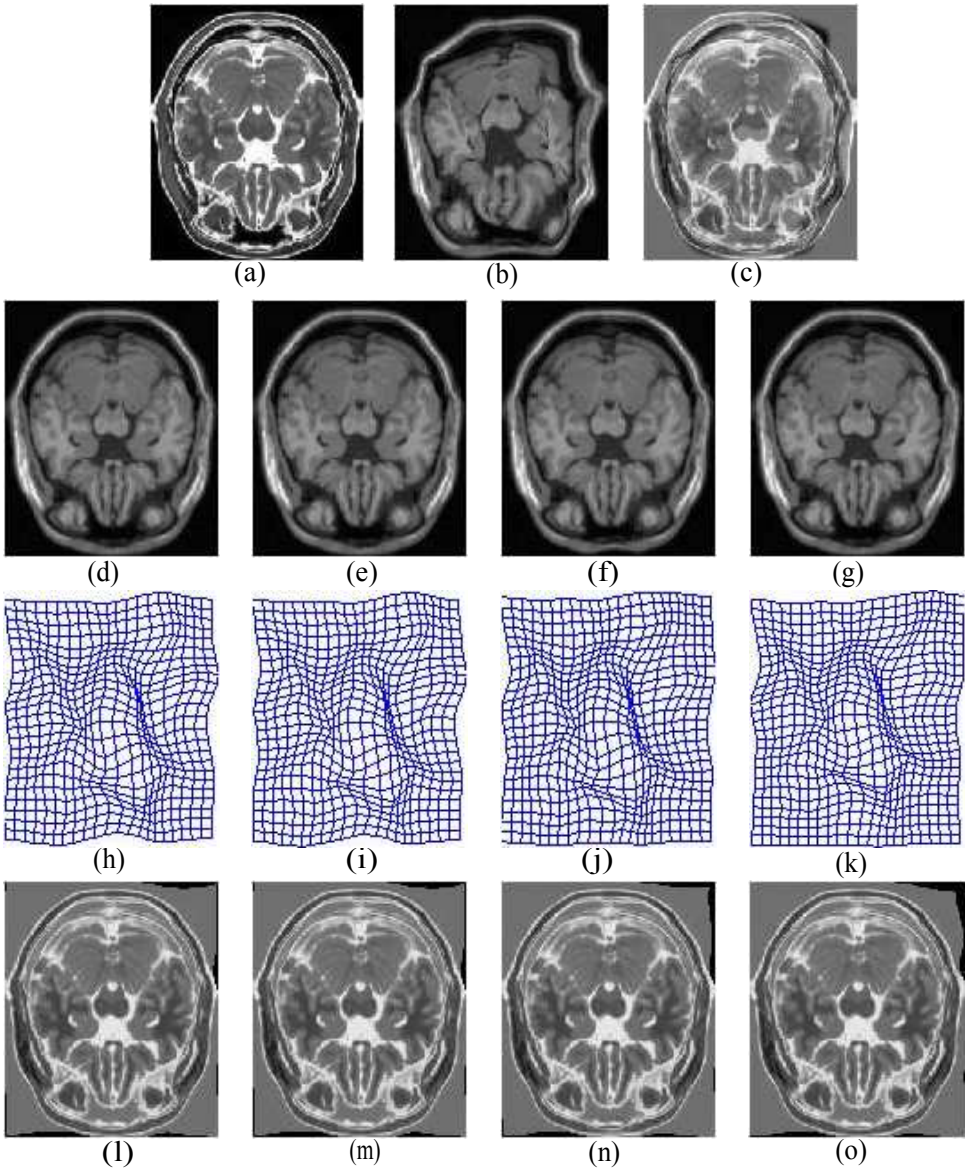

Figure 4.6: (a) Reference image, (b) Floating image, (c) Difference image before registration, (d-g) Registered image using B-spline, P-spline, NURBs and AP-spline transformation, (h-k) Corresponding final transformed grid, (l-o) Difference image after registration for Case II

Similarly, for Case III, a deformed PD weighted image is considered as the floating image which is to be registered, with respect to the reference image i.e T2 weighted MR image. The images are shown in Fig. 4.9 (a,b). Though the structures have similar anatomical information, the images are multi-modal due to different tissue characteristics. The registered images, final transformer grids along with the difference images after registration using the proposed AP-spline and other transformation schemes are shown in Fig. 4.9 (d-g), (h-k) and (l-o) respectively.

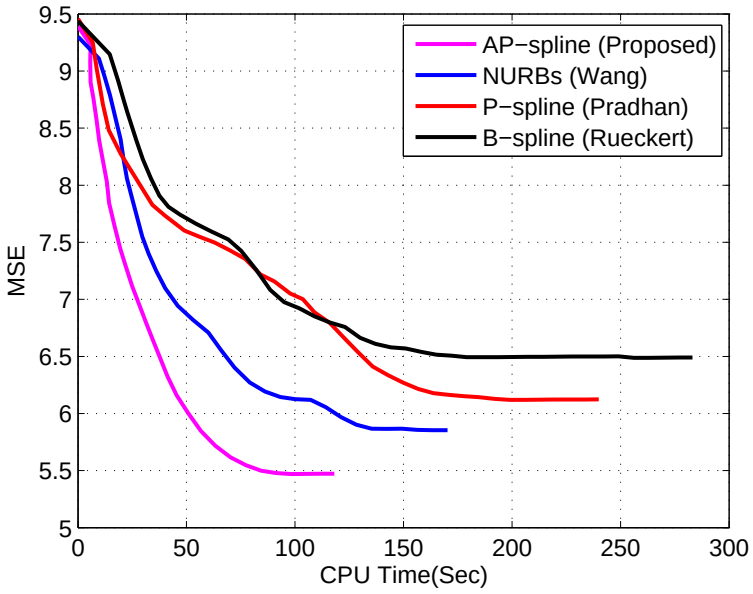

Figure 4.7: Convergence of different transformation method for Case II

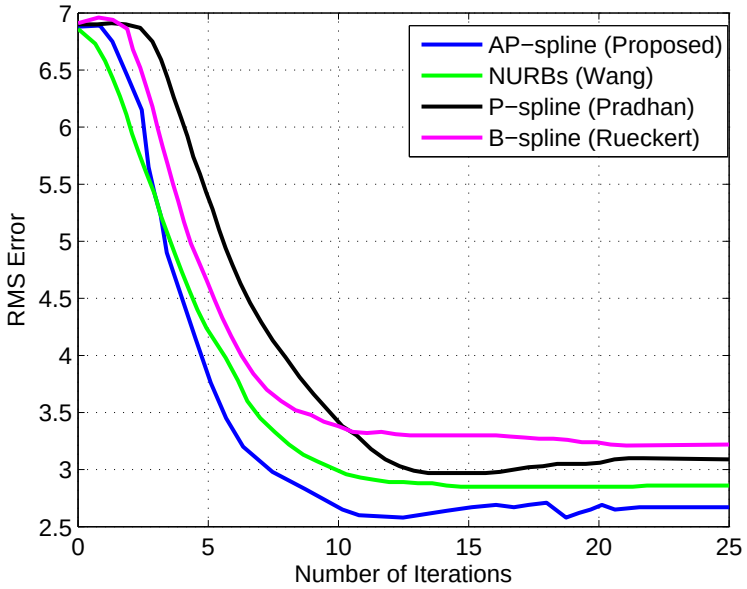

Figure 4.8: RMS error curve for different transformation method for Case II

Table 4.2: Performance Measures for Case II

Method	SM method	SM value	MSE	UQI	Comp time (s)
	SMI	1.73	5.43	0.81	104
	QMI	1.78	5.35	0.77	134
B-spline	EMI	1.84	5.28	0.72	165
Interpolation	**SR-EMI**	**1.89**	**5.21**	**0.69**	**180**
	SMI	1.76	5.40	0.78	175
	QMI	1.80	5.32	0.73	190
P-spline	EMI	1.84	5.26	0.69	208
Interpolation	**SR-EMI**	**1.95**	**5.18**	**0.64**	**239**
	SMI	1.80	5.39	0.76	90
	QMI	1.86	5.31	0.71	117
NURBS	EMI	1.91	5.22	0.66	123
Interpolation	**SR-EMI**	**1.98**	**5.13**	**0.62**	**155**
	SMI	1.86	5.26	0.72	73
Adaptive P-spline	QMI	1.91	5.20	0.68	87
Interpolation	EMI	1.96	5.12	0.64	99
Proposed	**SR-EMI**	**2.05**	**5.03**	**0.61**	**110**

Table 4.3: Performance Measures for Case III

Method	SM method	SM value	MSE	UQI	Comp time (s)
	SMI	2.51	4.48	0.78	152
	QMI	2.59	4.39	0.71	165
B-spline	EMI	2.63	4.31	0.68	177
Interpolation	**SR-EMI**	**2.78**	**4.25**	**0.62**	**189**
	SMI	2.62	4.44	0.73	186
	QMI	2.68	4.35	0.67	195
P-spline	EMI	2.72	4.26	0.63	208
Interpolation	**SR-EMI**	**2.84**	**4.18**	**0.58**	**216**
	SMI	2.68	4.34	0.67	128
	QMI	2.74	4.29	0.62	139
NURBS	EMI	2.80	4.22	0.58	151
Interpolation	**SR-EMI**	**2.94**	**4.11**	**0.52**	**166**
	SMI	2.72	4.38	0.63	108
Adaptive P-spline	QMI	2.79	4.22	0.59	121
Interpolation	EMI	2.85	4.13	0.56	139
Proposed	**SR-EMI**	**3.04**	**4.02**	**0.48**	**147**

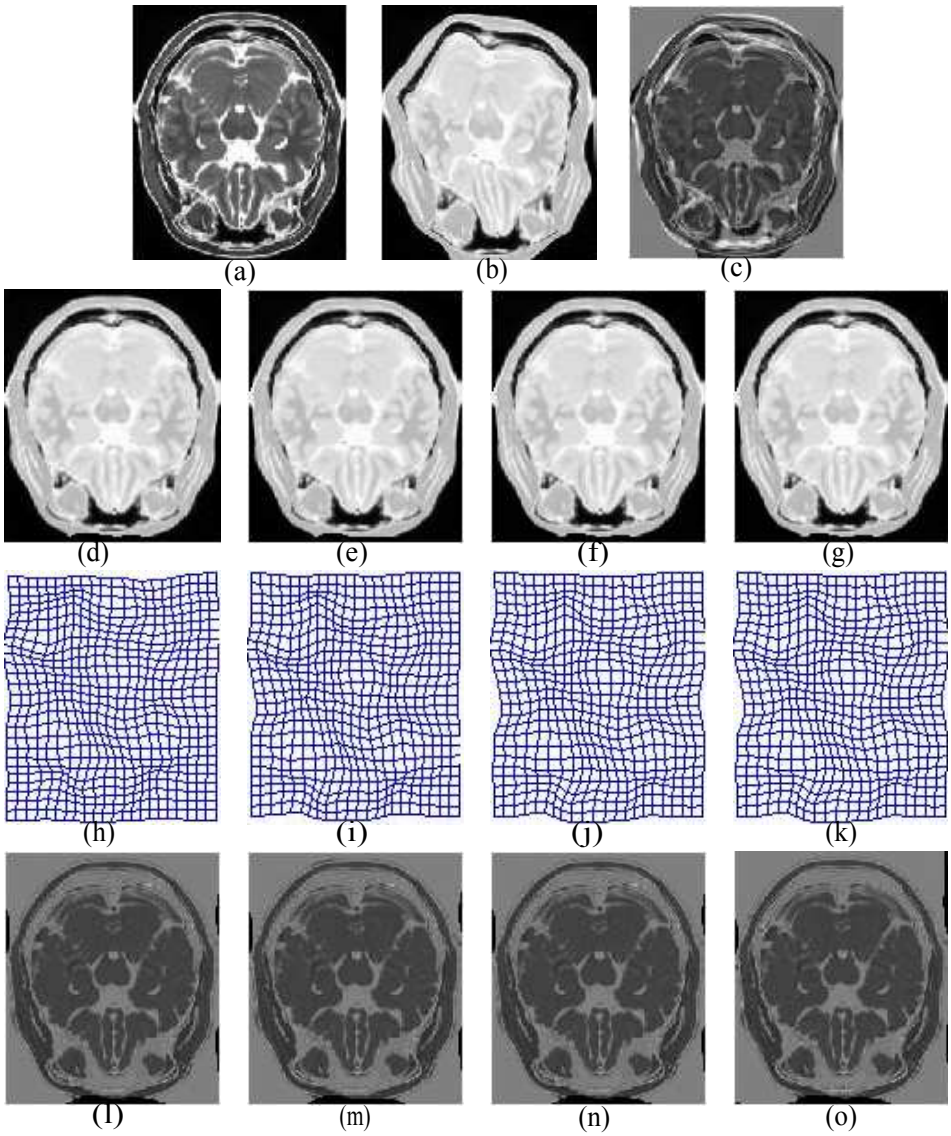

Figure 4.9: (a) Reference image, (b) Floating image, (c) Difference image before registration, (d-g) Registered image using B-spline, P-spline, NURBs and AP-spline transformation, (h-k) Corresponding final transformed grid, (l-o) Difference image after registration for Case III

In order to evaluate the proposed registration schemes, we have performed a quantitative validation. The SM value along with the performance measures such as MSE, UQI and computation time are tabulated in Table 4.3. The SM value is found to be higher in case of AP-spline as compared to P-spline and other spline based transformation methods. It demonstrates that the proposed method, AP-spline has locally transformed the deformation grid and outperforms than those of other existing schemes. It is also found that, the AP-spline scheme significantly reduces the mean square error (MSE) of different tissues as compared to P-spline, B-spline and NURBs based interpolation methods. This shows that improvement in registration accuracy due to the adaptive penalization of the weighted factor, that is incorporated into P-spline

based interpolation method.

Table 4.4: Performance Measures for Case IV

Method	SM method	SM value	MSE	UQI	Comp time (s)
	SMI	2.46	4.76	0.79	175
	QMI	2.53	4.69	0.73	189
B-spline	EMI	2.62	4.61	0.64	203
Interpolation	**SR-EMI**	**2.72**	**4.52**	**0.58**	**221**
	SMI	2.52	4.63	0.73	191
	QMI	2.61	4.59	0.68	209
P-spline	EMI	2.68	4.52	0.59	224
Interpolation	**SR-EMI**	**2.76**	**4.44**	**0.53**	**233**
	SMI	2.60	4.56	0.69	153
	QMI	2.69	4.49	0.63	164
NURBS	EMI	2.73	4.41	0.56	178
Interpolation	**SR-EMI**	**2.80**	**4.32**	**0.49**	**186**
	SMI	2.69	4.48	0.65	126
Adaptive P-spline	QMI	2.78	4.39	0.58	139
Interpolation	EMI	2.81	4.30	0.52	148
Proposed	**SR-EMI**	**2.90**	**4.21**	**0.45**	**160**

4.4.2 Pre and post operative brain MR image data set

In pursuance of validating the proposed registration method, another set of brain MR images of the same subject is also considered as the reference and floating image, which are shown in Fig. 4.10 (a,b). Fig. 4.10 (c-f) shows the registered images using B-spline, P-spline, NURBs and AP-spine based transformation for non-rigid registration framework. The difference images after registration are shown in Fig. 4.10 (g-j). The final transformed grids after reformation of the floating image with respect to the reference image using proposed AP-spline, P-spline and other existing transformation based registration methods are shown in Fig. 4.10 (k-n). The SM values along with the performance measures are tabulated in Table 4.4. From the table, it is observed that, the SM value is higher in case of registration scheme using AP-spline transformation with SR-EMI similarity measure as compared to SR-EMI with NURBs based and SR-EMI with P-spline based registration scheme. Similarly, the MSE and UQI values are found to be lower in case of the proposed scheme rather than the existing schemes. Also, the computation time of AP-spline and SR-EMI based registration scheme is 160 sec, which is lower than SR-EMI with P-spline based and SR-EMI with NURBs based registration schemes. From all these simulation based observations, we found that the proposed Adaptive P-spline interpolation based registration scheme performs

best when the similarity measure is considered as salient region based enhanced mutual information (SR-EMI). It can efficiently align the deformed floating images with respect to the reference image with more accuracy and faster convergence.

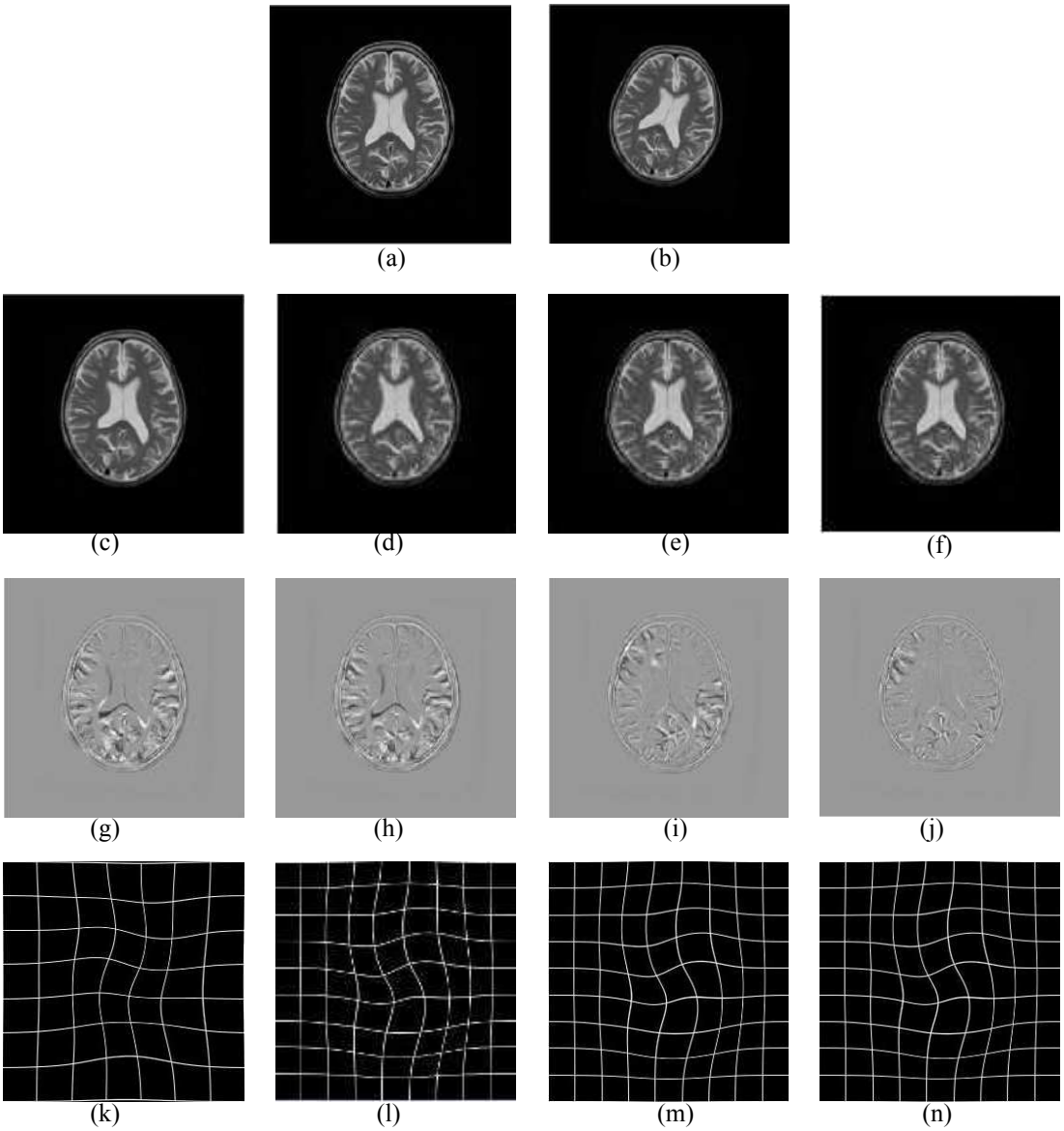

Figure 4.10: (a) Reference image, (b) Floating image, (c-f) Registered image using B-spline, P-spline, NURBs and AP-spline transformation, (g-j) Corresponding difference images, (k-n) Final transformed grid after registration for Case IV

4.5 Summary

The prime objective of this chapter is to transform the deformed floating images with non-rigid registration framework. B-spline interpolation is popularly used for non-rigid image registration. But, it fails to reform properly in the presence of local deformations. To overcome this problem, penalized spline (P-spline) interpolation based registration method is proposed, incorporating a penalty term as a weighted term to the B-spline interpolation method. The penalty term penalizes the local deformation in the image grid to transform smoothly and efficiently. But, the computation time is comparatively higher due to the computation of a penalty term at each grid point of the deformed image. To reduce the computational burden, an adaptive P-spline (AP-spline) interpolation based registration method is proposed, where only locally deformed grid points are penalized in stead of the whole image grid in the registration process. To validate the proposed P-spline and AP-spline interpolation based registration, the experimental analysis has been performed on several multi-modal brain MR images those are geometrically deformed. The combination of the proposed AP-spline interpolation with SR-EMI similarity measure based registration scheme outperforms the similar existing algorithms, such as SR-EMI + NURBs, SR-EMI + P-spline, and SR-EMI + B-spline in terms of MSE, UQI, and computation time. The computation time for SR-EMI + AP-spline interpolation method is reduced due to adaptive knot selection in the image grid. The MSE and UQI values are comparatively lower in case of SR-EMI + AP-spline based registration scheme.

Though AP-spline interpolation based registration algorithm registered the deformed image properly, the degree of freedom is comparatively higher, which becomes a bottleneck for optimizing the transformation parameters. Therefore, evolutionary based approaches are adopted for optimizing the transformation parameters in non-rigid registration procedure, which are discussed in the following chapter.

Chapter 5

Hybrid Evolutionary Technique for Transformation Optimization

This chapter describes about optimization of the similarity measure within a given class of geometric transformations for the registration framework. For the optimization of the similarity metric local methods were used. As the functions of the similarity metric with respect to the transformation parameters are non-convex and irregular, local optimization methods may not converge at optimum transformation parameters. Therefore global optimization techniques are required to get the optimum transformation parameters for more accurate mapping and subsequently obtain accurate registration. In this chapter, a new hybrid evolutionary based optimization method is proposed, to yield optimum transformation which leads to accurate registration. The proposed method is validated with both rigid and non-rigid transformed multi-modal brain images.

5.1 Introduction

The registration process is viewed as an optimization problem, where the registration criterion is the maximization of the cost function i.e. similarity measure over the search space of spatial transformation parameters. Starting with a set of initial parameters, the optimization procedure iteratively searches for a solution by evaluating the cost function at different positions in the search space. In this chapter, the similarity measure is considered as the cost function and is maximized for optimal registration.

For the optimization of the similarity measure, local methods or global methods are used [36, 109]. Local methods such as steepest descent gradient, Powell's direction set usually trap in a local optimum and obtain a large mean-registration error. Hence, the selection of good initial values are necessary for these techniques [1]. Evolutionary based optimization methods are very popular and successfully applied in image processing [37, 110, 111]. Genetic algorithm (GA) and particle swarm optimization (PSO) are some popular global optimization techniques used in image processing [112]. Though Genetic algorithm (GA) is a powerful scheme for global optimization, it takes a longer computation time and lacks the fine tuning capability. Particle swarm optimization (PSO) is a stochastic population based technique. A comparative study on genetic algorithm and particle swarm optimization is drawn in [113]. PSO is more effective and extremely simple algorithm in comparison with GA and other global optimization algorithms. It was used for multi-modal image registration with a variation of hybrid techniques [114]. A new diagonal gradient-type method for large scale unconstrained optimization was proposed by [115].

In this chapter, the focus is towards the maximization of the similarity metric for rigid and non-rigid transformed images. A new hybrid evolutionary computation based optimization algorithm is developed to optimize the transformation parameters for non-rigid registration of multi-modal images. The algorithm hybridizes the notion of BF and Quantum behaved PSO algorithm to reduce the misalignment or mean-registration error. For this purpose, the deformed transformation parameters are initialized. Subsequently the similarity measure is optimized by updating the transformation parameters, where the parameters were interpolated by an adaptive P-spline interpolation method. The process continues until the floating image and reference image align properly. The proposed hybrid algorithm outperforms as compared to other existing global optimization techniques.

The rest of the chapter is organized as follows. Section 5.2 describes the basic concept of global and local optimization technique used for the registration process. The one dimensional direction search Powell method and other existing evolutionary based optimization schemes are also included in this chapter. The proposed evolutionary

optimization algorithm is explained in detail in Section 5.3. Section 5.4 presents the performance analysis with experimental results of the proposed method and those in existing literature [37, 116, 117]. Finally, summary is drawn in Section 5.5.

5.2 Materials and Methods

5.2.1 Powell's Optimization Technique

Powell′s direction set method only requires evaluations of the cost function. The method finds the N-dimensional minimum of the function by repeatedly minimizing it in one-dimension along a set of N different directions, each time starting from the minimum found in the previous direction using a one-dimensional line minimization method. Powell′s method incorporates a scheme to construct a set of conjugate directions iteratively. The set of directions is initialized with the basis vectors in each dimension in parameter space, but after each iteration in which all directions in the set are optimized over in turn, the overall distance moved in parameter space into that iteration is taken as a new direction.

Powell′s algorithm exactly minimizes the cost function in (N +1) dimension line [118]. Here, the direction set to the parameter basis vectors reinitialized each time and a new direction is found for the final optimization. Due to differences in image resolution in different directions and due to the specific shape of the objects in the scene, different parameters are considered and are optimized, which might strongly influence optimization performance and registration robustness. The powell optimization method has been successfully applied for medical image registration in [119, 120]. A comparative study is drawn for multi-modal brain image matching in [121]. For rigid registration of multi-modal brain images, optimization of the translation transformations tx, ty, and rotation along ϕ_x are considered. Therefore, optimization of the parameters are obtained using Powell′s optimization scheme in each iteration for tx, ty, ϕ_x.

5.2.2 Particle Swarm Optimization Algorithm

In the swarm algorithm, basically the particles track a deterministic way of life by an updated velocity formulation through random acceleration coefficients. The conventional PSO algorithm has a weak local search ability, which deteriorates the global search ability of the algorithm. Hence, a trade-off between exploitation and exploration is essential for improved functioning of the algorithm with a favorable convergence speed. So, many variations of PSO have been offered by putting an inertia weight into the velocity update equation. Also a constriction factor was added in the velocity update equation, to keep off the velocity restriction during convergence by Clerc *et al.* [122]. Zheng *et al.* proposed some improved PSO algorithm for image

registration [116]. Many researchers proved the conventional GA and PSO fail to find the global optimum well. So, a new approach named hybrid particle swarm optimization (HPSO), was proposed which incorporated the sub-population and crossover of GA into the conventional PSO [123]. Though, HPSO algorithm is faster and accurate, the drawback is about the non accuracy in the presence of large shear distortion between images [124]. An adaptive accelerated particle swarm optimization approach is proposed by Ludwig [125].

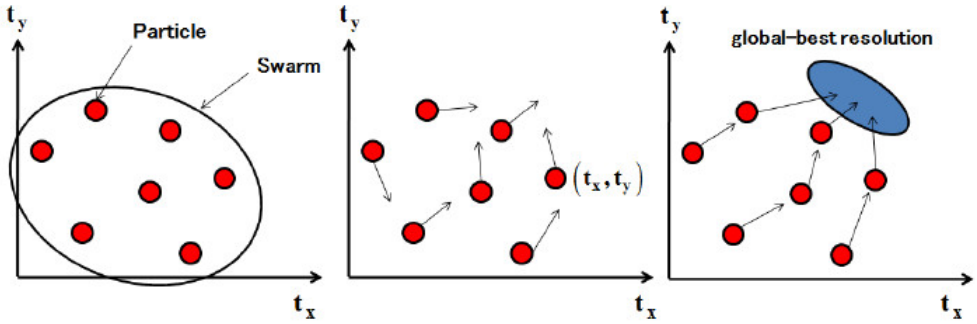

Figure 5.1: Example of PSO

5.2.3 Quantum behaved Particle Swarm Optimization Algorithm

Several probabilistic PSO algorithms have been proposed to cast along the particle trajectories with direct sampling by a random number generator, from a scattering of practical benefits. Quantum behaved PSO (QPSO) is a kind of probabilistic algorithm, inspired by quantum mechanics and trajectory analysis of PSO [126]. The algorithm employs a scheme based on a quantum delta potential well model, which samples about the previous best positions. During the search process, the update equation customize an adaptive approach for easier carry out with fewer parameters to adjust. Equally, it does not necessitate velocity vector for particles and has fewer parameters to adjust which makes the implementation easier [127]. Xi *et al.* improved the algorithm by introducing a weighted mean to find the best position of the particle and enhanced the performance as compared to the former method [128]. The flow chart of QPSO is shown in Fig. 5.2. Assuming each individual particle moves with a δ potential in the search space with a center of potential p_{ij} and solving Schrodinger equation of one-dimensional δ potential well, the probability density function S is defined as

$$S(X_{ij}(t+1)) = \frac{1}{W_{ij}}(t)F(X_{ij}(t+1)) \tag{5.1}$$

where $W_{ij}(t)$ is the standard deviation of the distribution, determining the search scope of each particle. The position of the particle is obtained by employing the Monte Carlo

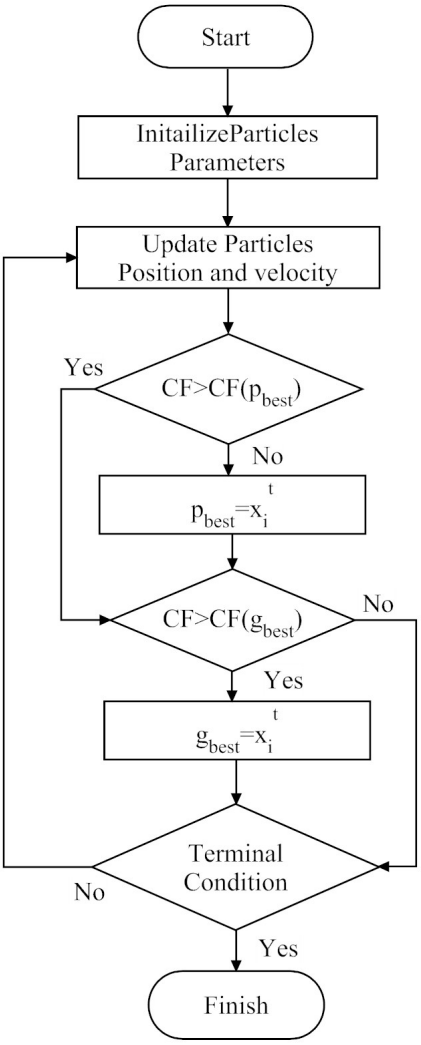

Figure 5.2: Flow chart of QPSO

method as:

$$X_{ij}(t+1) = P_{ij}(t) \pm \frac{W_{ij}}{1} ln(1/r) \tag{5.2}$$

where r is the random number uniformly distributed in (0,1). For evaluation of $W_{ij}(t)$, mean best position of the population was introduced into PSO [128]. The global point, denoted as m, is defined as the mean of the p_{best} positions of all particles. That is

$$m(t) = \frac{1}{M}\sum_{i=1}^{M} P_{i.1}(t), \frac{1}{M}\sum_{i=1}^{M} P_{i.2}(t), ..., \frac{1}{M}\sum_{i=1}^{M} P_{i.n}(t) \tag{5.3}$$

where M is the population size and P_i is the p_{best} position of particle i. The values of $W_{ij}(t)$ is determined by

$$W_{ij}(t) = 2\beta.|m_j(t) - X_{ij}(t)|$$

Thus the position is calculated as

$$X_{ij}(t+1) = P_{ij}(t) \pm \beta |m_j(t) - X_{ij}(t)| ln(1/r) \tag{5.4}$$

where

$$P_{i,j} = (c_1 P_{ij}(t) + c_2 P_{gj}(t))/(c_1 + c_2) \tag{5.5}$$

where β is called contraction-expansion coefficient, which is used as a tuner to control the convergence speed. c_1 and c_2 are the acceleration coefficients. Equation 5.4 is the position vector which is added to the particle swarm optimization. Steps of QPSO algorithm are as follows:

1. Initialize population randomly.
2. Calculate m_{best} using Equation 5.3
3. Calculate particle position using Equation 5.2
4. Update P_{best} using Equation 5.5
5. Update G_{best} using Equation 5.4
6. Until termination criterion is met.

5.2.4 Bacterial Foraging Algorithm

Bacterial foraging paradigm is a bio-inspired distributed non gradient global optimization method introduced by Passino [129, 130]. The algorithm is inspired by group foraging behavior of bacteria. A foraging bacteria takes foraging in the expression of the constraints represented by its own physiology and environment. i.e. the social animals, like E. coli - a bacterium, search for nutrients to maximize the energy acquired per unit time. Also the specific bacteria communicates with other by sending signals. Bacterial foraging optimization (BFO) algorithm has been used as a global optimization algorithm for fuzzy logic based image enhancement of degraded images by Hanmandlu *et al.* [131]. To know the particular degradation of the image, the parameters of the operator were found by optimizing the image entropy using the bacterial foraging algorithm. This approach worked well for underexposed images but fails for overexposed images and mixed exposed images. Wang *et al.* employed a probability density gradient based interest point detector to extract the stable point features precisely. To discard the outliers in the initial matches he proposed a robust technique, global parallax histogram based filter and tested for inter-frame registration [132]. Bacterial foraging algorithm has been successfully applied to medical image registration [37]. The foraging process is classified into four steps, such as chemotaxis, swarming, reproduction and elimination and dispersal described in [133].

1. **Chemotaxis**: The bacteria swim and tumble through flagella to succeeded the chemotaxis step. The effective approach that a bacterium performs in its total lifetime is switching between swimming and tumbling. If $C(i)$ is the step size specified by the tumble in a random direction and $\theta^i(j,k,l)$ is i^{th} bacterium at j^{th} chemotactic, k^{th} reproductive and l^{th} elimination-dispersal step, then the bacterium undertaking in the chemotaxis step is represented by

$$\theta^i(j+1,k,l) = \theta^i(j,k,l) + C(i)\frac{\delta(i)}{\delta^T(i)\delta(i)} \tag{5.6}$$

where δ indicates a vector in the random direction, between [-1, 1].

2. **Swarming**: Bacteria move in a striking ring by following the produced nutrient gradient of the group by consuming the food. When nutrient is high, bacteria releases the attractant and concentrate to a group producing concentric patterns of clusters with high compactness. The spatial order rest on both the outward activities of the group and local issues of the attractant, which serves as an attraction pointer between bacteria to gather. The cell to cell gesturing for the bacteria is represented by the function.

$$J_{cc}(\theta, P(j,k,l)) = \sum_{i=1}^{S} J_{cc}(\theta, \theta^i(j,k,l)) = \sum_{i=1}^{S}[-d_{attractant}exp(-w_{attractant} \tag{5.7}$$
$$\sum_{m=1}^{p}(\theta_m - \theta_m^i)^2)] + \sum_{i=1}^{S}[-h_{repellant}exp(-w_{repellant}\sum_{m=1}^{p}(\theta_m - \theta_m^i)^2)]$$

where $J_{cc}(\theta, P(j,k,l))$ is the objective function varying w.r.t time, S is the total number of bacteria, number of variables to be optimized is p and $d_{attractant}, w_{attractant}, h_{repellant}, w_{repellant}$ are the coefficients preferred according to the problem.

3. **Reproduction**: In this tone, the unhealthy bacterium expires and the healthier bacterium splits into two bacteria, which are located in the same location to prevent the population of the bacteria constant.

4. **Elimination and Dispersal**: Elimination occurs when local significant increase in high temperature kills the population of bacteria present in a neighborhood with high absorption of foods. A sudden forceful flow of water spread bacteria from one place to some other. The evacuation and the dispersal step affect the chemotactic progress due to demolition, but they too bear the consequence of assisting in chemotaxis, as dispersal places bacteria near noble nutrition sources.

The steps of BFA are as follows:

1. Initialize parameters n, S, N_c , N_s , N_re , N_ed , P_ed , $c(i)(i = 1, 2...S)$, θ^i where n: Dimension of the search space, S: The number of bacteria in the population, N_c: No. of Chemotactix steps, N_re: The number of reproduction steps, N_ed: The number of elimination-dispersal events, P_ed: Elimination-dispersal with probability, $c(i)$: The size of the step taken in the random direction specified by the tumble. θ^i: Position vector

2. Elimination-dispersal step: For (ell=1 to N_ed)

3. Reproduction step: For (k=1 to N_re)

4. Chemotaxis loop:

   (a) For (j=1 to N_c) For (i=1 to S) Evaluate the cost function $J(i, j, k, l) = J(i, j, k, l) + J_{cc}(\theta^i(j, k, l), P(j, k, l))$

   (b) Store the best cost function in $J_{last} = J(i, j, k, l)$

   (c) Tumbling: Generate a random direction and compute the new bacterium position as $J(i, j + 1, k, l)$ with an addition of attractant-repellant effect

   (d) Swimming:

      i. initializing m = 0

      ii. While $m < N_s$

         - if $J(i, j+1, k, l) < J_{last}$ then $J_{last} = J(i, j+1, k, l)$ move in the same direction and compute a new cost as in Step 4c.
         - else $m = N_s$ to force the exit from the loop

5. If $j < N_c$, go to previous step. Continue chemotaxis since the life of the bacteria is not over.

6. Reproduction:

   (a) Compute each bacteria health in chemotaxis loop as $J^i_{health} = \sum_{j=1}^{N_c+1} J(i, j, k, l)$

   (b) Sort bacteria in ascending order of health of bacteria where S_r bacteria with highest values dies with the remaining bacteria of best values split .

7. If $k < N_{re}$, then Step 3 continues to start the chemotactic loop for new generation.

8. Elimination - dispersal: For i=1,....,S with P_{ed}, eliminate and disperse each bacteria. If a bacteria is eliminated, another one dispersed to a random location in the optimization domain. If $l < Ned$, then Step 2 continues, else stop.

5.3 Proposed Optimization Algorithm: Hybrid BF-QPSO

Bacterial Foraging algorithm (BFA) is a non gradient global optimization technique where E-coli bacteria models a trial solution by chemotactic movement. During chemotaxis, the algorithm depends on random search direction, which delays to reach the global solution. To improve the convergence speed along with accuracy of the BFA, the notion of Quantum behaved Particle Swarm Optimization (QPSO) is hybridized in the chemotaxis step of BFA for optimization of multi-modal transformation functions. This hybrid BF-QPSO algorithm emphasizes on a wide usage of the ability of BFA to acquire a new tenacity in the dispersed procedure and analogous search ability of QPSO influenced by the swarm intelligent algorithm. The local search of the algorithm performs during the chemotactic movement procedure of BFA which is accomplished by a QPSO operator. The flowchart of the proposed BF-QPSO is shown in Fig. 5.3.

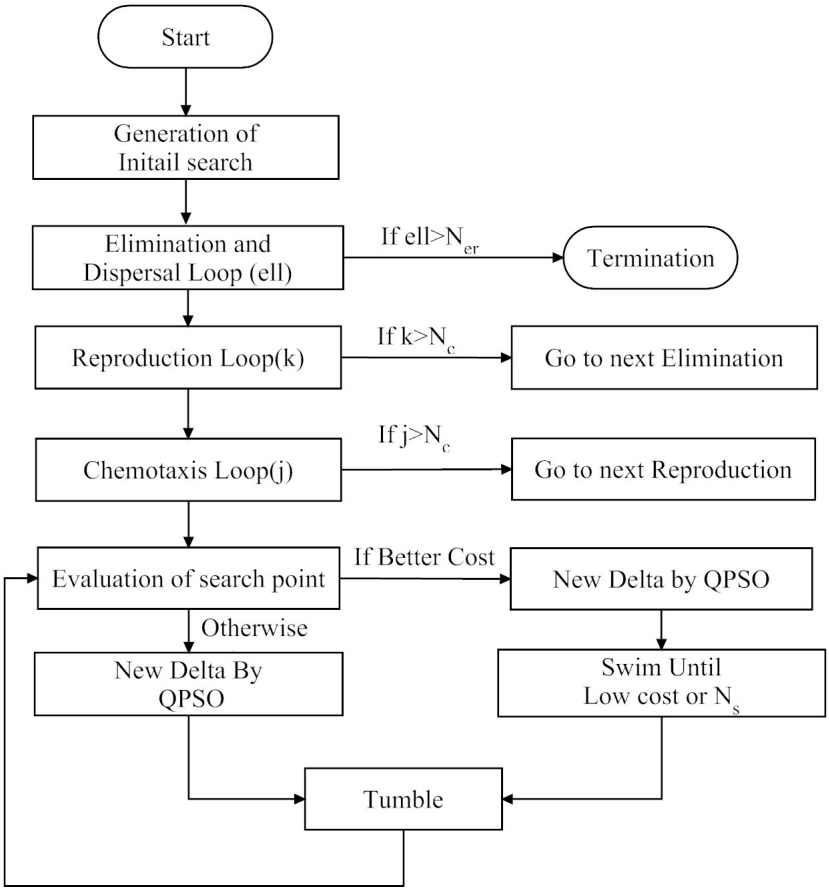

Figure 5.3: Flow chart of proposed BF-QPSO

In BF-QPSO, each bacterium gets transmutated by a QPSO operator after undergoing a chemotactic step. The bacterium is stochastically concerned near the global best position obtained and earlier heading direction from an entire population.

The QPSO operator eliminates the cognitive component. The steps of the BF-QPSO algorithm are as follows:

1. Initialize parameters n, S, N_c , N_s , N_{re} , N_{ed} , P_{ed} , $c(i)(i = 1, 2...S)$, δ, $C1$, $C2$, $R1$, $R2$. where n: Dimension of the search space, S: The number of bacteria in the population, N_c: Number of Chemotactix steps, N_{re}: The number of reproduction steps, N_{ed}: The number of elimination-dispersal events, P_{ed}: Elimination-dispersal with probability, $C(i)$:Step size taken in the random direction specified by the tumble. δ: The inertia weight. $C1$: Swarm Coefficient. $\theta(i, j, k)$: Position vector of the i^{th} bacterium, in j^{th} chemotactic step, and k^{th} reproduction. V_i: Velocity vector of the i^{th} bacterium.

2. For (k=1: N_{re}) For (j=1: N_c) For (i=1: S)

   (a) Evaluate the cost function $J(i, j, k)$

   (b) Store the best cost function in J_{best}, as $J_{best} = J(i, j, k)$

   (c) Tumble by generating a random vector Δ_i with each bacteria and move with $\theta(i, j + 1, k) = \theta(i, j, k) + C1\frac{\Delta_i}{\sqrt{\Delta_i^T \Delta_i}}$ and compute $J(i, j + 1, k)$

   (d) Swimming step initialized with swim length m=0
   While $m < N_s$

   - if $J(i, j+1, k) < J_{best}$ then $J_{best} = J(i, j+1, k)$ move in the same direction and compute a new cost as in .
   - else $m = N_s$ to exit from the loop

3. Chemotaxis step: Update the cost function $J(i, j, k)$ along with the position vector of the best position θ_{gbest} using Equation 5.2 and fitness of the best position $J_{best}(i, j, k)$ using Equation 5.4.

4. Reproduction:

   (a) Compute each bacteria health in the chemotaxis loop as $J^i_{health} = \sum_{j=1}^{N_c+1} J(i, j, k)$

   (b) Bacteria is sorted in ascending order of health of bacteria where S_r bacteria with highest values dies with the remaining bacteria of best values split .

5. If $k < N_{re}$, go to step 1. As the specified number of reproduction steps is not reached, the next generation in the chemotaxis loop starts.

6. Elimination-dispersal: For i=1,....,S with P_{ed}, each bacteria eliminates and disperses.

5.4 Simulation and Results

Extensive experiments have been carried out to evaluate the performance of proposed optimization scheme used for the registration of multi-modal images. The focus is on the optimization of FFD-based registration, where the transformation contains local deformation during image acquisition. As FFD-based registration allows more flexibility during the reformation of the deformed image for analysis, the computation time increases significantly due to a high degree of freedom. Hence, global as well as local optimization techniques are adopted to obtain the final transformed grid, that are controlled through proposed AP-spline interpolation and P-spline interpolation methods. The registration framework is tested under two proposed interpolation methods using both proposed SR-EMI, and EMI based similarity measures. All the combinations of the similarity measures and transformation methods are used in the non-rigid registration framework, where the transformation parameters are optimized with the proposed evolutionary based optimization algorithm named as BF-QPSO algorithm. For the validation, initially the values of step size, grid dimension, iteration number for the convergence, inertia weight, swarm coefficient were set to find the optimum cost function.

To evaluate the performance of the proposed BF-QPSO optimization scheme for registration, simulated brain images such as coronal and axial brain MR T1 weighted images have been taken from database (http://brainweb.bic.mni.mcgill.ca/brainweb/). The spatial resolution of the images used is of size 256×256 pixels. The reference images are deformed with some geometric transformations, to generate the floating image. Two sets of real brain MR image data set of same subject are collected from (Ispat General Hospital, Rourkela) for validation of the proposed optimization scheme. Here, we emphasize on different evolutionary-based optimization schemes for registration procedure, to find the optimum cost function i.e. similarity measure. The comparison of the similarity measure value and some performance indices proves the accuracy and robustness of the proposed optimization schemes for deformed multi-modal images.

For QPSO algorithm, β is called contraction-expansion (CE) coefficient, which can be tuned to control the convergence speed of the algorithms. CE coefficient was set to decrease linearly with the iteration number from 1.0 to 0.5. The population size was 20, and the maximum number of iterations was 40. The inertia weight decreasing linearly from 0.9 to 0.4 and both of the acceleration coefficients C_1 and C_2 were set to 2.

For BF-QPSO algorithm, the number of bacteria in population, s is set to 400. Number of chemotactic steps, $N_c = 20$; Maximum number of swim steps, $N_s = 10$; Number of reproduction steps, $N_{re} = 16$; Number of elimination/dispersal steps, $N_{ed} = 2$; Probability of dispersal, $P_{ed} = 0.25$; Size of the move step $C_{ij} = 0.001$.

In this work, the simulation based experimentation on registration have been performed with four different cases (reference image with floating image). The proposed algorithm is executed 30 times and resulting average similarity value is tabulated in the corresponding tables.

- **Case I**: Axial MR T1 weighted image with deformed T1 weighted image
- **Case II**: Coronal MR T1 weighted image with deformed T1 weighted image
- **Case III**: Pre and post operative brain MR image
- **Case IV**: Pre and post operative brain MR image

5.4.1 Axial MR T1 and deformed T1 image data set

For an evaluation of the proposed optimization scheme, a set of axial brain MR images are considered. In Case I, a set of mono-modal image i.e simulated axial T1 weighted image and its deformed image are also demonstrated, where Fig. 5.4 (a) is the reference image and Fig. 5.4 (b) is the floating image respectively. The registered image using SR-EMI based similarity measure with the AP-spline based interpolation scheme using BFA and QPSO algorithm are shown in Fig. 5.4 (c,d) and their difference image with respect to the reference image are shown in Fig. 5.4 (f,g) respectively. The final transformed grids for these optimization algorithm, where the images are registered are shown in Fig. 5.4 (i-j). The registered image using an evolutionary based hybrid BF-QPSO algorithm, along with its difference image and final transformed grid are shown in Fig. 5.4 (e,h,k) respectively.

Different performance measures such as MRE and SSIM are computed to evaluate the efficiency of the proposed optimization scheme for the nonrigid registration method. The SM values along with MRE, SSIM, and computation time for different evolutionary based optimization schemes such as PSO, QPSO, BFA, and BF-PSO using SR-EMI with AP-spline based interpolation, SR-EMI with P-spline based interpolation, EMI with AP-spline based interpolation, and EMI with P-spline based interpolation schemes are tabulated in Table 5.1. From the table, it is observed that, the SM value using BFA is 1.75, which is more than that of QPSO and PSO based optimization scheme, but the computation time for BFA is 118 sec., which is more as compared to QPSO and PSO. Hence, to find the optimum transformed grid faster, BFA and QPSO algorithms are hybridized to obtain higher SM value with a less computation time. The optimized SM value is found to be 1.96 with a computation time of 103 sec for the proposed BF-QPSO algorithm based registration scheme. After hybridization, the computation time reduced as compared to BFA and BF-PSO algorithm based registration.

The convergence of RMS error curves against a number of iteration of the proposed optimization scheme based registration is compared with BFA, QPSO, BF-PSO based registration schemes, and is shown in Fig. 5.5. From the plot, it is observed that the RMS error value is 5.3, for the proposed BF-QPSO based optimization scheme, which is lower as compared to other existing optimization schemes. The obtained SM values with AP-spline interpolation + SR-EMI based similarity measure using all aforementioned optimization schemes is plotted in Fig. 5.6. From this plot, it is clearly visible that the SM value using the BF-QPSO scheme is higher i.e. 1.96, where as in case of BF-PSO, QPSO and BFA, it is 1.86, 1.75, and 1.70 respectively. Also, it is observed that, the similarity measure value is converged after 10 iteration, whereas all other methods require more number of iteration for convergence of the similarity measure. It signifies the efficiency of the registration scheme with faster convergence.

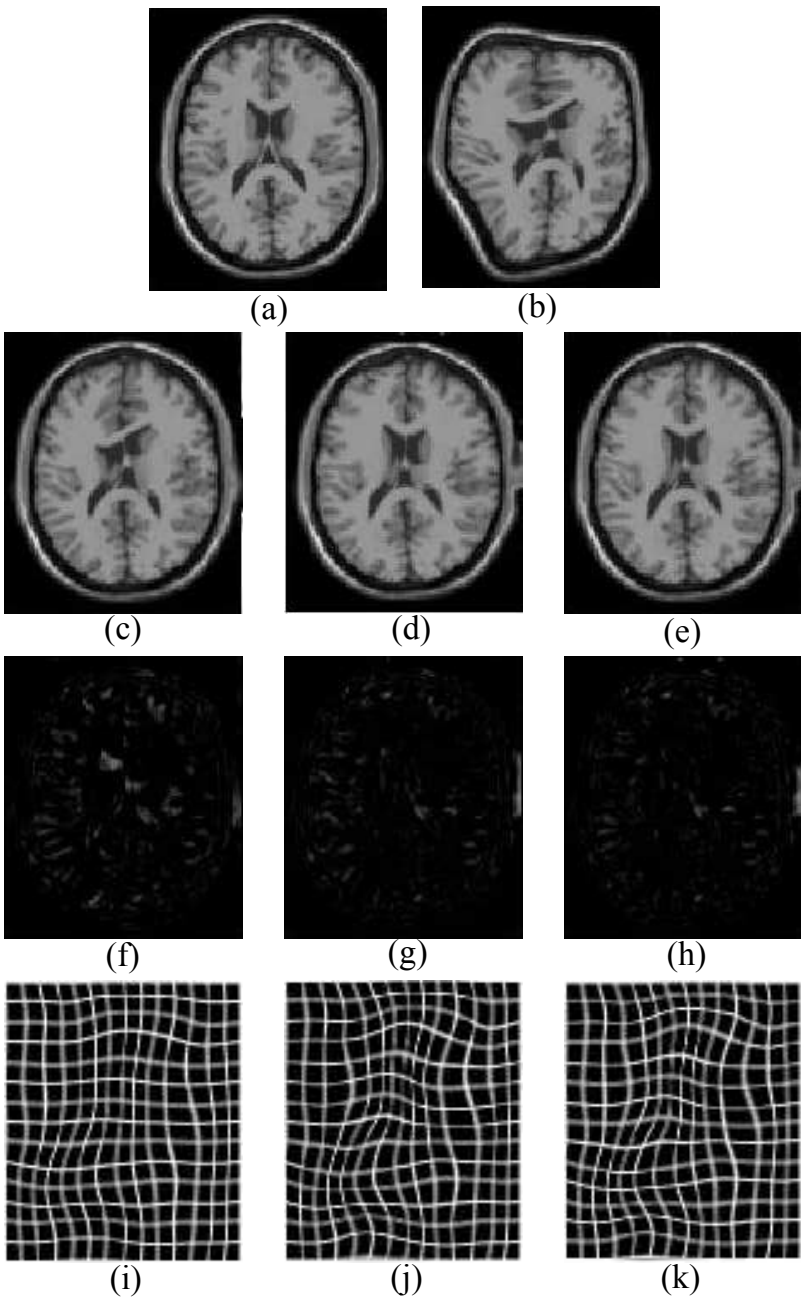

Figure 5.4: (a) Reference image, (b) Floating image, (c-e) Registered images using BFA, QPSO, BF-QPSO with AP-spline interpolation and SR-EMI similarity measure, (f-h) Corresponding difference images, (i-k) Final transformed grid respectively for Case I

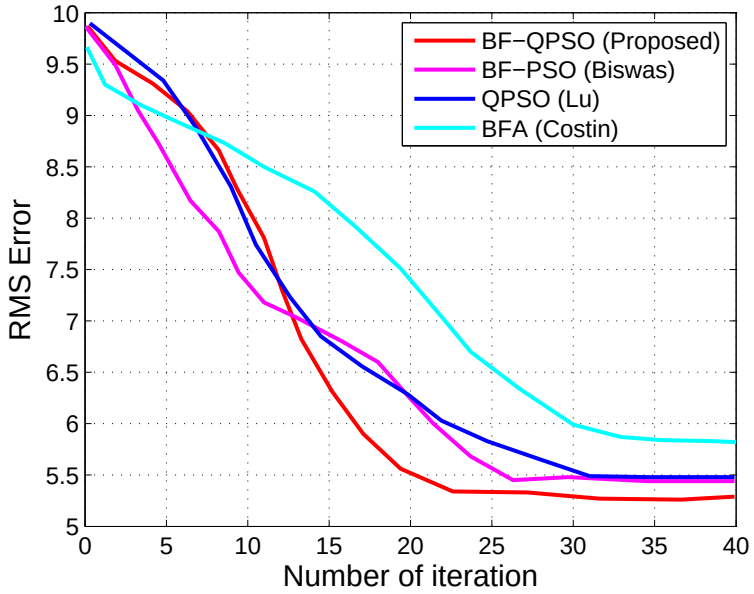

Figure 5.5: RMS error for different optimization methods for Case I

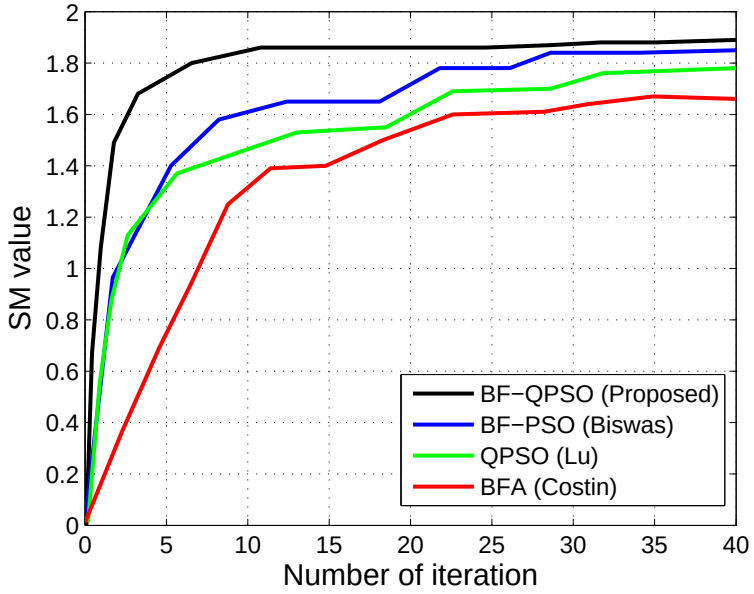

Figure 5.6: SM value for different optimization methods for Case I

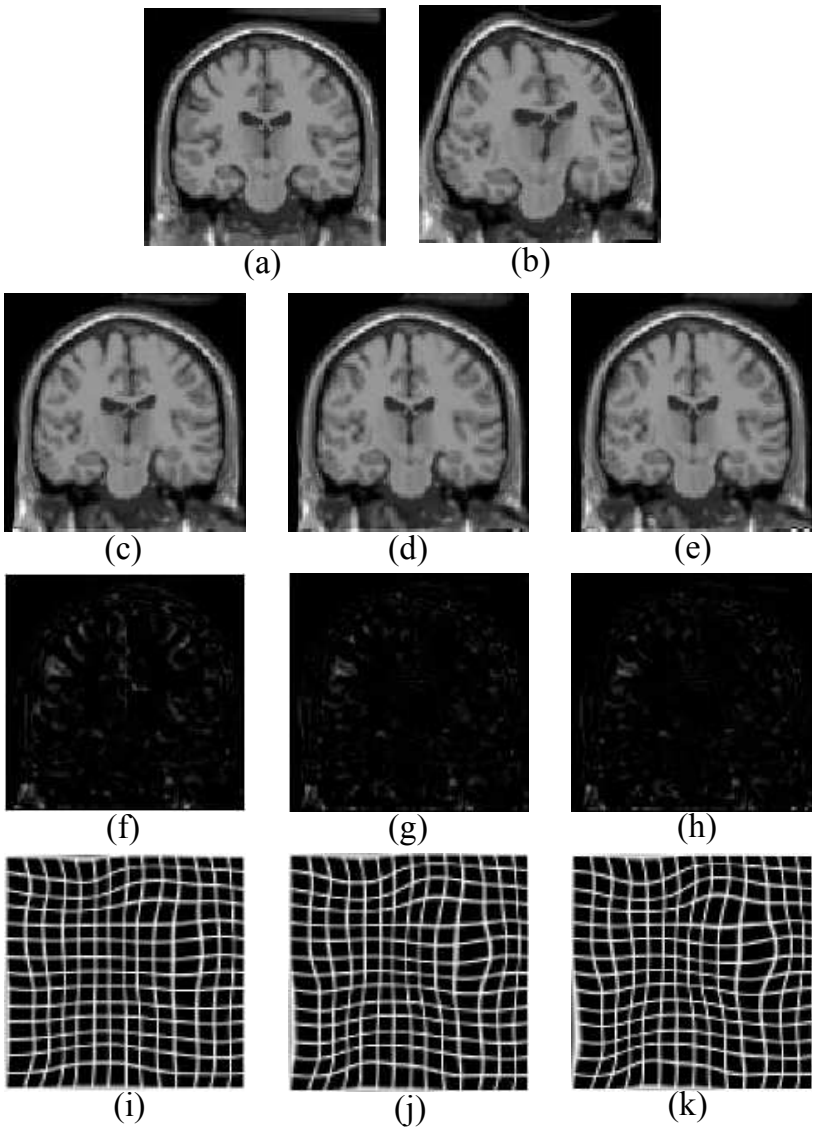

Figure 5.7: (a) Reference image, (b) Floating image, (c-e) Registered image using BFA, QPSO, BF-QPSO with AP-spline interpolation and SR-EMI similarity measure, (f-h) Corresponding difference images, (i-k) Final transformed grid respectively for Case II

Table 5.1: Performance Measures for Case I

Optimization Method	SM and Interpolation method	SM Value	MRE	SSIM	Computation Time (sec)
PSO	**SR-EMI using AP-spline**	**1.63**	**8.96**	**0.718**	**82**
	EMI using AP-spline	1.58	9.23	0.703	85
	SR-EMI using P-spline	1.49	12.57	0.681	87
	EMI using P-spline	1.45	12.94	0.672	98
QPSO	**SR-EMI using AP-spline**	**1.70**	**8.86**	**0.722**	**78**
	EMI using AP-spline	1.63	9.14	0.708	82
	SR-EMI using P-spline	1.53	12.32	0.695	89
	EMI using P-spline	1.49	12.82	0.680	93
BFA	**SR-EMI using AP-spline**	**1.75**	**8.68**	**0.728**	**118**
	EMI using AP-spline	1.69	9.01	0.714	125
	SR-EMI using P-spline	1.62	12.09	0.699	138
	EMI using P-spline	1.52	12.63	0.687	144
BF-PSO	**SR-EMI using AP-spline**	**1.86**	**8.18**	**0.731**	**109**
	EMI using AP-spline	1.74	8.33	0.720	115
	SR-EMI using P-spline	1.71	11.89	0.698	124
	EMI using P-spline	1.59	12.34	0.692	138
BF-QPSO Proposed	**SR-EMI using AP-spline**	**1.96**	**7.38**	**0.739**	**103**
	EMI using AP-spline	1.83	8.05	0.726	107
	SR-EMI using P-spline	1.80	11.28	0.707	118
	EMI using P-spline	1.67	12.03	0.703	129

5.4.2 Coronal MR T1 and deformed T1 image data set

In Case II, another set of healthy coronal T1 weighted image is considered as the reference image whereas deformed T1 weighted image is taken as the floating image and shown in Fig. 5.7 (a,b) respectively. The registered images with optimum transformed parameter using BFA, QPSO algorithm and BF-QPSO algorithm are shown in Fig. 5.7 (c)-(e), where the SR-EMI is used as similarity measure and transformed with the AP-spline interpolation method. Fig. 5.7 (f)-(h), shows the difference images with respect to the reference image with the final transformed grids using the AP-spline interpolation method are shown in Fig. 5.7 (i)-(k) respectively. The optimum SM value, along with performance measures such as MRE, SSIM, and computation time are tabulated in Table 5.2. From the table, it is observed that, the SM value is 2.08 in case of proposed BF-QPSO scheme, where as the MRE value is 6.32, which is lower as compared to other evolutionary based registration schemes. The SM value is enhanced due to the combination of the proposed SR-EMI similarity measure with the AP-spline interpolation method. It is also observed that, the computation time for the proposed scheme is lower due to the hybridization of QPSO technique with BF algorithm. The

optimization technique efficiently maximized the SM value within a comparable time period.

Table 5.2: Performance Measures for Case II

Optimization Method	SM and Interpolation method	SM Value	MRE	SSIM	Computation Time (sec)
PSO	**SR-EMI using AP-spline**	**1.87**	**7.39**	**0.801**	**76**
	EMI using AP-spline	1.68	8.85	0.74	83
	SR-EMI using P-spline	1.59	10.89	0.734	90
	EMI using P-spline	1.48	12.72	0.724	96
QPSO	**SR-EMI using AP-spline**	**1.92**	**7.37**	**0.804**	**73**
	EMI using AP-spline	1.73	8.82	0.75	75
	SR-EMI using P-spline	1.65	10.81	0.743	78
	EMI using P-spline	1.53	12.63	0.732	86
BFA	**SR-EMI using AP-spline**	**1.96**	**7.35**	**0.809**	**112**
	EMI using AP-spline	1.82	8.76	0.783	118
	SR-EMI using P-spline	1.72	10.71	0.752	120
	EMI using P-spline	1.62	12.48	0.748	126
BF-PSO	**SR-EMI using AP-spline**	**1.98**	**7.02**	**0.818**	**104**
	EMI using AP-spline	1.89	8.65	0.789	108
	SR-EMI using P-spline	1.76	10.37	0.758	109
	EMI using P-spline	1.67	12.09	0.749	116
BF-QPSO Proposed	**SR-EMI using AP-spline**	**2.08**	**6.32**	**0.826**	**95**
	EMI using AP-spline	1.93	8.55	0.798	98
	SR-EMI using P-spline	1.79	10.02	0.764	104
	EMI using P-spline	1.71	11.79	0.758	106

5.4.3 Pre and post operative brain MR image data set

In Case III, one more set of pre and post operative real brain MR images is also validated with the proposed optimization based registration method, where the reference image and the floating image are shown in Fig. 5.8 (a,b) respectively. The registered images using the existing optimization algorithms BFA, BF-QPSO are shown in Fig. 5.8 (d,e) and the paired image after registration are shown in Fig. 5.8 (j,k) respectively. The transformed grids for final registered images using these algorithms are displayed in Fig. 5.8 (g-h) respectively. Fig. 5.8 (f,i,l) represent, the registered image, transformed grid, and difference image using hybrid BF-QPSO algorithm respectively. The performance of the proposed hybrid BF-QPSO algorithm is compared with the aforementioned optimization schemes in terms of performance measures such as MRE, SSIM, and computation time, that are recorded in Table 5.3. From the table, it is observed that, the computation time for PSO, QPSO, BFA and BF-PSO are 91 sec, 88 sec, 123 sec, and

118 sec respectively. For the QPSO based registration, the computation time is lower as compared to PSO based registration, but the SM value obtained using QPSO is higher than that of the PSO based registration scheme. Though the SM value obtained using BF algorithm is improved than PSO and QPSO based scheme, it requires more time for optimization. Hence, to obtain the maximum SM value with less computation time, the QPSO algorithm is employed in the chemotaxis step of BF algorithm for faster convergence. The computation time after hybridization becomes 105 sec., which is lower than that of BFA and BF-PSO based registration scheme. At the same time, the SM value is more i.e. 2.54.

Table 5.3: Performance Measures for Case III

Optimization Method	SM and Interpolation method	SM Value	MRE	SSIM	Computation Time (sec)
PSO	**SR-EMI using AP-spline**	**2.22**	**9.21**	**0.801**	**91**
	EMI using AP-spline	2.10	9.52	0.810	97
	SR-EMI using P-spline	2.08	10.21	0.798	101
	EMI using P-spline	1.89	10.98	0.778	109
QPSO	**SR-EMI using AP-spline**	**2.28**	**9.15**	**0.809**	**88**
	EMI using AP-spline	2.18	9.44	0.812	96
	SR-EMI using P-spline	2.12	10.15	0.801	100
	EMI using P-spline	1.98	10.86	0.782	103
BFA	**SR-EMI using AP-spline**	**2.39**	**9.02**	**0.817**	**123**
	EMI using AP-spline	2.26	9.33	0.814	136
	SR-EMI using P-spline	2.22	10.06	0.805	142
	EMI using P-spline	2.02	10.73	0.798	149
BF-PSO	**SR-EMI using AP-spline**	**2.43**	**8.84**	**0.828**	**118**
	EMI using AP-spline	2.34	9.25	0.816	128
	SR-EMI using P-spline	2.32	9.93	0.809	136
	EMI using P-spline	2.09	10.62	0.804	142
BF-QPSO Proposed	**SR-EMI using AP-spline**	**2.54**	**8.78**	**0.835**	**105**
	EMI using AP-spline	2.39	9.01	0.826	112
	SR-EMI using P-spline	2.38	9.86	0.812	125
	EMI using P-spline	2.18	10.51	0.808	129

Similarly, in Case IV, another set of pre and post operative real brain MR images of same subject is also validated with the proposed hybrid BF-QPSO algorithm. Fig. 5.9 (a, b) are the pre-operative and post-operative brain MR images considered as reference and floating image. The image pair before registration is shown in Fig. 5.9 (c). The registered images using the BF and QPSO algorithms along with the proposed optimization algorithm are shown in Fig. 5.9 (d-f) with their final transformed grids in Fig. 5.9 (g-i) respectively. The corresponding paired image after registration are

Table 5.4: Performance Measures for Case IV

Optimization Method	SM and Interpolation method	SM Value	MRE	SSIM	Computation Time (sec)
QPSO	**SR-EMI using AP-spline**	**1.43**	**7.68**	**0.778**	**88**
	EMI using AP-spline	1.39	9.28	0.722	95
	SR-EMI using P-spline	1.28	10.86	0.705	98
	EMI using P-spline	1.22	11.21	0.699	108
BFA	**SR-EMI using AP-spline**	**1.55**	**7.61**	**0.782**	**111**
	EMI using AP-spline	1.46	9.08	0.748	122
	SR-EMI using P-spline	1.39	10.94	0.739	129
	EMI using P-spline	1.28	11.32	0.727	135
BF-PSO	**SR-EMI using AP-spline**	**1.63**	**7.48**	**0.791**	**105**
	EMI using AP-spline	1.52	8.91	0.778	118
	SR-EMI using P-spline	1.48	11.02	0.783	120
	EMI using P-spline	1.36	11.54	0.762	126
BF-QPSO Proposed	**SR-EMI using AP-spline**	**1.86**	**7.37**	**0.809**	**101**
	EMI using AP-spline	1.73	8.81	0.787	113
	SR-EMI using P-spline	1.56	11.28	0.799	111
	EMI using P-spline	1.42	11.62	0.773	118

shown in Fig. 5.9 (j-l) respectively. Comparing Fig. 5.9 (c) and (l), it is found that, the images are registered properly by maximizing the similarity measure using SR-EMI using the proposed BF-QPSO algorithm. The post operative image is transformed with respect to the pre operative brain MR image using the AP-spline interpolation method. The performance measures calculated for this case are tabulated in Table 5.4. Comparing the computation time of the proposed scheme with the other existing scheme, it is observed that, the SR-EMI using AP-spline method needs less computation time as compared to SR-EMI using P-spline method, when optimized using the proposed BF-QPSO algorithm. The performance is also compared with that of the hybrid BF-PSO method using the AP-spline interpolation method and the P-spline interpolation method. Both proposed similarity measures, i.e. SR-EMI and EMI are considered for alignment measure.

The similarity metric value signifies the alignment between the two images after registration process. Higher the similarity measure value implies accurate alignment of the images. In Case IV, the computation time is 101 sec., which is lower as compared to BF-PSO and BFA techniques. The mean registration error (MRE) is also tabulated by considering the registered image with respect to the reference images. In our proposed scheme the MRE is significantly reduced to 7.37, as compared to other evolutionary based optimization schemes. The less value of MRE signifies the best alignment of the images.

In, AP-spline interpolation, in order to smoothen the non-convex and irregular shape of the medical images, a penalized term is imposed adaptively to the B-spline bases, where the deformation is more. Though, bacterial foraging algorithm is a global optimization technique, it requires more time for optimum solution in tumbling process. QPSO algorithm has fewer parameters to be optimized as it does not require the velocity updation, whereas PSO needs more time. Also the contraction-expansion coefficient controls the convergence speed of QPSO algorithm. The hybridized BF-PSO algorithm registered the image but needs more time for convergence. After hybridizing BF and QPSO algorithm, the convergence rate seems faster with better accuracy in terms of computation time and MRE. For, quantitative analysis, Fig. 5.10, the convergence rate is shown through the RMS error curve. From the plot, it is observed that, the RMS value significantly reduced to 5.5 after 20 iterations. But, in case of BF optimization schemes, RMS error is nearly about 6. The optimum SM value obtained for the four evolutionary based optimization techniques for this case is shown in Fig. 5.11. From this, it is observed that, BF-QPSO needs 15 iterations to obtain the optimum similarity measure value, whereas BF-PSO, QPSO, and BFA need 25 to 35 iteration for the optimum SM value. Also, the SM value is comparatively more in case of BF-QPSO scheme.

After validation of all the cases, with all combination of similarity measure and interpolation methods, we observed that, SR-EMI + AP-spline outperforms as compared to SR-EMI +P-spline, EMI + AP-spline, and EMI + P-spline methods. For all cases, the SM value becomes higher, wehereas the MRE and SSIM value significantly reduced with a comparable computation time.

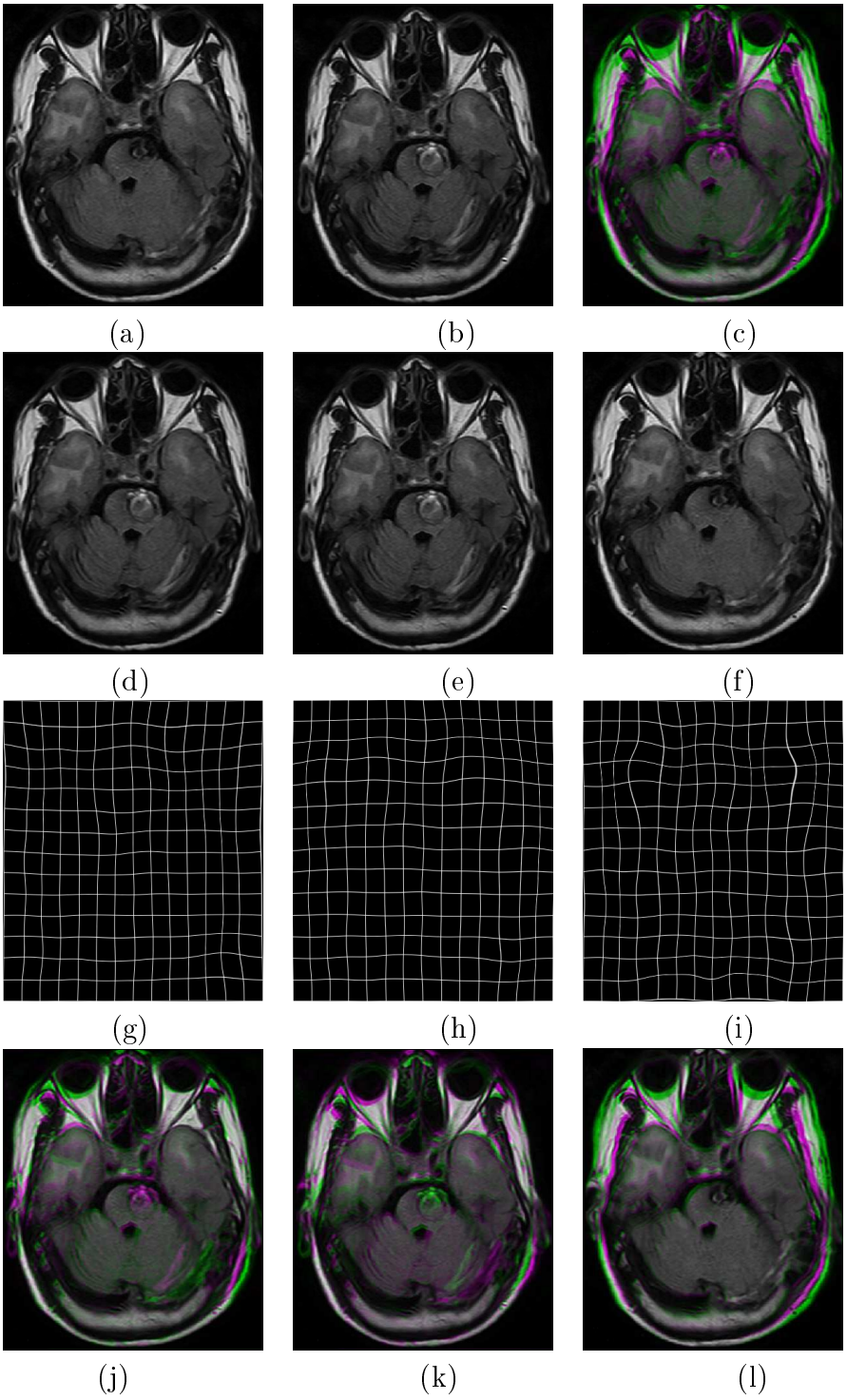

Figure 5.8: (a) Reference image, (b) Floating image, (c) Paired image before registration, (d-f) Registered image using BFA, QPSO, BF-QPSO with AP-spline interpolation and SR-EMI similarity measure, (g-i) Final transformed grid, (j-l) Paired image after registration respectively for Case III

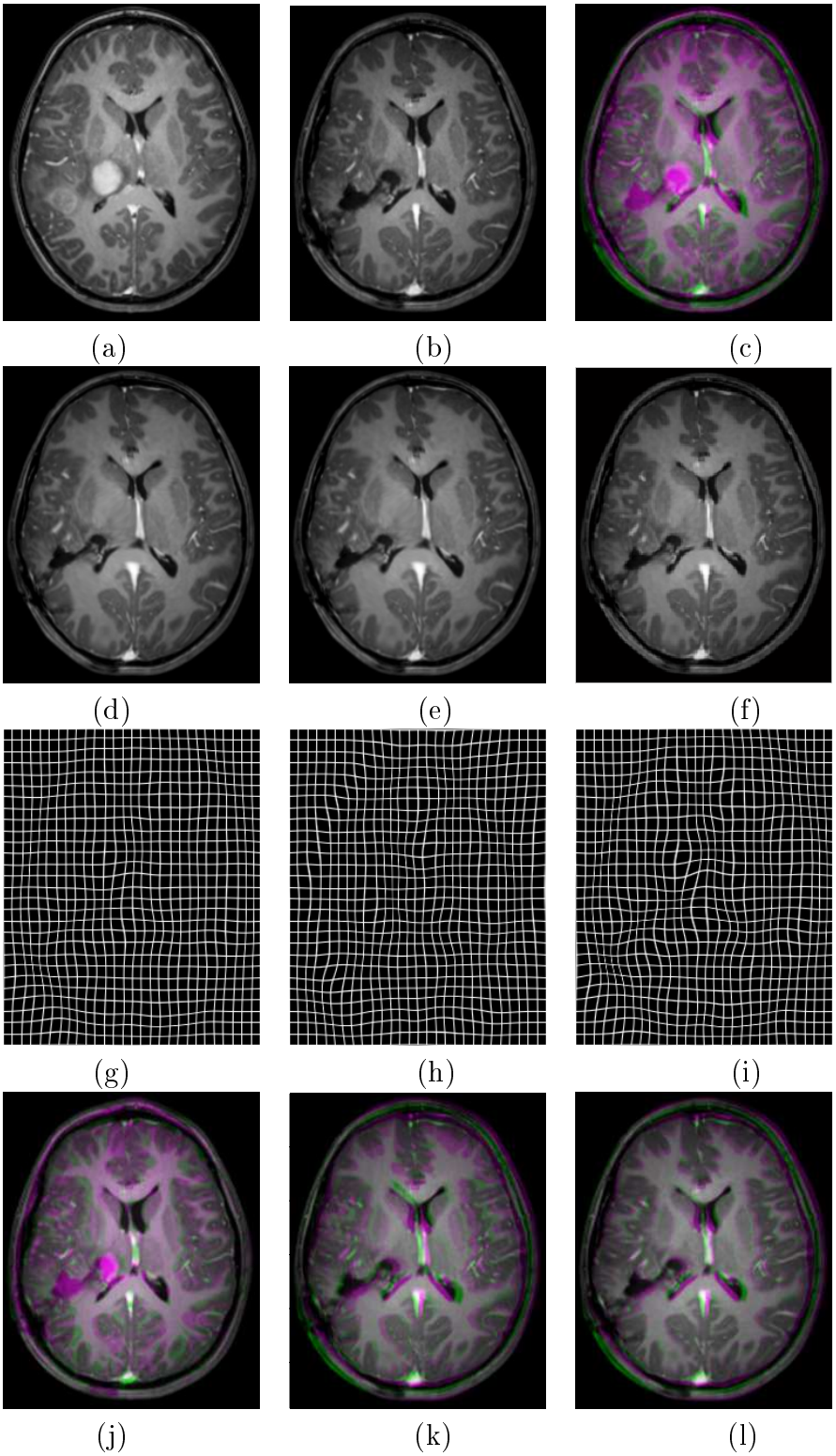

Figure 5.9: (a) Reference image, (b) Floating image, (c) Paired image before registration, (d-f) Registered image using BFA, QPSO, BF-QPSO with AP-spline interpolation and SR-EMI similarity measure, (g-i) Final transformed grid (j-l) Paired image after registration respectively for Case IV

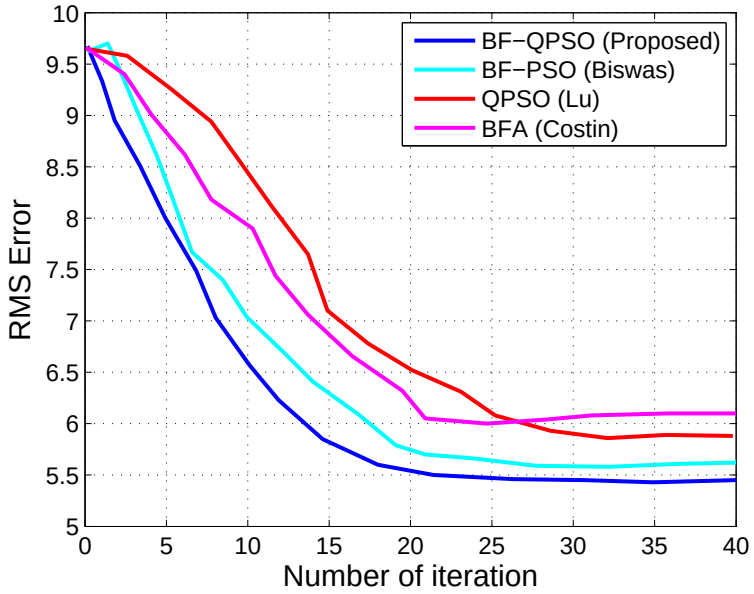

Figure 5.10: RMS error for different optimization methods for Case IV

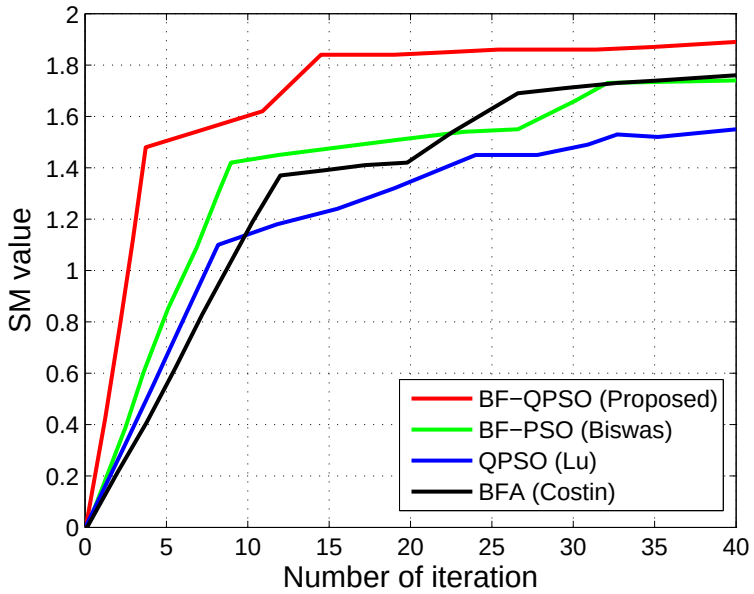

Figure 5.11: SM value for different optimization methods for Case IV

5.5 Summary

In this chapter, the optimization of similarity measures within a given class of geometric transformations is the primary focus. Though Powell optimization technique is used for rigid and affine registration, it fails to optimize in case of non-rigid registration due to the higher degree of parameters. Hence, evolutionary based optimization techniques are adopted to find the transformation grid in the non-rigid registration framework. Though bacterial foraging algorithm optimizes the transformation parameters globally, it suffers from the computational burden due to the step of chemotaxis. Again, quantum behaved optimization technique optimizes the parameters faster than that of PSO algorithm but traps locally. To overcome the difficulty of BFA, a new hybridization technique is proposed embodying the QPSO algorithm in the chemotaxis step of BFA. The proposed algorithm is named as BF-QPSO algorithm. The global search is incorporated through the bacterial foraging optimization technique whereas the local search is incorporated through QPSO algorithm. To validate the proposed hybrid algorithm, simulation has been performed on various multi-modal non-rigid brain images. The optimization of SR-EMI similarity measure with the AP-spline interpolation method is found to be faster convergent than that of existing state of the art. The performance of the proposed BF-QPSO is validated with various multi-modal brain image and compared with the performance of the existing algorithm such as QPSO, BFA, and BF-PSO algorithm. Both proposed P-spline and AP-spline interpolation methods are considered for the transformation of deformed images. For similarity measure, proposed EMI and SR-EMI are considered for the registration framework. Different combinations of the similarity measure along with interpolation methods are considered for the registration of non-rigid images. The performance analysis shows that the BF-QPSO based registration algorithm outperforms similar existing evolutionary algorithms in terms of MRE, SSIM and computation time.

Chapter 6

Conclusion and Future Scopes

6.1 Summary of the Work

This dissertation is focused on the development of efficient registration techniques for multi-modal brain images, where intensity based registration is considered. The process of brain image registration has been divided into three tasks such as similarity measure criterion, transformation and optimization. There are four contributions which are depicted in this dissertation, two of them are focused on the task of similarity measure criterion, and the other two are on the transformation and the step of optimization respectively. For the similarity measure criterion, we proposed two novel methods to augment the efficacy of some existing conventional information theoretic based similarity measure i.e. mutual information. To yield the accurate deformation in the transformation grid, we proposed the P-spline and adaptive P-spline interpolation based approach that are validated with deformed brain images. Moreover, a hybrid optimization technique is also proposed to obtain an optimum cost function with transformation parameter of nonrigid brain image registration. The summary of the thesis is discussed as follows.

In Chapter 2, we proposed a qualitative-quantitative measure of relative information based similarity measure known as Enhance Mutual Information (EMI), to overcome the drawback of conventional mutual information and to confront the efficiency of QMI. MI leads to misalignment when resolution of the input images change, due to lack of qualitative information. We proposed a new similarity measure to overcome the drawback by incorporating qualitative information with joint utility or saliency. The saliency is a qualitative aspect of the information defined from the images, considered as a weighting factor to the mutual information. The saliency used in QMI has scale invariant property. Motivated by the information theoretic measures, a new similarity

measure, EMI is proposed using the weighted relative information of the images. The EMI is found to gain more information than that of QMI. The proposed registration method using EMI is validated with various multi-modal brain images with translation, rotation and scaling transformations. The performance analysis shows that the proposed EMI based registration scheme outperforms the existing QMI, SMI, RMI, and NMI based registration schemes in terms of MRE, SSIM, NCC, PSNR, and UQI. It is observed that, MRE, UQI values are lower in case of the proposed scheme. At the same time, SSIM, NCC, and PSNR values are higher for the proposed scheme as compared to other existing schemes.

The drawback of the saliency measure used in EMI is that, it does not take care of the prospective and projective changes. Hence, scale invariant saliency fail to extract the salient region of the images properly that are affine transformed. To conquer this problem, affine invariant salient region based weighted parameter is incorporated into EMI based registration algorithm, which is proposed in Chapter 3. The proposed similarity measure incorporating the affine invariant saliency is named as SR-EMI. This affine invariant saliency not only enhances the similarity measure value but also reduces the MRE and NCC metrics as compared to EMI and QMI based registration schemes. Experiments show that the proposed SR-EMI is more robust than EMI methods in case of 2D affine brain image registration. The projective and prospective transformations are taken care with the affine invariant salient region.

In Chapter 4, the deformed brain MR image registration is carried out using spline based transformation. This type of registration is known as non-rigid registration, which has application in case of real medical image analysis, to know the treatment planning during surgery. Here, the registration process is performed on the image grid that are applied to reform the geometrically deformed images. The similarity measure is maximized within the constrains of a transformation model during the registration process. B-spline based interpolation has incorporated to model the deformed grid of the floating image. But, it fails to register intra tissues of brain by property of sensitivity to distribution of intensity. To overcome this bottleneck, penalized spline (P-spline) interpolation based registration method is proposed. Though, P-spline interpolation based method reform the deformed grid with a regularization or penalty term, the computation time of P-spline is quite higher than that of the B-spline based interpolation technique, due to the computation of penalty term at each grid point. Hence, an adaptive method is proposed which is based on the notion of NURBs. The proposed adaptive P-spline (AP-spline) based registration technique successfully obtained the reformed grid by transforming the deformed floating image with less computation time than that of the P-spline interpolation based registration method. From the experimental results, it is observed that the proposed AP-spline interpolation with the

proposed SR-EMI based registration method is more efficient than that of P-spline and B-spline based registration approach, in terms of some performance measures i.e. MSE, RMS, UQI and computation time. The proposed method not only aligns the shape structure of deformed brain very well, but also reasonably maintain the correspondence of local deformation.

Finally, in Chapter 5, we proposed a hybrid evolutionary based optimization method named bacterial foraging - quantum behaved particle swarm optimization (BF-QPSO), a new optimization technique for deformed brain images, to improve the accuracy and efficiency of the registration procedure. In, past several years, PSO and QPSO have been successfully applied for rigid medical image registration. Though QPSO converges faster, it traps at local optimum. Similarly, the bacterial foraging algorithm is a global optimization scheme used for medical image registration, but the computation time is more to obtain optimal convergence. For trade of between the global and local search, hybrid evolutionary technique is proposed using the notion of the bacterial foraging (BF) algorithm and quantum behaved particle swarm optimization (QPSO) technique for registration of non-rigid images. The proposed hybrid optimization technique is validated for rigid and nonrigid brain image registration. In case of rigid brain image registration, we applied BF-QPSO to both simulated data and real brain image dataset to obtain the robustness of the algorithm. Similarly, for nonrigid registration, the simulation results prove the faster convergence of the proposed hybrid algorithm than that of other similar techniques. In order to compare with the other conventional methods, PSO, BFA, QPSO, and BF-PSO are also experimented for each dataset. In this chapter both the P-spline and AP-spline interpolation scheme are applied for non-rigid registration. The proposed similarity measures i.e. EMI and SR-EMI are considered for alignment measurement. After exhaustive study, it is found that SR-EMI + AP-spline interpolation with BF-QPSO optimization based registration method outperforms the other proposed combination schemes, i.e, SR-EMI + P-spline + BF-QPSO, SR-EMI + AP-spline + BF-PSO etc. Considering all combinations, the computation time is lowest i.e in SR-EMI using AP-spline interpolation based registration scheme optimized with BF-QPSO.

6.2 Future Scope of Research

Medical imaging plays a significant role in modern healthcare and will continue to do as patient-specific care is emerging. The new era will even further increase the number of possible clinical applications utilizing image registration. In addition to focus on further improvement in non-rigid image registration, several interesting research directions are discussed next.

1. Segmentation based registration: Our ongoing efforts are focused on non-rigid registration. In the future, we intend to develop an image registration approach followed by a segmentation method for possible clinical applications. Segmentation discriminates the most likely structures and aids certain information. Prior information of the shapes or relative positions of internal structures may help in the registration process and will assist the clinician for analysis.

2. 3D image registration: For surgical assistance, 3D image registration is necessary for proper analysis during treatment planning. In the future, the proposed non-rigid registration framework may be extended to world 3D environment.

3. Group-wise image registration: Another possible future work direction is to extend the proposed Enhanced mutual information similarity measure to register a set of multiple images. The key idea is to register all image frames to the average (mean) image.

4. Image fusion: Another possible future work direction is image fusion. It would be of great interest to fuse images after their registration. Images are usually registered for the purpose of combining or comparing them, enabling the fusion of information in the images. Incorporating image fusion with our nonrigid registration algorithm will provide a systematic framework which extracts information from input images such that the fused image provides better information for human or machine perception as compared to any of the input images.

5. Regularization terms: In this dissertation, free form deformation based non-rigid registration is performed. Regularization terms or penalty terms are incorporated in to B-spline interpolation for transformation of local deformations. The possible future work is, the choice of diffusion regularizer, for implementation of curvature or linear elasticity within non-grid positions.

Appendix

Appendix-A

In this appendix, the maximum information obtained by Equation (2.22) is described. Also its lower and upper bounds to prove the inequality is given.

Considering the function

$$\zeta\left(R_1\, R_2\, ...\, R_n\; W_1\, W_2\, ...\, W_n\right) = -\sum_{i=1}^{n} R_i log R_i + \sum_{i=1}^{n} R_i W_i + \lambda(\sum_{i=1}^{n} R_i - 1) \tag{6.1}$$

where λ is the lagrange multiplier and is a real positive number. The function ζ is maximum with respect to R_i for fixed w_i coincides with the maximum of function $H_1(R, W)$. The conditions for extreme is given by

$$\begin{cases} \frac{\partial \zeta(R_1\, R_2\, ...\, R_n\; W_1\, W_2\, ...\, W_n)}{\partial R_i} = 0 \quad 1 < i \leq n \\ \sum\limits_{i=0}^{n} P_i = 1 \end{cases} \tag{6.2}$$

applying (6.2) on the function (6.1) we obtain

$$R_i = \frac{2^{Wi}}{\sum_{i=0}^{n} 2^{Wi}} \tag{6.3}$$

$i = 1, 2, ..., n$ This extreme is maximum because,

$$\frac{\partial^2 \zeta}{\partial R_i^2} = -\frac{\sum_{i=0}^{n} 2^{Wi}}{2^{w_i} ln 2} \; < 0$$

and

$$\frac{\partial^2 \zeta}{\partial R_i R_j} = 0 \qquad when \;\; i \neq j \tag{6.4}$$

Applying (6.4) into $H_4(R/F, W) = -\sum_{n=1}^{N} R_n log(R_i/F_i) + \sum_{n=1}^{N} W_n R_n$ we will get $max_{R_i} H_4(R/F, W) = log_2\left(\sum_{i=0}^{n} 2^{Wi}\right)$. The maximum value obtained when $R_i = \frac{2^{Wi}}{\sum_{i=0}^{n} 2^{Wi}}$ for each i. Hence, the derivative provides an easy method for finding the optimum probabilities, which maximizes the entropy (2.22).

The bounds of new similarity measure using the inequalities derived by Halliwell et al. [134] provides the improved lower and upper bound on relative entropy given by (2.22).

Let $R_i, F_i > 0$ where $1 \neq i \neq n$ and $\sum_{i=0}^{n} R_n = 1 = \sum_{i=0}^{n} F_n$

Then the following estimate holds

$$\sum_{i=1}^{n} \frac{f_i(f_i - r_i)^2}{(f_i)^2 + (max(f_i r_i))^2} \leq \sum_{i=1}^{n} R_i log \frac{R_i}{F_i} \leq \frac{f_i(f_i - r_i)^2}{(f_i)^2 + (min(f_i r_i))^2} \tag{6.5}$$

The inequality is refinement of Shanon inequality given by $\sum_{i=1}^{n} R_i log \geq 0$. Replacing f_i by $R_i = \frac{2^{Wi}}{\sum_{i=0}^{n} 2^{Wi}}$ in the above inequality

$$\sum_{i=1}^{n} \frac{\frac{2^{Wi}}{\sum_{i=0}^{n} 2^{Wi}} \left(\frac{2^{Wi}}{\sum_{i=0}^{n} 2^{Wi}} - r_i\right)^2}{\left(\frac{2^{Wi}}{\sum_{i=0}^{n} 2^{Wi}}\right)^2 + \left(max\left(\frac{2^{Wi}}{\sum_{i=0}^{n} 2^{Wi}} r_i\right)\right)^2} \leq log\left(\sum_{i=0}^{n} 2^{Wi}\right)$$

$$-H^*(R,W) \leq \sum_{i=1}^{n} \frac{\frac{2^{Wi}}{\sum_{i=0}^{n} 2^{Wi}} \left(\frac{2^{Wi}}{\sum_{i=0}^{n} 2^{Wi}} - r_i\right)^2}{\left(\frac{2^{Wi}}{\sum_{i=0}^{n} 2^{Wi}}\right)^2 + \left(max\left(\frac{2^{Wi}}{\sum_{i=0}^{n} 2^{Wi}} r_i\right)\right)^2} \tag{6.6}$$

which gives

$$log\left(\sum_{i=0}^{n} 2^{Wi}\right) - \sum_{i=1}^{n} \frac{\frac{2^{Wi}}{\sum_{i=0}^{n} 2^{Wi}} \left(\frac{2^{Wi}}{\sum_{i=0}^{n} 2^{Wi}} - r_i\right)^2}{\left(\frac{2^{Wi}}{\sum_{i=0}^{n} 2^{Wi}}\right)^2 + \left(min\left(\frac{2^{Wi}}{\sum_{i=0}^{n} 2^{Wi}} r_i\right)\right)^2} \leq H^*(R,W)$$

$$\leq \sum_{i=1}^{n} \frac{\frac{2^{Wi}}{\sum_{i=0}^{n} 2^{Wi}} \left(\frac{2^{Wi}}{\sum_{i=0}^{n} 2^{Wi}} - r_i\right)^2}{\left(\frac{2^{Wi}}{\sum_{i=0}^{n} 2^{Wi}}\right)^2 + \left(max\left(\frac{2^{Wi}}{\sum_{i=0}^{n} 2^{Wi}} r_i\right)\right)^2} \tag{6.7}$$

This proves the equality holds in the above inequality if $R_i = \frac{2^{Wi}}{\sum_{i=0}^{n} 2^{Wi}}$ for each i. The relative entropy has two advantages a) gives maximum information and b) minimizing the transmission time for source information.

Bibliography

[1] L. G. Brown, "A survey of image registration techniques," *ACM computing surveys (CSUR)*, vol. 24, no. 4, pp. 325–376, 1992.

[2] U. C. Pati, P. K. Dutta, and A. Barua, "Feature level fusion of range and intensity images of an object," *International Journal of Computational Vision and Robotics*, vol. 1, no. 1, pp. 2–33, 2009.

[3] B. Spottiswoode, D. Van den Heever, Y. Chang, S. Engelhardt, S. Du Plessis, F. Nicolls, H. Hartzenberg, and A. Gretschel, "Preoperative three-dimensional model creation of magnetic resonance brain images as a tool to assist neurosurgical planning," *Stereotactic and functional neurosurgery*, vol. 91, no. 3, pp. 162–169, 2013.

[4] D. Loeckx, P. Slagmolen, F. Maes, D. Vandermeulen, and P. Suetens, "Nonrigid image registration using conditional mutual information," *Medical Imaging, IEEE Transactions on*, vol. 29, no. 1, pp. 19–29, 2010.

[5] T. Rohlfing, C. R. Maurer Jr, D. A. Bluemke, and M. A. Jacobs, "Volume-preserving nonrigid registration of mr breast images using free-form deformation with an incompressibility constraint," *Medical Imaging, IEEE Transactions on*, vol. 22, no. 6, pp. 730–741, 2003.

[6] D. Ruan, J. A. Fessler, M. Roberson, J. Balter, and M. Kessler, "Nonrigid registration using regularization that accomodates local tissue rigidity," in *Medical Imaging*. International Society for Optics and Photonics, 2006, pp. 614 412–614 412.

[7] M. Staring, S. Klein, and J. P. Pluim, "A rigidity penalty term for nonrigid registration," *Medical physics*, vol. 34, no. 11, pp. 4098–4108, 2007.

[8] N. J. Tustison and B. B. Avants, "Explicit b-spline regularization in diffeomorphic image registration," *Front. Neuroinform*, vol. 7, no. 39, 2013.

[9] S. Alkaabi and F. Deravi, "Iterative transform parameter refinement for image registration," 2005.

[10] F. P. Oliveira and J. M. R. Tavares, "Medical image registration: a review," *Computer methods in biomechanics and biomedical engineering*, vol. 17, no. 2, pp. 73–93, 2014.

[11] B. Zitova and J. Flusser, "Image registration methods: a survey," *Image and vision computing*, vol. 21, no. 11, pp. 977–1000, 2003.

[12] F. Maes, A. Collignon, D. Vandermeulen, G. Marchal, and P. Suetens, "Multimodality image registration by maximization of mutual information," *Medical Imaging, IEEE Transactions on*, vol. 16, no. 2, pp. 187–198, 1997.

[13] C. Studholme, D. L. Hill, and D. J. Hawkes, "An overlap invariant entropy measure of 3d medical image alignment," *Pattern recognition*, vol. 32, no. 1, pp. 71–86, 1999.

[14] R. Shekhar and V. Zagrodsky, "Mutual information-based rigid and nonrigid registration of ultrasound volumes," *Medical Imaging, IEEE Transactions on*, vol. 21, no. 1, pp. 9–22, 2002.

[15] G. K. Rohde, A. Aldroubi, and B. M. Dawant, "The adaptive bases algorithm for intensity-based nonrigid image registration," *Medical Imaging, IEEE Transactions on*, vol. 22, no. 11, pp. 1470–1479, 2003.

[16] A. Andronache, M. von Siebenthal, G. Székely, and P. Cattin, "Non-rigid registration of multi-modal images using both mutual information and cross-correlation," *Medical image analysis*, vol. 12, no. 1, pp. 3–15, 2008.

[17] M. P. Heinrich, M. Jenkinson, M. Bhushan, T. Matin, F. V. Gleeson, J. M. Brady, and J. A. Schnabel, "Non-local shape descriptor: a new similarity metric for deformable multi-modal registration," in *Medical Image Computing and Computer-Assisted Intervention–MICCAI 2011*. Springer, 2011, pp. 541–548.

[18] H. Rivaz and D. L. Collins, "Self-similarity weighted mutual information: A new nonrigid image registration metric," in *Medical Image Computing and Computer-Assisted Intervention–MICCAI 2012*. Springer, 2012, pp. 91–98.

[19] T. M. Lehmann, C. Gonner, and K. Spitzer, "Survey: Interpolation methods in medical image processing," *Medical Imaging, IEEE Transactions on*, vol. 18, no. 11, pp. 1049–1075, 1999.

[20] D. Rueckert, L. I. Sonoda, C. Hayes, D. L. Hill, M. O. Leach, and D. J. Hawkes, "Nonrigid registration using free-form deformations: application to breast mr images," *Medical Imaging, IEEE Transactions on*, vol. 18, no. 8, pp. 712–721, 1999.

[21] D. Rueckert, P. Aljabar, R. A. Heckemann, J. V. Hajnal, and A. Hammers, "Diffeomorphic registration using b-splines," in *Medical Image Computing and Computer-Assisted Intervention–MICCAI 2006*. Springer, 2006, pp. 702–709.

[22] A. Sotiras, C. Davatzikos, and N. Paragios, "Deformable medical image registration: A survey," *Medical Imaging, IEEE Transactions on*, vol. 32, no. 7, pp. 1153–1190, 2013.

[23] M. Unser, "Splines: A perfect fit for signal and image processing," *Signal Processing Magazine, IEEE*, vol. 16, no. 6, pp. 22–38, 1999.

[24] A. Diou, Y. Voisin, L. L. Y. Voon, G. Moreels, and J. Clairemidi, "Some applications of b-spline functions in image processing," *Graphics/Vision Interface*, 1998.

[25] U. M, "Splines: a perfect fit for medical imaging," in *Keynote address, SPIE Symposium on Medical Imaging*. Springer, 2002, pp. 1–12.

[26] X. Zhuang, S. Arridge, D. J. Hawkes, and S. Ourselin, "A nonrigid registration framework using spatially encoded mutual information and free-form deformations," *Medical Imaging, IEEE Transactions on*, vol. 30, no. 10, pp. 1819–1828, 2011.

[27] M. Khader and A. B. Hamza, "An entropy-based technique for nonrigid medical image alignment," in *Combinatorial Image Analysis*. Springer, 2011, pp. 444–455.

[28] S. Y. Chun and J. A. Fessler, "A simple regularizer for b-spline nonrigid image registration that encourages local invertibility," *Selected Topics in Signal Processing, IEEE Journal of*, vol. 3, no. 1, pp. 159–169, 2009.

[29] J. Du, S. Tang, T. Jiang, and Z. Lu, "Intensity-based robust similarity for multimodal image registration," *International Journal of Computer Mathematics*, vol. 83, no. 1, pp. 49–57, 2006.

[30] P. H. Eilers and B. D. Marx, "Flexible smoothing with b-splines and penalties," *Statistical science*, pp. 89–102, 1996.

[31] T. J. Jacobson, *An Investigation of NURBS-based Deformable Image Registration*. Virginia Commonwealth University, 2014.

[32] J. C. Rajapakse, R. G. Meegama, and L. S. Ho, "Nurbs-based analysis of gender-related variability of the human brain surface," in *Control, Automation, Robotics and Vision, 2002. ICARCV 2002. 7th International Conference on*, vol. 1. IEEE, 2002, pp. 520–524.

[33] J. Wang and T. Jiang, "Nonrigid registration of brain mri using nurbs," *Pattern Recognition Letters*, vol. 28, no. 2, pp. 214–223, 2007.

[34] S. Lahmiri and M. Boukadoum, "New approach for automatic classification of alzheimer's disease, mild cognitive impairment and healthy brain magnetic resonance images," *Healthcare Technology Letters*, vol. 1, no. 1, pp. 32–36, 2014.

[35] P. Thévenaz and M. Unser, "Optimization of mutual information for multiresolution image registration," *Image Processing, IEEE Transactions on*, vol. 9, no. 12, pp. 2083–2099, 2000.

[36] R. He and P. A. Narayana, "Global optimization of mutual information: application to three-dimensional retrospective registration of magnetic resonance images," *Computerized Medical Imaging and Graphics*, vol. 26, no. 4, pp. 277–292, 2002.

[37] H. Costin and S. Bejinariu, "Medical image registration by means of a bio-inspired optimization strategy," *The Computer Science Journal of Moldova*, vol. 20, no. 2, p. 59, 2012.

[38] H. Luan, F. Qi, Z. Xue, L. Chen, and D. Shen, "Multimodality image registration by maximization of quantitative–qualitative measure of mutual information," *Pattern Recognition*, vol. 41, no. 1, pp. 285–298, 2008.

[39] W. M. Wells, P. Viola, H. Atsumi, S. Nakajima, and R. Kikinis, "Multi-modal volume registration by maximization of mutual information," *Medical image analysis*, vol. 1, no. 1, pp. 35–51, 1996.

[40] P. Viola and W. M. Wells III, "Alignment by maximization of mutual information," *International journal of computer vision*, vol. 24, no. 2, pp. 137–154, 1997.

[41] J. P. Pluim, J. A. Maintz, and M. A. Viergever, "Mutual-information-based registration of medical images: a survey," *Medical Imaging, IEEE Transactions on*, vol. 22, no. 8, pp. 986–1004, 2003.

[42] J. P. Pluim, Maintz, and M. A. Viergever, "Image registration by maximization of combined mutual information and gradient information," *Medical Imaging, IEEE Transactions on*, vol. 19, no. 8, pp. 809–814, 2000.

[43] D. B. Russakoff, C. Tomasi, T. Rohlfing, and C. R. Maurer Jr, "Image similarity using mutual information of regions," in *Computer Vision-ECCV 2004*. Springer, 2004, pp. 596–607.

[44] Y. W. Chen and C. L. Lin, "Pca based regional mutual information for robust medical image registration," in *Advances in Neural Networks–ISNN 2011*. Springer, 2011, pp. 355–362.

[45] J. D. Lee, C. H. Huang, Y. H. Weng, K. J. Lin, and C. T. Chen, "An automatic mri/spect registration algorithm using image intensity and anatomical feature as matching characters: application on the evaluation of parkinson's disease," *Nuclear medicine and biology*, vol. 34, no. 4, pp. 447–457, 2007.

[46] D. B. Russakoff, T. Rohlfing, and C. R. Maurer Jr, "Fast intensity-based 2d-3d image registration of clinical data using light," in *Computer Vision, 2003. Proceedings. Ninth IEEE International Conference on.* IEEE, 2003, pp. 416–422.

[47] T. Rohlfing and C. R. Maurer Jr, "Intensity-based non-rigid registration using adaptive multilevel free-form deformation with an incompressibility constraint," in *Medical Image Computing and Computer-Assisted Intervention–MICCAI 2001.* Springer, 2001, pp. 111–119.

[48] A. Roche, X. Pennec, G. Malandain, and N. Ayache, "Rigid registration of 3-d ultrasound with mr images: a new approach combining intensity and gradient information," *Medical Imaging, IEEE Transactions on*, vol. 20, no. 10, pp. 1038–1049, 2001.

[49] L. Junck, J. G. Moen, G. D. Hutchins, M. B. Brown, and D. E. Kuhl, "Correlation methods for the centering, rotation, and alignment of functional brain images." *Journal of nuclear medicine: official publication, Society of Nuclear Medicine*, vol. 31, no. 7, pp. 1220–1226, 1990.

[50] A. V. Cideciyan, "Registration of ocular fundus images," *IEEE Engineering in medicine and biology*, vol. 14, no. 1, pp. 52–58, 1995.

[51] X. Lu, S. Zhang, H. Su, and Y. Chen, "Mutual information-based multimodal image registration using a novel joint histogram estimation," *Computerized Medical Imaging and Graphics*, vol. 32, no. 3, pp. 202–209, 2008.

[52] J. V. Hajnal, N. Saeed, A. Oatridge, E. J. Williams, I. R. Young, and G. M. Bydder, "Detection of subtle brain changes using subvoxel registration and subtraction of serial mr images." *Journal of computer assisted tomography*, vol. 19, no. 5, pp. 677–691, 1995.

[53] R. P. Woods, S. T. Grafton, C. J. Holmes, S. R. Cherry, and J. C. Mazziotta, "Automated image registration: I. general methods and intrasubject, intramodality validation," *Journal of computer assisted tomography*, vol. 22, no. 1, pp. 139–152, 1998.

[54] T. M. Cover and J. A. Thomas, *Elements of information theory.* John Wiley & Sons, 2012.

[55] D. D. V. D. S. Collignon, Maes and M. G., "Automated multimodality image registration based on information theory," *Information processing in Medical Imaging*, pp. 263–274, 1995.

[56] E. Parzen, "On estimation of a probability density function and mode," *The annals of mathematical statistics*, pp. 1065–1076, 1962.

[57] J. Li, K. Wu, X. Zhang, and M. Ding, "Image quality assessment based on multi-channel regional mutual information," *AEU-International Journal of Electronics and Communications*, vol. 66, no. 9, pp. 784–787, 2012.

[58] E. Haber and J. Modersitzki, "Intensity gradient based registration and fusion of multi-modal images," in *Medical Image Computing and Computer-Assisted Intervention–MICCAI 2006.* Springer, 2006, pp. 726–733.

[59] R. Bhagalia, J. Fessler, B. Kim *et al.*, "Gradient based image registration using importance sampling," in *Biomedical Imaging: Nano to Macro, 2006. 3rd IEEE International Symposium on.* IEEE, 2006, pp. 446–449.

[60] M. Belis and S. Guiasu, "A quantitative-qualitative measure of information in cybernetic systems (corresp.)," *Information Theory, IEEE Transactions on*, vol. 14, no. 4, pp. 593–594, 1968.

[61] V. Mani *et al.*, "Survey of medical image registration," *Journal of Biomedical Engineering and Technology*, vol. 1, no. 2, pp. 8–25, 2013.

[62] H. Taneja and R. Tuteja, "Characterization of a quantitative-qualitative measure of relative information," *Information sciences*, vol. 33, no. 3, pp. 217–222, 1984.

[63] J. Kapur, "New qualitative-quantitative measure of information," *National Academy Science Letters-India*, vol. 9, no. 2, pp. 51–54, 1986.

[64] D. Hooda, "On a generalized measure of relative useful information," *Soochow Journal of Mathematics*, vol. 12, pp. 23–32, 1986.

[65] V. Munteanu and D. Tarniceriu, "Optimal coding for qualitative sources on noiseless channels," *The Annals of Dunarea De Jos University of Galati Fascicle II (Electrotechnics, Electronics, Automatic Control, Informatics)*, 2006.

[66] K. C. Jain and S. Amit, "On a new quantitative-qualitative measure of information," *Journal of Applied Mathematics, Statistics and Informatics (JAMSI)*, vol. 4, no. 2, 2008.

[67] A. Srivastava, "Some new bounds of weighted entropy measures," *Cybernetics and Information Technologies*, vol. 11, no. 3, 2011.

[68] T. Kadir, D. Boukerroui, and M. Brady, "An analysis of the scale saliency algorithm," *OUEL No: 2264*, vol. 3, pp. 1–38, 2003.

[69] X. Huang, Y. Sun, D. Metaxas, F. Sauer, and C. Xu, "Hybrid image registration based on configural matching of scale-invariant salient region features," in *Computer Vision and Pattern Recognition Workshop, 2004. CVPRW'04. Conference on.* IEEE, 2004.

[70] C. R. Maurer Jr, J. M. Fitzpatrick, M. Y. Wang, R. L. Galloway, R. J. Maciunas, and G. S. Allen, "Registration of head volume images using implantable fiducial markers," *Medical Imaging, IEEE Transactions on*, vol. 16, no. 4, pp. 447–462, 1997.

[71] J. Maver, "Self-similarity and points of interest," *Pattern Analysis and Machine Intelligence, IEEE Transactions on*, vol. 32, no. 7, pp. 1211–1226, 2010.

[72] J. S. Hare and P. H. Lewis, "Scale saliency: applications in visual matching, tracking and view-based object recognition," 2003.

[73] T. Liu, Z. Yuan, J. Sun, J. Wang, N. Zheng, X. Tang, and H.-Y. Shum, "Learning to detect a salient object," *Pattern Analysis and Machine Intelligence, IEEE Transactions on*, vol. 33, no. 2, pp. 353–367, 2011.

[74] K. Duncan and S. Sarkar, "Saliency in images and video: a brief survey," *Computer Vision, IET*, vol. 6, no. 6, pp. 514–523, 2012.

[75] L. Itti and C. Koch, "A saliency-based search mechanism for overt and covert shifts of visual attention," *Vision research*, vol. 40, no. 10, pp. 1489–1506, 2000.

[76] T. Kadir and M. Brady, "Saliency, scale and image description," *International Journal of Computer Vision*, vol. 45, no. 2, pp. 83–105, 2001.

[77] D. G. Lowe, "Object recognition from local scale-invariant features," in *Computer vision, 1999. The proceedings of the seventh IEEE international conference on*, vol. 2. Ieee, 1999, pp. 1150–1157.

[78] T. Kadir, A. Zisserman, and M. Brady, "An affine invariant salient region detector," in *Computer Vision-ECCV 2004*. Springer, 2004, pp. 228–241.

[79] S. Pradhan and D. Patra, "Enhanced mutual information based medical image registration," *IET Image Processing*, vol. 10, no. 5, pp. 418 – 427, 2016.

[80] J. Zheng, J. Tian, K. Deng, X. Dai, X. Zhang, and M. Xu, "Salient feature region: a new method for retinal image registration," *Information Technology in Biomedicine, IEEE Transactions on*, vol. 15, no. 2, pp. 221–232, 2011.

[81] A. Toet, "Computational versus psychophysical bottom-up image saliency: A comparative evaluation study," *Pattern Analysis and Machine Intelligence, IEEE Transactions on*, vol. 33, no. 11, pp. 2131–2146, 2011.

[82] P. Manipoonchelvi and K. Muneeswaran, "Region-based saliency detection," *Image Processing, IET*, vol. 8, no. 9, pp. 519–527, 2014.

[83] D. Mahapatra and Y. Sun, "Rigid registration of renal perfusion images using a neurobiology-based visual saliency model," *Journal on Image and Video Processing*, vol. 2010, p. 4, 2010.

[84] Y. Ou, A. Sotiras, N. Paragios, and C. Davatzikos, "Dramms: Deformable registration via attribute matching and mutual-saliency weighting," *Medical image analysis*, vol. 15, no. 4, pp. 622–639, 2011.

[85] Z. Chen, J. Yuan, and Y.-P. Tan, "Hybrid saliency detection for images," *Signal Processing Letters, IEEE*, vol. 20, no. 1, pp. 95–98, 2013.

[86] D. S. Gilles, "Robust description and matching of images," Ph.D. dissertation, University of Oxford, 1999.

[87] K. Mikolajczyk, T. Tuytelaars, C. Schmid, A. Zisserman, J. Matas, F. Schaffalitzky, T. Kadir, and L. Van Gool, "A comparison of affine region detectors," *International journal of computer vision*, vol. 65, no. 1-2, pp. 43–72, 2005.

[88] N. Bruce and J. Tsotsos, "Saliency based on information maximization," in *Advances in neural information processing systems*, 2005, pp. 155–162.

[89] J. Zhang and A. Rangarajan, "Affine image registration using a new information metric," in *Computer Vision and Pattern Recognition, 2004. CVPR 2004. Proceedings of the 2004 IEEE Computer Society Conference on*, vol. 1. IEEE, 2004, pp. I–848.

[90] J. Tsao, "Interpolation artifacts in multimodality image registration based on maximization of mutual information," *Medical Imaging, IEEE Transactions on*, vol. 22, no. 7, pp. 854–864, 2003.

[91] J. P. Pluim, J. A. Maintz, and M. A. Viergever, "Interpolation artefacts in mutual information-based image registration," *Computer vision and image understanding*, vol. 77, no. 2, pp. 211–232, 2000.

[92] B. Likar and F. Pernuš, "A hierarchical approach to elastic registration based on mutual information," *Image and vision computing*, vol. 19, no. 1, pp. 33–44, 2001.

[93] H. m. Chen and P. K. Varshney, "Mutual information-based ct-mr brain image registration using generalized partial volume joint histogram estimation," *Medical Imaging, IEEE Transactions on*, vol. 22, no. 9, pp. 1111–1119, 2003.

[94] R. Szeliski and J. Coughlan, "Spline-based image registration," *International Journal of Computer Vision*, vol. 22, no. 3, pp. 199–218, 1997.

[95] D. Mattes, D. R. Haynor, H. Vesselle, T. K. Lewellen, and W. Eubank, "Pet-ct image registration in the chest using free-form deformations," *Medical Imaging, IEEE Transactions on*, vol. 22, no. 1, pp. 120–128, 2003.

[96] M. Holden, "A review of geometric transformations for nonrigid body registration," *Medical Imaging, IEEE Transactions on*, vol. 27, no. 1, pp. 111–128, 2008.

[97] E. Haber and J. Modersitzki, "Numerical methods for image registration," 2004.

[98] D. Loeckx, F. Maes, D. Vandermeulen, and P. Suetens, "Nonrigid image registration using free-form deformations with a local rigidity constraint," in *Medical Image Computing and Computer-Assisted Intervention–MICCAI 2004*. Springer, 2004, pp. 639–646.

[99] S. McKinley and M. Levine, "Cubic spline interpolation," *College of the Redwoods*, vol. 45, no. 1, pp. 1049–1060, 1998.

[100] Z. Xie and G. E. Farin, "Image registration using hierarchical b-splines," *Visualization and Computer Graphics, IEEE Transactions on*, vol. 10, no. 1, pp. 85–94, 2004.

[101] K. Rajab, "Knowledge guided non-uniform rational b-spline (nurbs) for supporting design intent in computer aided design (cad) modeling," Ph.D. dissertation, 2011.

[102] C. M. Crainiceanu, D. Ruppert, and R. J. Carroll, "Spatially adaptive bayesian p-splines with heteroscedastic errors," 2004.

[103] D. Ruppert, "Selecting the number of knots for penalized splines," *Journal of computational and graphical statistics*, 2012.

[104] B. D. Marx, "P-spline varying coefficient models for complex data," in *Statistical Modelling and Regression Structures*. Springer, 2010, pp. 19–43.

[105] W. Li, S. Xu, G. Zhao, and L. P. Goh, "Adaptive knot placement in b-spline curve approximation," *Computer-Aided Design*, vol. 37, no. 8, pp. 791–797, 2005.

[106] S. Pradhan and D. Patra, "Rmi based non-rigid image registration using bf-qpso optimization and p-spline," *AEU-International Journal of Electronics and Communications*, vol. 69, no. 3, pp. 609–621, 2015.

[107] A. Pawar, Y. Zhang, X. Wei, Y. Jia, T. Rabczuk, C. L. Chan, and C. Anitescu, "An adaptive non-rigid image registration technique using hierarchical b-splines," in *Computational Vision and Medical Image Processing V: (VipIMAGE 2015, Tenerife, Spain, October 19-21, 2015)*. CRC Press, 2015, p. 3.

[108] M. S. Hansen, R. Larsen, B. Glocker, and N. Navab, "Adaptive parametrization of multivariate b-splines for image registration," in *Computer Vision and Pattern Recognition, 2008. CVPR 2008. IEEE Conference on*. IEEE, 2008, pp. 1–8.

[109] G. K. Matsopoulos, N. A. Mouravliansky, K. K. Delibasis, and K. S. Nikita, "Automatic retinal image registration scheme using global optimization techniques," *Information Technology in Biomedicine, IEEE Transactions on*, vol. 3, no. 1, pp. 47–60, 1999.

[110] H. Talbi and M. Batouche, "Particle swam optimization for image registration," in *Information and Communication Technologies: From Theory to Applications, 2004. Proceedings. 2004 International Conference on*. IEEE, 2004, pp. 397–398.

[111] Y. Lu, Z. Liao, and W. Chen, "An automatic registration framework using quantum particle swarm optimization for remote sensing images," in *Wavelet Analysis and Pattern Recognition, 2007. ICWAPR'07. International Conference on*, vol. 2. IEEE, 2007, pp. 484–488.

[112] J. Kennedy, "Particle swarm optimization," in *Encyclopedia of machine learning*. Springer, 2011, pp. 760–766.

[113] A. Das and M. Bhattacharya, "Affine-based registration of ct and mr modality images of human brain using multiresolution approaches: comparative study on genetic algorithm and particle swarm optimization," *Neural Computing and Applications*, vol. 20, no. 2, pp. 223–237, 2011.

[114] M. P. Wachowiak, R. Smolíková, Y. Zheng, J. M. Zurada, and A. S. Elmaghraby, "An approach to multimodal biomedical image registration utilizing particle swarm optimization," *Evolutionary Computation, IEEE Transactions on*, vol. 8, no. 3, pp. 289–301, 2004.

[115] M. Farid, W. J. Leong, and L. Zheng, "A new diagonal gradient-type method for large scale unconstrained optimization," *University politehnica of bucharest scientific bulletin series a applied mathematics and physics*, vol. 75, no. 1, pp. 57–64, 2013.

[116] L. T. Zheng and R. F. Tong, "Image registration algorithm using an improved pso algorithm," in *Computing and Intelligent Systems*. Springer, 2011, pp. 198–203.

[117] A. Biswas, S. Dasgupta, S. Das, and A. Abraham, "Synergy of pso and bacterial foraging optimization a comparative study on numerical benchmarks," in *Innovations in Hybrid Intelligent Systems*. Springer, 2007, pp. 255–263.

[118] M. J. Powell, "A view of algorithms for optimization without derivatives," *Mathematics Today-Bulletin of the Institute of Mathematics and its Applications*, vol. 43, no. 5, pp. 170–174, 2007.

[119] X. Xu and R. D. Dony, "Differential evolution with powell's direction set method in medical image registration," in *Biomedical Imaging: Nano to Macro, 2004. IEEE International Symposium on*. IEEE, 2004, pp. 732–735.

[120] J. Zhang, P. Huo, J. Teng, X. Wang, and S. Wang, "Medical image registration algorithm with generalized mutual information and pso-powell hybrid algorithm," in *International Conference in Swarm Intelligence*. Springer, 2010, pp. 160–166.

[121] J. Bernon, V. Boudousq, J. Rohmer, M. Fourcade, M. Zanca, M. Rossi, and D. Mariano-Goulart, "A comparative study of powell's and downhill simplex algorithms for a fast multimodal surface matching in brain imaging," *Computerized Medical Imaging and Graphics*, vol. 25, no. 4, pp. 287–297, 2001.

[122] M. Clerc and J. Kennedy, "The particle swarm-explosion, stability, and convergence in a multidimensional complex space," *Evolutionary Computation, IEEE Transactions on*, vol. 6, no. 1, pp. 58–73, 2002.

[123] F. Ayatollahi, S. B. Shokouhi, and A. Ayatollahi, "A new hybrid particle swarm optimization for multimodal brain image registration," 2012.

[124] C.-L. Lin, A. Mimori, and Y.-W. Chen, "Hybrid particle swarm optimization and its application to multimodal 3d medical image registration," *Computational intelligence and neuroscience*, vol. 2012, p. 6, 2012.

[125] S. A. Ludwig, "Repulsive self-adaptive acceleration particle swarm optimization approach," *Journal of Artificial Intelligence and Soft Computing Research*, vol. 4, no. 3, pp. 189–204, 2014.

[126] J. Sun, B. Feng, and W. Xu, "Particle swarm optimization with particles having quantum behavior," in *Congress on Evolutionary Computation*, 2004.

[127] S. Yang, M. Wang, and L. Jiao, "A quantum particle swarm optimization," in *Evolutionary Computation, 2004. CEC2004. Congress on*, vol. 1. IEEE, 2004, pp. 320–324.

[128] M. Xi, J. Sun, and W. Xu, "An improved quantum-behaved particle swarm optimization algorithm with weighted mean best position," *Applied Mathematics and Computation*, vol. 205, no. 2, pp. 751–759, 2008.

[129] N. Sharma and S. Sharma, "Bio-inspired optimization techniques and their application to biomedical engineering," *Indian Journal of Industrial and Applied Mathematics*, vol. 3, no. 1s, pp. 114–127, 2012.

[130] K. M. Passino, "Biomimicry of bacterial foraging for distributed optimization and control," *Control Systems, IEEE*, vol. 22, no. 3, pp. 52–67, 2002.

[131] M. Hanmandlu, O. P. Verma, N. K. Kumar, and M. Kulkarni, "A novel optimal fuzzy system for color image enhancement using bacterial foraging," *Instrumentation and Measurement, IEEE Transactions on*, vol. 58, no. 8, pp. 2867–2879, 2009.

[132] Y. Wang, J. Huang, J. Liu, and X. Tang, "An efficient image-registration method based on probability density and global parallax," *AEU-International Journal of Electronics and Communications*, vol. 64, no. 12, pp. 1148–1156, 2010.

[133] S. Das, A. Biswas, S. Dasgupta, and A. Abraham, "Bacterial foraging optimization algorithm: theoretical foundations, analysis, and applications," in *Foundations of Computational Intelligence Volume 3*. Springer, 2009, pp. 23–55.

[134] G. T. Halliwell and P. R. Mercer, "A refinement of an inequality from information theory," *J. Inequal. Pure Appl. Math*, vol. 5, no. 1, 2004.

Dissemination of Work

Journal

1. Smita Pradhan, Dipti Patra, "Enhanced Mutual Information based medical image registration", **IET Image Processing**, vol. 10 (5), pp. 418-427, 2016.

2. Smita Pradhan, Dipti Patra, "RMI Based Non-rigid Image Registration Using BF-QPSO Optimization and P-spline", **AEU-International Journal of Electronics and Communications, Elsevier**, vol. 69 (3), pp. 609-621, 2015.

Conference

1. Smita Pradhan, Dipti Patra, "Nonrigid medical image registration using adaptive knot selection in P-spline", Tech Sym-2016, IIT, Kharagpur, India (Accepted) .

2. Smita Pradhan, Ajay Singh, Dipti Patra, "Enhanced Mutual Information based multi-modal brain MR image registration using phase congruency", ICACNI-2016, NIT, Rourkela, India (Accepted) .

3. Smita Pradhan, Dipti Patra, "Image Registration of Medical Images using Ripplet Transform", Computer Vision Image Processing (CVIP), IIT Roorkee, India, 2016.

4. Smita Pradhan, Dipti Patra, "P-spline based Nonrigid brain MR image registration using Regional Mutual Information", Annual IEEE India Conference (INDICON), IIT Mumbai, India, 2013.

5. Smita Pradhan, Dipti Patra, "Nonrigid Image Registration of Brain MR images using Normalized Mutual Information", Second International conference on SocProS, IET, Jaipur, India, 2012.